Acoustical Methods for Cavitation Control in Shockwave Lithotripsy and Histotripsy

by

Hedieh Alavi Tamaddoni

A dissertation submitted in partial fulfillment
of the requirements for the degree of
Doctor of Philosophy
(Biomedical Engineering)
in The University of Michigan
2019

Doctoral Committee:

Associate Research Scientist Timothy L. Hall, Co-Chair
Associate Professor Zhen Xu, Co-Chair
Professor J. Brian Fowlkes
Professor William W. Roberts

Hedieh Alavi Tamaddoni

alavi@umich.edu

ORCID iD: 0000-0001-8271-8654

DEDICATION

To maman, Hanieh,

and

Hossein

TABLE OF CONTENTS

LIST OF FIGURES

ABSTRACT

The overall goal of the work presented in this dissertation is to develop acoustic mechanisms to modulate, or manipulate, cavitation events in histotripsy and lithotripsy therapies in order to achieve efficient and fast histotripsy, high shock rate lithotripsy, and active tissue protection. We investigated the effects of applying properly tuned low pressure acoustic pulses before and during therapy in order to control the cavitation threshold, the shape of the resulting bubble cloud, and the behavior and interactions of residual microbubbles.

Histotripsy is a tissue ablation method that utilizes focused high amplitude ultrasound to generate a cavitation bubble cloud that mechanically fractionates tissue. Effective histotripsy depends on initiation, control, and maintenance of cavitation bubble clouds in the targeted area. The work in this dissertation seeks to develop active tissue protection techniques by modulating the pressure threshold of bubble cloud initiation and focal sharpening using bubble suppressing pulses. We demonstrated that by applying a properly tuned low pressure pulse sequence before and/or during shock scattering histotripsy therapy, both the cavitation initiation pressure threshold and the growth of the cavitation bubble can be modified. This mechanism can be used to produce well defined lesions with minimal collateral damage. It can also be a way to actively protect soft tissue from cavitation damage during both lithotripsy and histotripsy by increasing the pressure threshold for bubble cloud initiation in the periphery zone.

Cavitation also plays a significant role in the efficacy of stone comminution during shockwave lithotripsy (SWL). Although cavitation on the surface of urinary stones helps to improve stone fragmentation, cavitation bubbles along the propagation path may shield or block subsequent shockwaves and potentially induce collateral tissue damage. At low firing rates, there is sufficient time for the majority of the bubbles to passively dissolve, while at high firing rates the per shockwave efficacy is significantly reduced due to pre-focal persisting bubbles. We investigated acoustic methods for removing residual bubble nuclei in order to avoid shielding effects. Previous *in vitro* work has shown that applying low amplitude acoustic waves after each shockwave can force bubbles to consolidate and enhance SWL efficacy. In this work, the feasibility of applying acoustic bubble coalescence (ABC) *in vivo* was examined. We further optimized the parameters of bubble coalescing pulses, and conducted a feasibility investigation of bubble dispersion by forcing the residual bubble nuclei to disperse from the propagation path away or toward the targeted area before the arrival of the next therapy pulse. These results suggest that manipulation of residual bubbles after each shockwave can be further optimized by acoustic bubble coalescence and dispersion, which can reduce the shielding effect of residual bubble nuclei more efficiently than relying only on immediate coalescence of residual bubbles, resulting in a more efficient SWL treatment.

CHAPTER 1

Introduction

The overall goal of the work presented in this dissertation is to improve the efficacy and safety of histotripsy and lithotripsy by means of cavitation control. This research can be separated into two categories: 1) investigation of modulation of cavitation initiation pressure threshold by applying a properly tuned low pressure acoustic pulse sequence before and/or during histotripsy pulses, and 2) investigation of acoustical methods to avoid shielding and memory effects of persisting cavitation bubbles in high rate shockwave lithotripsy and histotripsy. This chapter will give a brief introduction on shock scattering histotripsy and shockwave lithotripsy, and then go on to explore the issues with remnant residual microbubbles in shockwave lithotripsy or histotripsy.

1.1 Cavitation Threshold for Shock Scattering Histotripsy

One of the objectives of this work is to achieve active tissue protection during histotripsy treatment by modulating cavitation threshold by applying bubble suppressing pulses. In histotripsy, and particularly at lower pressures with shock scattering, the treatment is highly dependent on generating and maintaining a dense bubble cloud at the target.

Histotripsy is a cavitation-based ultrasound therapy that can achieve tissue fractionation through a mechanical process using controlled cavitation bubble clouds. Through histotripsy, a dense cloud of micron-sized cavitation bubbles is generated at a targeted area by applying a focused, microsecond long, high amplitude ultrasound pulse sequence at a very low duty cycle (typically less than 1%) [1-5]. The erosion caused by histotripsy results not by liquefying the tissue through high temperature, but rather through mechanical stress caused by oscillation and collapse of the cavitation bubble cloud [4-5]. Histotripsy cavitation bubble cloud can be generated by applying a negative pressure exceeding a distinct threshold (which appears to be intrinsic to the medium called intrinsic threshold, about 25 to 30 MPa in soft tissue) or at lower pressures by means of shock scattering [6-12]. The shock scattering from initial bubbles has the opposite polarity to that of the incident wave, and when combined with the incoming wave, it creates a high negative pressure which results in growth of a dense bubble cloud [6-7].

Previous studies have shown a correlation between the histotripsy cavitation bubble clouds and the lesions that they produce [13]. As a result, bubble clouds with scattered cavitation would result in collateral tissue damage. Generating a dense and confined cavitation bubble cloud would be necessary to minimize potential damage. It has been shown that cavitation preconditioning pulses can be applied before histotripsy pulses for active focal sharpening, in order to control cavitation in the periphery of the focus, which would result in more precise and well-confined lesions [14].

In this work, we investigate the effect of applying preconditioning and bubble suppressing pulses before and during shock scattering histotripsy on cavitation initiation pressure threshold. Cavitation initiation displays a stochastic nature affected by existing nuclei populations in the

medium. By applying bubble suppressing pulses during treatment, after each pulse, the residual nuclei are forced to coalesce. This effect can decrease the probability of nuclei presence at the focus, shock scattering from which is to boost the negative pressure. As a result, the probability of shock scattering at each pressure level is decreased, which is to say it will increase the pressure threshold. This mechanism can be used for tissue hardening, active focal sharpening and active protection of the part of the tissue that needs to be protected from cavitation.

1.2 Enhanced Shockwave Lithotripsy

Shockwave lithotripsy (SWL) is a non-invasive method for treatment of urinary stones. SWL is utilized to replace the surgical removal of urinary stones with the fragmentation of those stones by applying acoustic energy from outside of the body. One of the main issues with the current clinical use of SWL is the incomplete fragmentation of stones. These incomplete fragments can cause extreme pain when they are discarded. The larger fragments and large volume of fragments may cause ureteral obstruction, which would result in pain, and may even require secondary surgery in order to remove these fragments. These incomplete fragments can also act as nidus for additional stone formation [15-17]. The newer option for treating renal stones is ureteroscopic laser lithotripsy which has been shown to achieve better stone free rates than SWL, likely a direct result of the smaller residual stone fragment size at the end of treatment and the opportunity to actively extract fragments. The research in this proposal aims to reestablish SWL as an effective and competitive first line treatment for urinary stones to supplement ureteroscopy.

The fragmentation of renal calculi by SWL is understood to be produced through mechanical stresses caused by a combination of incident shockwaves and the collapse of cavitation bubbles on the surface of the urinary stones [18-19]. Although mechanical stress generated by the

incident shockwave causes the initial disintegration of the stone, cavitation is a necessary component for efficient fragmentation, and particularly for producing fine passable fragments (<2mm) [19]. The effect of cavitation on the fragmentation process is thought to be primarily through erosion on the stone surface, but it may also help in the formation of crack lines through which damage is spread from the surface into the bulk of the stone. This damage on the surface of the stone makes the structure weaker and as a result more susceptible to subsequent shockwaves [19-21]. The growth and collapse lifespan of a cavitation bubble cloud produced by a lithotripter shockwave has been shown to be on the order of 1ms – much shorter than the interval between shockwaves at typical lithotripter firing rates of 0.5–2Hz. However, the residual micron-sized bubbles following a cavitation cloud collapse have a longer lifespan on the order of 1 second, and thus, a large fraction would be expected to persist between subsequent shockwaves, particularly at higher firing rates [22-25]. On subsequent pulses, these nuclei absorb energy from the negative pressure phase of the lithotripter waveform, thus reducing cavitation on the surface of the stone. This in turn reduces the efficacy of stone comminution [22].

A strong rate dependency in the efficacy of histotripsy [26], and shockwave lithotripsy has been shown by many *in vitro* [22, 27-29], *in vivo* [30], and human studies [31-33]. It is hypothesized that a major component of this effect is due to the presence of cavitation bubbles persisting between subsequent pulses or shockwaves which shield or attenuate the amplitude of subsequent histotripsy pulse or lithotripter shockwaves [26, 34-37]. At low firing rates, there is sufficient time for a majority of the bubbles to passively dissolve, while at high firing rates, efficacy is significantly reduced due to persisting bubbles. The solution that this dissertation proposes for overcoming the adverse effects of persisting bubbles is Acoustic Bubble Coalescence

and Dispersion (ABCD), which forces cavitation bubbles to coalesce or disperse away from the propagation path before the arrival of the next therapy pulse [27, 34, 38].

1.3 Cavitation Bubble Behavior

One of the objectives of this dissertation is to model and simulate the physical characteristics and behavior of cavitation bubbles generated by shockwave lithotripsy or histotripsy in order to optimize acoustic bubble coalescence and dispersion processes and to gain a better understanding of cavitation bubble behavior.

It has been widely known that lowering the shockwave rate or histotripsy PRF would reduce interference from the persisting cavitation bubbles. Here, we are developing a novel technique for achieving the same effect by actively removing cavitation bubbles from the propagation path using acoustic radiation forces generated by a low amplitude sound field. The mechanism of bubble coalescence occurs through the acoustic field inducing size oscillations in the bubbles, which gives rise to two major forces. The primary Bjerknes force describes the tendency of bubbles smaller (or larger) than resonant size to move up (or down) a pressure gradient and congregate at pressure antinodes (or nodes). The secondary Bjerknes force describes an attractive (or repulsive) force between bubbles which are oscillating in phase (or out of phase) with one another depending on their size and the acoustic field frequency [39-45]. When optimized for the primary acoustic radiation force, this sound field will disperse bubbles away from the propagation path. Alternatively, the field can be optimized for the secondary radiation force, which stimulates the bubbles to coalesce, and hence, greatly reduces their shielding potential. In either case, cavitation is still able to occur on the surface of the stone, or at the focus of the histotripsy

transducer in soft tissue, and may even be enhanced due to the reduced interference from intervening cavitation bubbles along the propagation path.

1.4 Outline

The current chapter introduces objectives and motivations of the work presented in this dissertation, and provides an overview of treatment modalities for which cavitation control has been utilized in order to improve efficacy and safety, including cavitation initiation threshold in histotripsy and high rate shockwave lithotripsy.

Chapter 2 examines the feasibility of acoustically modulating cavitation initiation pressure threshold in the targeted area. We demonstrated that a low pressure acoustic pulse sequence applied before and/or during shock scattering histotripsy therapy can modulate the cavitation initiation pressure threshold and the growth of cavitation bubble clouds.

The study presented in chapter 3 demonstrates modeling and simulation of cavitation bubble behavior under different acoustic pulse sequences following a cavitation event in shockwave lithotripsy or histotripsy treatments in order to optimize ABCD processes and to gain a better understanding of cavitation bubble behavior.

Chapter 4 investigates enhanced high rate shockwave lithotripsy by applying acoustic bubble coalescence (ABC) pulses in an *in vivo* porcine model. The results confirm that acoustic bubble coalescence can reduce the shielding effect of residual bubble nuclei, resulting in a more efficient SWL treatment.

Chapter 5 explores the effects of applying low amplitude acoustic pulse sequences at different time delays after each lithotripsy shockwave, which would result in different interactions

among residual microbubbles during stone comminution. We hypothesized that by utilizing Acoustic Bubble Coalescence and Dispersion (ABCD), we can mitigate the shielding effect of residual cavitation bubbles more efficiently, and further improve the therapy efficacy particularly at higher pulse repetition rates.

Chapter 6 provides an overview of design and construction of non-focal transducer lenses with complex surface geometries using rapid prototyping stereolithography to produce more effective acoustic fields for bubble consolidation during lithotripsy or ultrasound therapy. We demonstrate a design methodology using an inverse problem technique to map the desired acoustic field back to the surface of the transducer lens to determine the correct phase shift at every point on the lens surface.

Finally, chapter 7 summarizes the findings and contributions of this dissertation and discusses future work in cavitation control in shockwave lithotripsy and histotripsy.

1.5 References

[1] Z. Xu, A. Ludomirsky, L. Y. Eun, T. L. Hall, B. C. Tran, J. B. Fowlkes, et al., "Controlled ultrasound tissue erosion," *IEEE Trans Ultrason Ferroelectr Freq Control*, vol. 51, no. 6, pp. 726-36, Jun. 2004.

[2] W. W. Roberts, T. L. Hall, K. Ives, J. S. Wolf, Jr., J. B. Fowlkes, and C. A. Cain, "Pulsed cavitational ultrasound: a noninvasive technology for controlled tissue ablation (histotripsy) in the rabbit kidney," *J. of Urology*, vol. 175, no. 2pp. 734-8, Feb. 2006.

[3] J. E. Parsons, C. A. Cain, G. D. Abrams, and J. B. Fowlkes, "Pulsed cavitational ultrasound therapy for controlled tissue homogenization," *Ultrasound in Medicine & Biology*, vol. 32, no. 1, pp. 115-29, Jan. 2006.

[4] J. E. Parsons, C. A. Cain and J. B. Fowlkes, "Spatial variability in acoustic backscatter as an indicator of tissue homogenate production in pulsed cavitational ultrasound therapy,"

in *IEEE Transactions on Ultrasonics, Ferroelectrics, and Frequency Control*, vol. 54, no. 3, pp. 576-590, Mar. 2007.

[5] Z. Xu, J. B. Fowlkes, E. D. Rothman, A. M. Levin, and C. A. Cain, "Controlled ultrasound tissue erosion: The role of dynamic interaction between insonation and microbubble activity," *Journal of the Acoustical Society of America*, vol. 117, no. 1, pp. 424–435, Jan. 2005.

[6] A. D. Maxwell, C. A. Cain, J. B. Fowlkes and Z. Xu, "Inception of cavitation clouds by scattered shockwaves," *2010 IEEE International Ultrasonics Symposium*, San Diego, CA, 2010, pp. 108-111.

[7] A. D. Maxwell, T. Y. Wang, C. A. Cain, J. B. Fowlkes, O. A. Sapozhnikov, M. R. Bailey, and Z. Xu, "Cavitation clouds created by shock scattering from bubbles during histotripsy," *Journal of the Acoustical Society of America*, vol. 130, pp. 1888–1898, Oct. 2011.

[8] A. D. Maxwell, C. A. Cain, T. L. Hall, J. B. Fowlkes, and Z. Xu, "Probability of cavitation for single ultrasound pulses applied to tissues and tissue-mimicking materials," *Ultrasound in Medicine & Biology*, vol. 39, pp. 449–465, Mar. 2013.

[9] E. Vlaisavljevich, A. D. Maxwell, M. Warnez, E. Johnsen, C. A. Cain, Z. Xu, "Histotripsy-induced cavitation cloud initiation thresholds in tissues of different mechanical properties." *Ultrasonics, Ferroelectrics, and Frequency Control, IEEE Transactions*, vol. 61, no.2, pp. 341-352, Feb. 2014.

[10] J. B. Fowlkes and L. A. Crum, "Cavitation threshold measurements for microsecond length pulses of ultrasound," *Journal of the Acoustical Society of America*, vol. 83, no. 6, pp. 2190–2201, Jun. 1988.

[11] J. B. Fowlkes, P. L. Carson, E. H. Chiang, and J. M. Rubin, "Acoustic generation of bubbles in excised canine urinary bladders," *Journal of the Acoustical Society of America*, vol. 89, no. 6, pp. 2740–2744, Jun. 1991

[12] K. W. Lin, et al., "Histotripsy beyond the intrinsic cavitation threshold using very short ultrasound pulses: microtripsy," *IEEE Trans Ultrason Ferroelectr Freq Control*, vol. 61, pp. 251-65, Feb 2014.

[13] A. D. Maxwell, T. Y. Wang, L. Yuan L, A. P. Duryea, Z. Xu, C. A. Cain, "A tissue phantom for evaluation of mechanical damage caused by cavitation," *Ultrasound Med. Biol*. vol. 36, pp. 2132–2143. Dec. 2010

[14] T. Y. Wang, Z. Xu, T. L. Hall, J. B. Fowlkes, W. W. Roberts and C. A. Cain, "Active focal zone sharpening for high-precision treatment using histotripsy," *IEEE Transactions on Ultrasonics, Ferroelectrics, and Frequency Control*, vol. 58, no. 2, pp. 305-315, Feb. 2011.

[15] Lingeman JE, Smith LH, Wood JR. Bioeffects and long term effects of ESWL. In: Urinary Calculi: ESWL, Endourology and Medical Therapy. Philadelphia: Lea & Febiger. 1989; 285.

[16] Politis G, Griffith DP. ESWL: Stone free efficacy based upon the stone size and location. *World J Urol*. 1987; 5: 255–258.

[17] Cass AS. Comparison of first generation (Dornier HM3) and second generation (Medstone STS) lithotriptors: treatment results with 13,864 renal and ureteral calculi. *J Urol*. 1995 Mar; 153 (3 Pt 1): 588-92. PMID: 7861488.

[18] M. Lokhandwalla, B. Sturtevant, "Fracture mechanics model of stone comminution in ESWL and implications for tissue damage," *Physics in medicine and biology*, vol. 45, no. 7, pp. 1923, Jul. 2000.

[19] S. Zhu, F. H. Cocks, G. M. Preminger, P. Zhong, "The role of stress waves and cavitation in stone comminution in shock wave lithotripsy," *Ultrasound in medicine & biology*, vol. 28, no. 5, pp. 661-71, May. 2002.

[20] P. Zhong, C. J. Chuong, G. M. Preminger, "Characterization of fracture toughness of renal calculi using a microindentation technique," *Journal of materials science letters*, vol. 12, no. 1, pp. 1460-2, Jan. 1993.

[21] A. P. Duryea, W. W. Roberts, C. A. Cain, and T. L. Hall, "Controlled cavitation to augment SWL stone comminution: mechanistic insights in vitro," *IEEE Trans Ultrason Ferroelectr Freq Control*, vol. 60, pp. 301-9, Feb 2013.

[22] Y. A. Pishchalnikov, J. A. McAteer, Jr. J. C. Williams, I. V. Pishchalnikova and R. J. Vonderhaar, "Why stones break better at slow shockwave rates than at fast rates: in vitro study with a research electrohydraulic lithotripter," *Journal of Endourology*, vol. 20, no. 8, pp. 537-41, Aug. 2006

[23] H. G. Flynn, "Generation of transient cavities in liquids by microsecond pulses of ultrasound," *Journal of the Acoustical Society of America*, vol. 72, no. 6, pp. 1926-32, Dec. 1982.

[24] J. B. Fowlkes and L. A. Crum, "Cavitation threshold measurements for microsecond length pulses of ultrasound," *Journal of the Acoustical Society of America*, vol. 83, no. 6, pp. 2190–2201, Jun. 1988.

[25] Y. A. Pishchalnikov, J. A. McAteer, I. V. Pishchalnikova, J. C. Williams, M. R. Bailey, and O. A. Sapozhnikov, "Bubble proliferation in shock wave lithotripsy occurs during inertial collapse," in *18th International Symposium on Nonlinear Acoustics*, 2008, pp. 460-463.

[26] T. Y. Wang, Z. Xu, T. L. Hall, J. B. Fowlkes, and C. A. Cain, "An efficient treatment strategy for histotripsy by removing cavitation memory," Ultrasound Med Biol, vol. 38, pp. 753-66, May 2012.

[27] A. P. Duryea, W. W. Roberts, C. A. Cain, H. A. Tamaddoni, and T. L. Hall, "Acoustic bubble removal to enhance SWL efficacy at high shock rate: an in vitro study," *J Endourol*, vol. 28, pp. 90-5, Jan 2014.

[28] M. J. Weir, N. Tariq, and R. J. Honey, "Shockwave frequency affects fragmentation in a kidney stone model," *J Endourol*, vol. 14, pp. 547-50, Sep 2000.

[29] A. Greenstein and H. Matzkin, "Does the rate of extracorporeal shock wave delivery affect stone fragmentation?," *Urology,* vol. 54, pp. 430-432, 1999.

[30] R. F. Paterson, D. A. Lifshitz, J. E. Lingeman, A. P. Evan, B. A. Connors, N. S. Fineberg, *et al.*, "Stone fragmentation during shock wave lithotripsy is improved by slowing the shock wave rate: studies with a new animal model," *J Urol*, vol. 168, pp. 2211-5, Nov 2002.

[31] K. T. Pace, D. Ghiculete, and M. Harju, "Shock wave lithotripsy at 60 or 120 shocks per minute: A randomized, double-blind trial," *The Journal of Urology*, vol. 174, pp. 595-599, 2005.

[32] E. Yilmaz, E. Batislam, M. Basar, D. Tuglu, C. Mert, and H. Basar, "Optimal frequency in extracorporeal shock wave lithotripsy: prospective randomized study," *Urology,* vol. 66, pp. 1160-4, Dec 2005.

[33] K. Madbouly, A. M. El-Tiraifi, M. Seida, S. R. El-Faqih, R. Atassi, and R. F. Talic, "Slow versus fast shock wave lithotripsy rate for urolithiasis: a prospective randomized study," *J Urol*, vol. 173, pp. 127-30, Jan 2005.

[34] A. P. Duryea, C. A. Cain, H. A. Tamaddoni, W. W. Roberts, and T. L. Hall, "Removal of Residual Nuclei Following a Cavitation Event using Low-Amplitude Ultrasound," *IEEE Trans Ultrason Ferroelectr Freq Control,* vol. 61, pp. 1619-26, Oct 2014.

[35] M. Delius, F. Ueberle, W. Eisenmenger, “Extracorporeal shock waves act by shock wave-gas bubble interaction,” *Ultrasound in medicine & biology*, vol. 24, no. 7, pp. 1055-9. Sep. 1998.

[36] A. Philipp, M. Delius, C. Scheffczyk, A. Vogel, W. Lauterborn, “Interaction of lithotripter-generated shock waves with air bubbles,” *The Journal of the Acoustical Society of America*, vol. 93, no. 5, pp. 2496-509, May. 1993.

[37] Y. A. Pishchalnikov, J. A. McAteer, M. R. Bailey, I. V. Pishchalnikova, J. C. Williams, and A. P. Evan, "Acoustic shielding by cavitation bubbles in shock wave lithotripsy (SWL)," in *17th International Symposium on Nonlinear Acoustics* 2005, pp. 319-322.

[38] H. Alavi Tamaddoni, W. W. Roberts, A. P. Duryea, C. A. Cain, T. L. Hall, “Enhanced High-Rate Shockwave Lithotripsy Stone Comminution in an In Vivo Porcine Model Using Acoustic Bubble Coalescence,” *Journal of endourology*, vol. *30*, no. 12, pp. 1321-1325, Dec. 2016.

[39] V. Bjerknes, *Fields of Force*, 1906.

[40] M. Kornfeld and L. Suvorov, "On the destructive action of cavitation," *Journal of Applied Physics*, vol. 15, no.6, pp. 495-506, 1944.

[41] F. G. Blake, "Bjerknes Forces in Stationary Sound Fields," *The Journal of the Acoustical Society of America*, vol. 21, no. 5, pp. 551-551, Jun. 1949.

[42] E. A. Neppiras, "Subharmonic and Other Low-Frequency Emission from Bubbles in Sound-Irradiated Liquids," *The Journal of the Acoustical Society of America*, vol. 46, no. 3B, pp. 587-601, Sep. 1969.

[43] L. A. Crum and A. I. Eller, "Motion of Bubbles in a Stationary Sound Field," *The Journal of the Acoustical Society of America*, vol. 48, no. 1B, pp. 181-189, Jul. 1970.

[44] L. A. Crum, "Bjerknes forces on bubbles in a stationary sound field," *The Journal of the Acoustical Society of America*, vol. 57, no 6, pp. 1363-1370, Jun. 1975.

[45] T. G. Leighton, *The Acoustic Bubble*. San Diego, CA: Academic Press Inc, 1997.

CHAPTER 2

Acoustic Methods for Modulating the Cavitation Initiation Pressure Threshold

A majority component of this chapter has been published in *IEEE Transactions on Ultrasonics, Ferroelectric, and Frequency Control* © 2018 IEEE. Reprinted, with permission, from [1].

2.1 Introduction

Histotripsy is a cavitation-based ultrasound therapy that produces tissue fractionation through a mechanical process using controlled cavitation bubble clouds [2]-[6]. During histotripsy, a dense cloud of micron size cavitation bubbles is generated in a targeted area by applying a focused, microseconds length, high amplitude ultrasound burst at a very low duty cycle (typically less than 1%). Studies suggest the erosion caused by histotripsy is not achieved by liquefying the tissue through high temperature, but rather through mechanical stress caused by oscillation and collapse of cavitation bubble clouds [5], [6]. A histotripsy cavitation bubble cloud can be directly generated by applying a negative pressure exceeding a distinct threshold, which appears to be intrinsic to the medium of about 25 to 30 MPa in soft tissue [7]-[12]. Another way to initiate a dense bubble cloud is via the shock-scattering mechanism where incoming acoustic waves are reflected and inverted by pre-existing single bubbles at the focus. When the reflected waves combine with subsequent incoming cycles (particularly if there are highly shocked nonlinear

waveforms due to nonlinear propagation), a sufficiently large negative pressure can be created to exceed the intrinsic threshold resulting in growth of a similarly dense bubble cloud [7], [8].

The primary motivation for this study is to develop a technique to reduce unintended tissue damage from cavitation during histotripsy or lithotripsy treatments by modulating the cavitation initiation pressure threshold. Specifically, this study investigates the incident pressure threshold to initiate and maintain bubble clouds through the shock-scattering mechanism when using various low amplitude acoustic pulse sequences. For histotripsy, effective therapy is highly dependent on generating and maintaining a dense bubble cloud at the targeted area [8]-[10]. Wang found that applying "cavitation suppressing" pulses to the periphery of the focus immediately before histotripsy pulses (called "preconditioning") reduced bubble formation in the periphery of the focus, resulting in smaller and better confined lesions [13].

Cavitation initiation for shock-scattering displays a stochastic nature affected by existing bubble nuclei populations in the medium. We hypothesized that by applying proper low pressure amplitude pulse sequences before or during histotripsy therapy, the initiation pressure threshold and growth pattern of cavitation bubble clouds could be modified. In previous *in vivo* and *in vitro* studies, applying low amplitude acoustic pulse sequences has shown to increase the efficacy of therapy in histotripsy [14]-[17] and lithotripsy [18], [19] by minimizing the shielding effect of bubbles. The residual micron sized bubbles following a cavitation cloud collapse [20], [21] have long dissolution times on the order of 1 second and thus a large fraction persist between subsequent pulses at PRFs > 1 Hz [11], [22]-[27]. For subsequent pulses, these nuclei absorb energy from the negative pressure phase of the histotripsy waveform [26]. Previous studies suggest that low

amplitude acoustic pulse sequences can overcome the adverse effects of persisting bubbles by forcing cavitation bubbles to coalesce, or disperse away from propagation path before the arrival of next therapy pulse [14], [18]. The same process of bubble coalescence may also have an effect on changing the initiation pressure threshold in shock-scattering histotripsy. In this study, we investigated the effect of applying low amplitude acoustic pulse sequences before and during shock scattering histotripsy on the cavitation initiation pressure threshold. We expect that the cavitation initiation pressure threshold for shock-scattering would increase due to a reduction in the probability of initial nuclei presence at the focus.

2.2 Methods

2.2.1 Experimental Setup

In a series of three experiments, histotripsy and low amplitude acoustic pulse sequences were applied targeting (A) a chamber of degassed water, (B) tissue phantom agarose gel, and (C) bovine liver tissue samples. Acoustic backscatter signals and optical imaging were used to detect and monitor initiation, maintenance and growth of resulting cavitation bubble cloud (Figure 2.1).

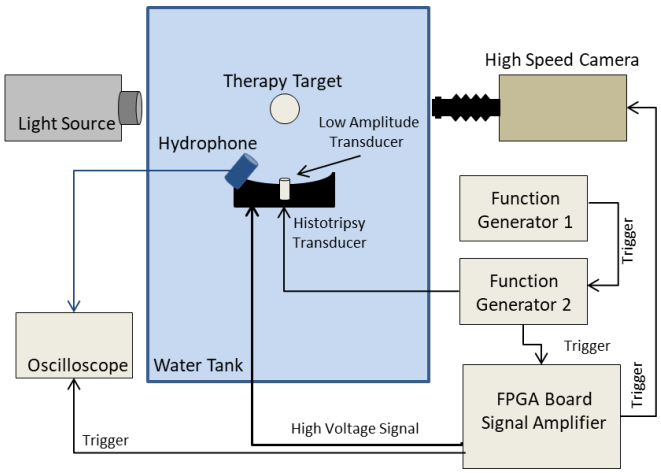

Figure 2.1. Schematic of the experimental setup. Histotripsy and low amplitude acoustic pulse sequences were applied targeting (A) a chamber of degassed water, (B) tissue phantom agarose gel, and (C) bovine liver tissue samples. Cavitation was monitored using acoustic backscatter signals and optical imaging obtained from a high speed camera positioned perpendicular to histotripsy transducer propagation axis.

2.2.1A Water

The transducers (described in sections 2.2.2 and 2.2.3) were placed in a water tank filled with degassed water to a dissolved oxygen level of 80% of saturation, at room temperature measure by a Traceable Digital Oxygen Meter (Control Co., Friendswood, TX, USA). Histotripsy pulses targeted a chamber of degassed deionized water with saturation below 80%. The gas concentration in the chamber was kept constant for all experiments by a circulation pump. The chamber components were made from polytetrafluoroethylene, glass, and 316 stainless steel. It is 150 mL cavitation chamber and has two glass windows to facilitate high speed photography, and two acoustic windows made from 12 μm-thick low density polyethylene membranes [9]. 4-6 trials were performed for each of the parameters.

2.2.1B Tissue Phantom Agarose Gel

Tissue phantoms were prepared by mixing agarose powder (Agarose Type VII, Sigma-Aldrich) with deionized water at 1% ratio. The solution was stirred and heated in a microwave until completely dissolved, degassed under high vacuum for half an hour, and then poured in a cylindrical gel holder 6 cm diameter and 7 cm height. It was then put into a refrigerator for an hour in order for the gel to solidify. After preparation, the phantom gel holder was mounted to an electronically controlled positioning system (VXM Stepping Motor Controller, Velmex Inc.,

Bloomfield, NY) in the water tank filled with degassed water with dissolved oxygen level of 15%-20% of saturation. Horizontal and vertical spacing of 7 mm was used between treatment spots for all of the trials of each set of parameters to minimize possible variations of the acoustic path and influence of previous treatments. The results of 10 trials for each of the parameters were collected.

2.2.1C Bovine Liver Tissue

Cavitation threshold modulation experiments were repeated on bovine liver samples *in vitro* for a subset of parameters. Whole livers were harvested and placed in degassed saline immediately after slaughter for transport. At the laboratory, these were sectioned into 5 cm cubes avoiding large vessels and then degassed under vacuum in saline for 6 hours. The pieces were then placed in a holder surrounded by 1% agarose (Agarose, Low Melt. Scientific Inc. Burton, MI) gel prepared the same as in A.II. After one hour cooling, the solidified gel with embedded tissue samples were ready for experiments. Samples were mounted on the positioning system and moved in steps of 5 mm horizontally and vertical in one central slice for each of the treatment spots. Water in the tank was highly degassed to below 15%. Since cavitation events cannot be observed by optical imaging in tissue, acoustic backscatter signals were the only measure for cavitation detection in the tissue experiments. 8-10 trials for each of the parameters were performed for histotripsy PRF of 100 Hz.

2.2.2 Acoustic Pulse Sequence

Histotripsy pulses were generated by a 1 MHz focused piezocomposite ultrasound transducer with 10 cm aperture and 9 cm focal length, with a hole in the center (Imasonic, Voray sur l'Ognon, France). The histotripsy transducer was driven by an in-house made system at a range of different pressure levels with negative peak/positive peak between 8/8 and 28/50 MPa.

Measurements and calibration of histotripsy waveform pressure was done by an in-house built fiber optic probe hydrophone [28] in degassed water at room temperature for lower pressures and extrapolated for higher pressures; since measurements for pressures higher than the intrinsic pressure cannot be done accurately due to cavitation initiation at the tip of the fiber. All calibrations were performed in degassed water. Pressure levels that are reported for experiments with agarose gel and liver tissue as targets in water tank are based on calibrated pressures in degassed water as well.

Low amplitude acoustic pulse sequences were produced by an in-house made single element transducer constructed from a 1 MHz disc of PZ36 material (Ferroperm Piezoceramics A/S, Kvistgaard, Denmark), with 20mm diameter and 1.5 mm thickness with an Accura 60 (3D Systems Inc., Rock Hill, SC, USA) acoustic lens matching layer. This transducer was driven by an ENI power amplifier (ENI, Inc., Rochester, NY) model AP 400B controllable power amplifier, for experiments in water and in agarose gel, and model A150 RF power amplifier for experiments in liver tissue. This transducer was placed in the central hole of the histotripsy transducer. The near field distance of the low amplitude transducer is about 67.5 mm, however, since the -3 dB beamwidth is about 85.0 mm in axial direction and 6.2 mm in lateral, this sound field fully covers the focus zone of histotripsy transducer and the extent of growth of the bubble cloud (less than 3 mm in lateral and 10 mm in axial direction in agarose gel), which grows toward the transducer along the axial axis [8]. The low amplitude transducer was calibrated by an HNR-0500 needle hydrophone (Onda Corporation, Sunnyvale, CA) for experiments in water and agarose gel, and an identical second transducer was used in experiments in liver tissue that was calibrated by a HGL hydrophone (hydrophone: ONDA HGL 0085, and amplifier: ONDA AH2010. ONDA Sunnyvale, Ca).

The experiments were performed with three different pulse schemes as shown in figure 2.2. First case was histotripsy only, in which 5 cycles of 1 MHz histotripsy pulses were fired at PRF 1, 10, or 100 Hz, with peak negative pressures from 10 to 28 MPa for 100 pulses. In the second case, bubble coalescence, each histotripsy pulse was followed by burst of 5,000 cycles of low amplitude acoustic pulses with pressure amplitude of 1 MPa, which were fired 500 µs (100 µs for experiments in liver tissue) after histotripsy pulses in order to allow the histotripsy cavitation bubble cloud to grow and collapse without interference. For the third case, preconditioning, a full second of low amplitude acoustic pulses with same pressure amplitude were applied before histotripsy treatment pulses.

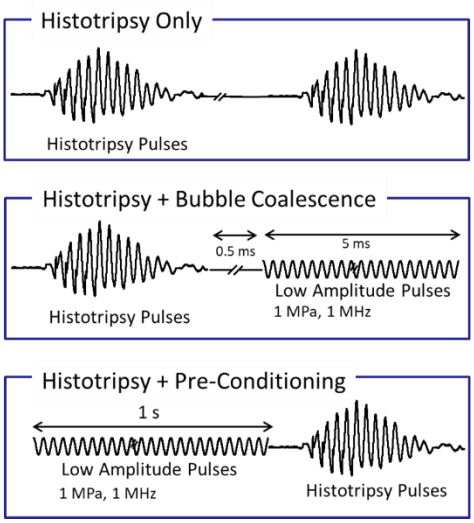

Figure 2.2. Three different pulse schemes for threshold modulation studies. Case 1: Histotripsy Only, in which five cycles of 1 MHz histotripsy pulses were applied for a range of different pressures. Case2: Histotripsy+Bubble Coalescence, in which each histotripsy pulse is followed by low amplitude acoustic pulses for duration of 5 ms. Case 3: Histotripsy+Pre-Conditioning, in which one full second of low amplitude acoustic pulses were applied immediately before the start of histotripsy treatment.

2.2.3 Detection and Monitoring

In these experiments, we used two different methods for monitoring and detecting cavitation events; the amplitude of the backscattered signal and the back-lit bubble cloud size.

The main measure for cavitation detection was the backscattered signal that was captured by an uncalibrated low frequency unfocused marine hydrophone (H1a, Aquarian Audio Products, Anacortes, WA), facing the focus of therapy transducer at about 30° angle; an increase in amplitude of the backscattered signal is an indicator for bubble cloud initiation. The energy of the acoustic backscatter signal of each pulse was calculated as the sum of voltage squared samples of each pulse, and normalized to the spatial peak pulse average intensity of the corresponding therapy pulses. The threshold for cavitation detection was then defined as the average of the uninitiated acoustic backscatter energy plus three standard deviations.

For experiment in water, the optical images from a high speed 1 megapixel CCD camera (Phantom V210, Vision Research) were recorded, and the area of backlit bubble cloud in each frame was checked against a threshold. The camera was triggered after each histotripsy pulse to record one image per pulse after about 70 μs delay to account for the sound traveling time from histotripsy transducer to the focus as well as the growth of bubble cloud. Bubble cloud was backlit by a continuous light source. For experiments in agarose gel a digital, 1.3-megapixel, CMOS camera (PN: FL3-U3–13Y3M-C, Flea 3, PointGrey, Richmond, BC, Canada) was used in the same setting, and for experiment in bovine liver tissue, no optical images were obtained.

In this study, bubble cloud initiation pressure threshold was defined as the lowest pressure at which bubble cloud is detected with probability of at least 50%, or the pressure at which the sigmoid curve fits to the data (in figures 2.3,2.5 and 2.6) given the probability=0.5 when pressures

exceeding the 50 percentile is not available. The percentage of pulses in which bubble cloud was detected is another measure used to evaluate the results.

2.3 Results

2.3.1 Experiment in Water

Figure 2.3 shows the percentage of pulses for which a bubble cloud was detected for a) PRF of 100 Hz and b) 1 Hz. All three cases were completed for PRF of 100 Hz, the results for pre-conditioning were not as significant even for 100 Hz, and as a result we did not repeat pre-conditioning case for 1 Hz. For PRF of 100 Hz, applying low amplitude acoustic pulse sequences during histotripsy significantly reduced the probability of cavitation initiation, effectively increasing the cavitation initiation pressure threshold. The threshold was increased from 20.3 MPa for histotripsy only chase to 21.2 MPa for pre-conditioning case, and to 24.5 MPa for bubble coalescence case. By Kolmogorov–Smirnov test over the non-zero part of the curves with 95% confidence level we can conclude that the three fit curves are statistically from different distributions. Kolmogorov–Smirnov test shows asymptotic p-value = 2.19e-4 between histotripsy only and bubble coalescence, and p = 0.047 for histotripsy only and pre-conditioning. At 1 Hz, no statistically significant difference was observed between histotripsy only chase and bubble coalescence case (p-value=0.41) and the predicted pressure threshold that fit the curve in figure 2.3b is 32.1 MPa for both cases. The asymptotic p-value = 0.19 per Kolmogorov–Smirnov test between the two curves in figure 2.3b shows no statistically significant difference.

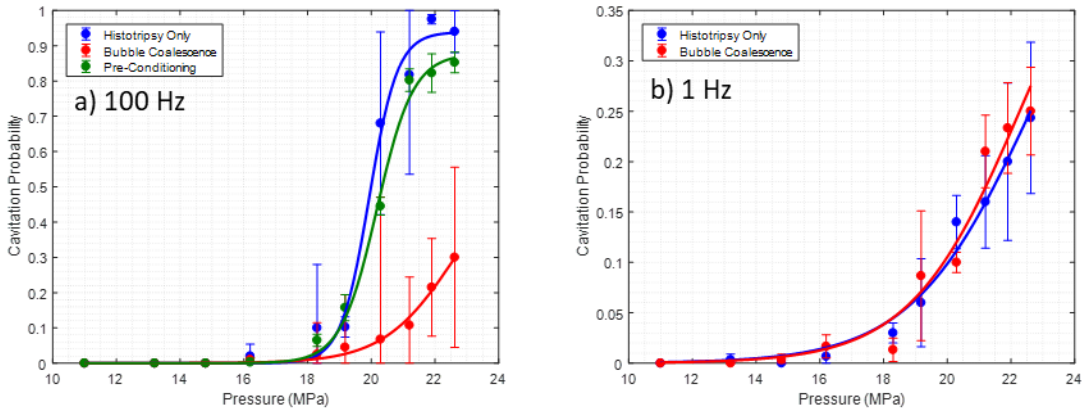

Figure 2.3. Cavitation probability for experiments in water for a) PRF 100 Hz and b) PRF 1 Hz

Investigating the backscattered signal, we realized that the effect of pre-conditioning at PRF of 100Hz is only significant in the beginning of the treatment. In other words, applying pre-conditioning is delaying the cavitation initiation, and after this delay of up to 30 pulses the same pattern is observed; figure 2.4 shows the pulse number at which bubble cloud initiation occurs for pressures close to threshold. In each of the first three pressures initiation is delayed when pre-conditioning is applied.

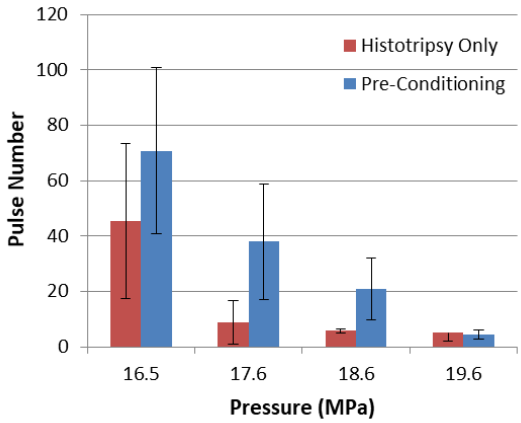

Figure 2.4. Number of pulses required to initiate cavitation bubble cloud for experiments in water for histotripsy only case and pre-conditioning with PRF 100 Hz.(p-value = 0.04)

2.3.2 Experiment in Tissue Phantom Agarose Gel

Results from experiments in agarose gel demonstrated that the applying low amplitude acoustic pulse sequences can increase the cavitation threshold in the targeted area. Figure 2.5 show the cavitation probability for different pressures at a) PRF of 100 and b) 1 Hz.

For PRF of 100 Hz, cavitation initiation threshold for both cases of bubble coalescence and pre-conditioning was increased from 16.5 MPa to 19.6 MPa. We observed a statistically significant difference between histotripsy only case and both bubble coalescence and pre-conditioning cases. Based on Kolmogorov–Smirnov test on non-zero part of the curves we can assert that the data points are from different distributions with asymptotic p-value of 3.11e-11 for histotripsy only and bubble coalescence curve, and 1.28e-7 between histotripsy only case and pre-conditioning curves.

For PRF of 1 Hz, cavitation initiation threshold for both cases of bubble coalescence and pre-conditioning was increased from 18.6 MPa to 21.5 MPa for 1 Hz PRF. Similarly, a statistically significant difference between histotripsy only case and both bubble coalescence and pre-conditioning cases was observed. Based on Kolmogorov–Smirnov test on non-zero part of the curves we can assert that the data points are from different distributions with asymptotic p-value of 0.024 for histotripsy only and bubble coalescence curve, and 1.47e-9 between histotripsy only case and pre-conditioning curve.

Unlike open water, the increase in threshold was maintained in lower PRF as well.

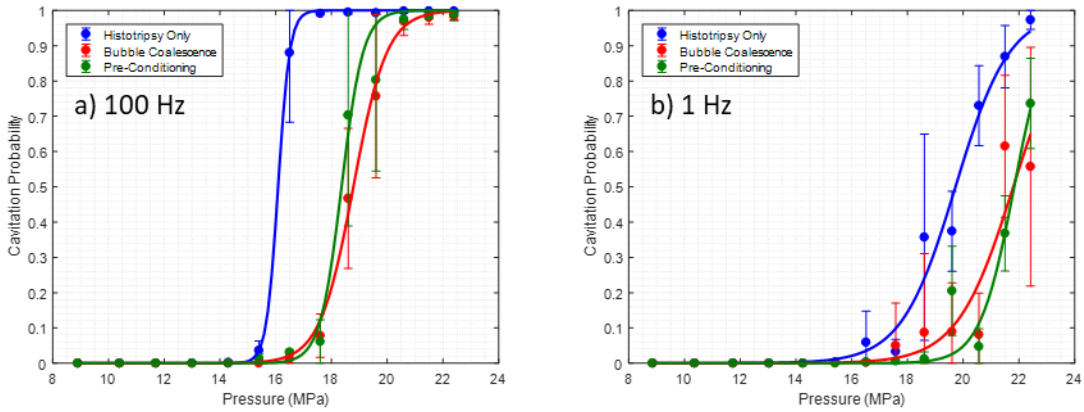

Figure 2.5. Cavitation probability for experiments in tissue phantom agarose gel for a) PRF 100 Hz and b) PRF 1 Hz

2.3.3 Experiment in Bovine Liver Tissue

The results from the experiment in tissue showed similar results to those obtained from experiments in the agarose tissue phantom gel. Applying low amplitude acoustic pulse sequences in both bubble coalescence and pre-conditioning cases resulted in an increase in the cavitation initiation threshold; for a PRF of 100 Hz, the threshold increased from 18 MPa for histotripsy only to about 20.3 MPa for both bubble coalescence and pre-conditioning cases. We observed statistically significant differences between all three cases. Based on Kolmogorov–Smirnov test on non-zero part of the curves we can assert that the data points are from different distributions with asymptotic p-value of 3.37e-5 for histotripsy only and bubble coalescence curve, and 1.65e-6 between histotripsy only case and pre-conditioning curves.

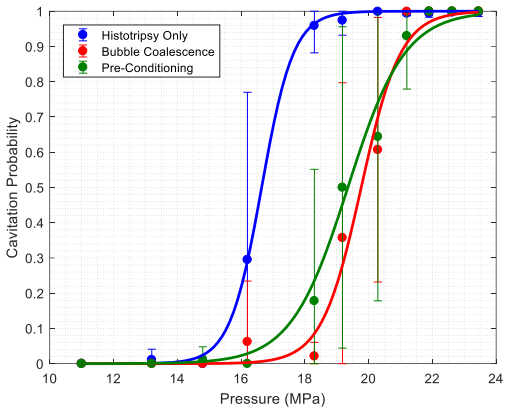

Figure 2.6. Cavitation probability for treatments in liver tissue for PRF 100 Hz

Qualitative analysis of backlit bubble cloud images showed that the shape and density of the resulting bubble cloud can also be modified through utilizing low amplitude acoustic pulses before and during treatment. By applying the low amplitude acoustic pulses, we were able to generate a dense cavitation bubble cloud at the focus, which would increase efficacy of the treatment, while decreasing scattered cavitation in the peripheral zone, which would reduce collateral damage. The size and shape differences of the resulting bubble cloud by shock scattering when pre-conditioning and bubble coalescence pulses were applied are illustrated in figure 2.7.

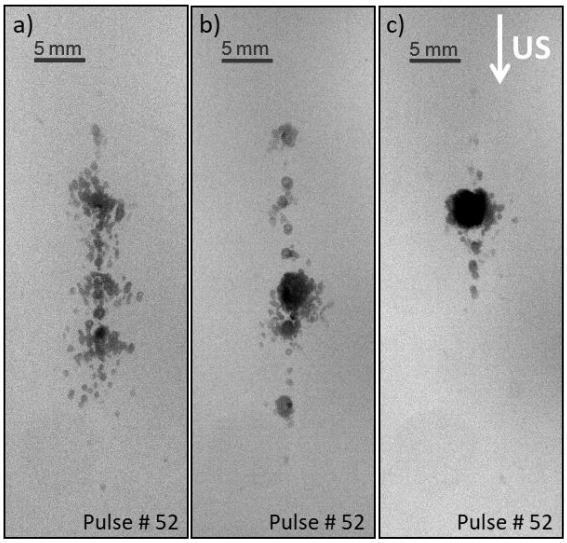

Figure 2.7. Cavitation bubble cloud in agarose gel generated by shock scattering at 22MPa with PRF 100Hz, a) histotripsy only, b) histotripsy with pre-conditioning, and c) histotripsy with bubble coalescence pulses.

2.4 Discussion

The results of this study suggest it may be possible to protect tissue during histotripsy or lithotripsy treatments by applying low amplitude acoustic pulse sequences to modulate the cavitation threshold. This mechanism could be used for tissue hardening, active focal sharpening, and protecting sensitive tissues or structures located close to a treatment target. Results from experiments in all three mediums of water, tissue phantom gel, and liver tissue generally confirmed our hypothesis and showed that applying low amplitude acoustic pulse sequences before or during shock scattering histotripsy treatment increases the cavitation initiation pressure threshold. For experiments in water at the low PRF of 1 Hz, we did not observe any statistically significant difference when low amplitude acoustic pulse sequences were applied for pre-conditioning or bubble coalescence cases. At higher rate, PRF of 100 Hz, the effect of low amplitude acoustic pulse sequences applied after each histotripsy pulse, the bubble coalescence case, was much more significant than pre-conditioning; pre-conditioning effect was only significant in the beginning of the treatment, after which generation and shape of the bubble cloud was similar to those of the histotripsy only cases. However, in experiments in agarose tissue phantom gel and in liver tissue, the effect of pre-conditioning persisted throughout the treatment and the results were similar to bubble coalescence cases. The difference in persistence of effect of pre-conditioning in water in comparison with agarose gel and tissue was expected since, in free water due to streaming, distribution of cavitation nuclei can change more rapidly than in agarose gel and soft tissue.

Despite the differences between pre-conditioning and bubble coalescence cases; pre-conditioning reduces pre-existing cavitation, and coalescence reduces residual cavitation by forced coalescence, still some of the same physical mechanism of forced coalescence is assumed to be in play in pre-conditioning as well. In pre-conditioning, similar to coalescence case, reduction of pre-existing nuclei at the focus and periphery of the focus by forced coalescence and dispersion, results in less scattered cavitation and a denser cavitation bubble cloud. Although the bubble clouds in pre-conditioning case and bubble coalescence case shown in figure 2.7 are not exactly similar, both has less scattered cavitation in comparison with histotripsy only case.

Cavitation initiation, particularly in shock scattering histotripsy, displays a stochastic nature affected by existing nuclei populations in the medium. By applying low amplitude acoustic pulse sequences during treatment, the residual nuclei are forced to coalesce. As a result of active bubble coalescence, the number existing bubbles in the vicinity of focus decreases, which consequently, reduces the probability of nuclei presence at the focus when the next therapy pulse arrives. Shock scattering from some existing nuclei at the focus is to generate a high negative pressure and initiate histotripsy bubble cloud. As a result, probability of shock scattering at any pressure level close to threshold is decreased, which translates to increase of the pressure threshold.

It is helpful to note that low amplitude acoustic pulse sequences or cavitation suppression pulses, as previously demonstrated in a number of studies [14]-[19], can be utilized to increase the efficacy of histotripsy and lithotripsy treatments at higher PRFs by avoiding or minimizing the memory effect and shielding effect of residual cavitation nuclei at the focal area and along the propagation path. At lower PRF, after each cavitation event there is sufficient time for a majority of the residual bubbles to passively dissolve away, while at higher rates the pulse efficacy is

significantly reduced due to persisting bubbles. Memory effect mainly explains how residual bubbles at the focal area contribute to this reduced efficacy, and shielding effect explains the attenuation of histotripsy pulses at the focus. On subsequent pulses, pre-focal residual bubbles absorb energy from the negative pressure phase of the histotripsy waveform and distort the waveform and attenuate its amplitude. Cavitation suppression pulses can be utilized to stimulate residual cavitation bubbles to coalesce and clear the path for the subsequent histotripsy pulses. Since cavitation suppression pulses in the current experimental setup design would result in removing bubbles from the propagation path as well as focal area, it would result in reducing attenuation of therapy signal at higher rates. This process potentially contributes to initiating and maintaining histotripsy bubble cloud at lower pressures. However, we still observed significant increase in initiation threshold when cavitation suppression pulses were used despite this process working in opposite direction. Therefore, we would expect to observe even more pronounced increase in initiation pressure threshold, with different experiment setup with cavitation suppression transducer firing at the focus perpendicular to the propagation path of histotripsy transducer. Consequently, if the same experiments were performed with histotripsy at intrinsic threshold instead of histotripsy by means of shock scattering, we would expect to observe decrease in initiation pressure threshold.

In this study, low pressure acoustic pulses were utilized during treatment to stimulate residual cavitation bubbles to coalesce. This mechanism occurs through the acoustic field, inducing size oscillations in the bubbles, and gives rise to two major forces [29]-[36]. The primary Bjerknes force describes the tendency of bubbles smaller than resonant size to move up a pressure gradient and congregate at pressure antinodes, and bubbles larger than resonant size to move down a pressure gradient and congregate at pressure nodes. The secondary Bjerknes force describes an

attractive force between bubbles which are oscillating in phase with one another, and a repulsive force between bubbles which are oscillating out of phase with one another, depending on their size and the acoustic field frequency. This secondary Bjerknes force is hypothesized to be the dominant factor bringing the remnant bubbles together to coalesce. During stable bubble oscillations, this force increases with higher amplitude and higher frequency of the driving sound field. The amplitude and frequency of cavitation suppression pulses in this study are set to mechanical index of one which would result in stable oscillation and maximum bubble coalescence [16]. Frequency of both pre-conditioning and bubble coalescence pulses were the same in these preliminary studies, each of which is subject to further optimization. The efficacy of forced bubble coalescence for a given bubble population is highly dependent on the driving frequency, particularly if its corresponding resonant size is close to the existing bubble nuclei size range. Based on the Minnaert formula [37], resonant size of driving frequency in this study is about diameter of 6 μm, which is in the range of micron size cavitation nuclei following the collapse of histotripsy bubble cloud, while range of stable and incidental bubbles prior to treatment is assumed to be three orders of magnitude smaller in range nanometer-sized nuclei [9,38-40]. Furthermore, pre-conditioning process is expected to rely on dispersion (primary Bjerknes forces), as well as coalescence (secondary Bjerknes forces), and as a result, since there are different phenomena in play in each mechanism, separate optimization for each mechanism, or combination of the two, can lead to even more pronounced change in initiation pressure threshold.

2.5 References

[1] H. Alavi Tamaddoni, W. W. Roberts, A. P. Duryea, C. A. Cain, and T. L. Hall, “Enhanced High-Rate Shockwave Lithotripsy Stone Comminution in an *in vivo* Porcine Model Using Acoustic Bubble Coalescence,” *Journal of Endourology*, vol. 30, no. 12, pp. 1321-1325, Dec. 2016.

[2] Z. Xu, A. Ludomirsky, L. Y. Eun, T. L. Hall, B. C. Tran, J. B. Fowlkes, et al., "Controlled ultrasound tissue erosion," *IEEE Trans Ultrason Ferroelectr Freq Control*, vol. 51, no. 6, pp. 726-36, Jun. 2004.

[3] W. W. Roberts, T. L. Hall, K. Ives, J. S. Wolf, Jr., J. B. Fowlkes, and C. A. Cain, "Pulsed cavitational ultrasound: a noninvasive technology for controlled tissue ablation (histotripsy) in the rabbit kidney," *J. of Urology*, vol. 175, no. 2pp. 734-8, Feb. 2006.

[4] J. E. Parsons, C. A. Cain, G. D. Abrams, and J. B. Fowlkes, "Pulsed cavitational ultrasound therapy for controlled tissue homogenization," *Ultrasound in Medicine & Biology*, vol. 32, no. 1, pp. 115-29, Jan. 2006.

[5] J. E. Parsons, C. A. Cain and J. B. Fowlkes, "Spatial variability in acoustic backscatter as an indicator of tissue homogenate production in pulsed cavitational ultrasound therapy," in *IEEE Transactions on Ultrasonics, Ferroelectrics, and Frequency Control*, vol. 54, no. 3, pp. 576-590, Mar. 2007.

[6] Z. Xu, J. B. Fowlkes, E. D. Rothman, A. M. Levin, and C. A. Cain, "Controlled ultrasound tissue erosion: The role of dynamic interaction between insonation and microbubble activity," *Journal of the Acoustical Society of America*, vol. 117, no. 1, pp. 424–435, Jan. 2005.

[7] A. D. Maxwell, C. A. Cain, J. B. Fowlkes and Z. Xu, "Inception of cavitation clouds by scattered shockwaves," *2010 IEEE International Ultrasonics Symposium*, San Diego, CA, 2010, pp. 108-111.

[8] A. D. Maxwell, T. Y. Wang, C. A. Cain, J. B. Fowlkes, O. A. Sapozhnikov, M. R. Bailey, and Z. Xu, "Cavitation clouds created by shock scattering from bubbles during histotripsy," *Journal of the Acoustical Society of America*, vol. 130, pp. 1888–1898, Oct. 2011.

[9] A. D. Maxwell, C. A. Cain, T. L. Hall, J. B. Fowlkes, and Z. Xu, "Probability of cavitation for single ultrasound pulses applied to tissues and tissue-mimicking materials," *Ultrasound in Medicine & Biology*, vol. 39, pp. 449–465, Mar. 2013.

[10] E. Vlaisavljevich, A. D. Maxwell, M. Warnez, E. Johnsen, C. A. Cain, Z. Xu, "Histotripsy-induced cavitation cloud initiation thresholds in tissues of different mechanical properties." *Ultrasonics, Ferroelectrics, and Frequency Control, IEEE Transactions*, vol. 61, no.2 , pp. 341-352. Feb. 2014.

[11] J. B. Fowlkes and L. A. Crum, "Cavitation threshold measurements for microsecond length pulses of ultrasound," *Journal of the Acoustical Society of America*, vol. 83, no. 6, pp. 2190–2201, Jun. 1988.

[12] J. B. Fowlkes, P. L. Carson, E. H. Chiang, and J. M. Rubin, “Acoustic generation of bubbles in excised canine urinary bladders, ,” *Journal of the Acoustical Society of America*, vol. 89, no. 6, pp. 2740–2744, Jun. 1991.e

[13] T. Y. Wang, Z. Xu, T. L. Hall, J. B. Fowlkes, W. W. Roberts and C. A. Cain, "Active focal zone sharpening for high-precision treatment using histotripsy," *IEEE Transactions on Ultrasonics, Ferroelectrics, and Frequency Control*, vol. 58, no. 2, pp. 305-315, Feb. 2011.

[14] A. P. Duryea, C. A. Cain, H. A. Tamaddoni, W. W. Roberts and T. L. Hall, "Removal of residual nuclei following a cavitation event using low-amplitude ultrasound," *IEEE Transactions on Ultrasonics, Ferroelectrics, and Frequency Control*, vol. 61, no. 10, pp. 1619-1626, Oct. 2014.

[15] A. P. Duryea, W. W. Roberts, C. A. Cain and T. L. Hall, "Removal of residual cavitation nuclei to enhance histotripsy erosion of model urinary stones," *IEEE Transactions on Ultrasonics, Ferroelectrics, and Frequency Control*, vol. 62, no. 5, pp. 896-904, May 2015.

[16] A. P. Duryea, H. A. Tamaddoni, C. A. Cain, W. W. Roberts and T. L. Hall, "Removal of residual nuclei following a cavitation event: a parametric study," *IEEE Transactions on Ultrasonics, Ferroelectrics, and Frequency Control*, vol. 62, no. 9, pp. 1605-1614, Sep. 2015.

[17] A. P. Duryea, C. A. Cain, W. W. Roberts and T. L. Hall,, "Removal of residual cavitation nuclei to enhance histotripsy fractionation of soft tissue," *IEEE Transactions on Ultrasonics, Ferroelectrics, and Frequency Control*, vol. 62, no. 12, pp. 2068-2078, Dec. 2015.

[18] A. P. Duryea, W. W. Roberts, C. A. Cain, H. A. Tamaddoni and T. L. Hall, “Acoustic bubble removal to enhance SWL efficacy at high shock rate: an in vitro study,” *Journal of Endourology*, vol. 28, no. 1, pp. 90-95, Jan. 2014.

[19] H. Alavi Tamaddoni, W. W. Roberts, A. P. Duryea, C. A. Cain, and T. L. Hall, *Journal of Endourology*, vol. 30, no. 12, pp. 1321-1325, Dec. 2016.

[20] Y. A. Pishchalnikov, J. A. McAteer, and J. C. Williams, Jr., "Effect of firing rate on the performance of shock wave lithotriptors," BJU International, vol. 102, no. 11, pp. 1681-6, Dec. 2008.

[21] R. Mettin, I. Akhatov, U. Parlitz, C. D. Ohl, and W. Lauterborn, "Bjerknes forces between small cavitation bubbles in a strong acoustic field," *Physical Review E*, vol. 56, no. 3, pp. 2924-2931, Sep. 1997.

[22] P. Huber, K. Jochle, and J. Debus, "Influence of shock wave pressure amplitude and pulse repetition frequency on the lifespan, size and number of transient cavities in the field of an electromagnetic lithotripter," *Physics in Medicine & Biology*, vol. 43, no. 10, pp. 3113-28, Oct. 1998.

[23] Y. A. Pishchalnikov, J. A. McAteer, I. V. Pishchalnikova, J. C. Williams, M. R. Bailey, and O. A. Sapozhnikov, "Bubble proliferation in shock wave lithotripsy occurs during inertial collapse," in *18th International Symposium on Nonlinear Acoustics*, 2008, pp. 460-463.

[24] Y. A. Pishchalnikov, J. C. Williams, and J. A. McAteer, "Bubble proliferation in the cavitation field of a shock wave lithotripter," *Journal of the Acoustical Society of America*, vol. 130, no. 2, pp. EL87-93, Aug. 2011.

[25] P. S. Epstein and M. S. Plesset, "On the stability of gas bubbles in liquid-gas solutions," *The Journal of Chemical Physics*, vol. 18, no. 11, pp. 1505-1509, 1950.

[26] Y. A. Pishchalnikov, J. A. McAteer, Jr. J. C. Williams, I. V. Pishchalnikova and R. J. Vonderhaar, "Why stones break better at slow shockwave rates than at fast rates: in vitro study with a research electrohydraulic lithotripter," *Journal of Endourology*, vol. 20, no. 8, pp. 537-41, Aug. 2006

[27] H. G. Flynn, "Generation of transient cavities in liquids by microsecond pulses of ultrasound," *Journal of the Acoustical Society of America*, vol. 72, no. 6, pp. 1926-32, Dec. 1982.

[28] J. E. Parsons, C. A. Cain, and J. B. Fowlkes, "Cost-effective assembly of a basic fiber-optic hydrophone for measurement of high amplitude therapeutic ultrasound fields," *Journal of the Acoustical Society of America*, vol. 119, no. 3, pp. 1432–1440, Mar. 2006.

[29] V. Bjerknes, *Fields of Force*, 1906.

[30] V. Bjerknes, *Die Kraftfelder*, 1909.

[31] M. Kornfeld and L. Suvorov, "On the destructive action of cavitation," *Journal of Applied Physics*, vol. 15, no.6, pp. 495-506, 1944.

[32] F. G. Blake, "Bjerknes Forces in Stationary Sound Fields," *The Journal of the Acoustical Society of America*, vol. 21, no. 5, pp. 551-551, Jun. 1949.

[33] E. A. Neppiras, "Subharmonic and Other Low-Frequency Emission from Bubbles in Sound-Irradiated Liquids," *The Journal of the Acoustical Society of America*, vol. 46, no. 3B, pp. 587-601, Sep. 1969.

[34] L. A. Crum and A. I. Eller, "Motion of Bubbles in a Stationary Sound Field," *The Journal of the Acoustical Society of America*, vol. 48, no. 1B, pp. 181-189, Jul. 1970.

[35] L. A. Crum, "Bjerknes forces on bubbles in a stationary sound field," *The Journal of the Acoustical Society of America*, vol. 57, no 6, pp. 1363-1370, Jun. 1975.

[36] T. G. Leighton, *The Acoustic Bubble*. San Diego, CA: Academic Press Inc, 1997.

[37] M. Minnaert, "XVI. On musical air-bubbles and the sounds of running water," *Philosophical Magazine Series 7*, vol. 16, no. 104, pp. 235-248, Aug. 1933.

[38] E. Vlaisavljevich, K. Lin, A. Maxwell, M. T. Warnez, L. Mancia, R. Singh, A. J. Putnam, B. Fowlkes, E. Johnsen, C. Cain, And Z. Xu, "Effects of Ultrasound Frequency and Tissue Stiffness on the Histotripsy Intrinsic Threshold for Cavitation" *Ultrasound in Medicine and Biology*, vol. 41, no. 6, pp. 1651 – 1667, 2015.

[39] A. Arvengas, E. Herbert, S. Cersoy, K. Davitt, and F. Caupin, "Cavitation in Heavy Water and Other Liquids." *J Phys Chem B*, vol. 115, pp. 14240–14245, Oct. 2011.

[40] E. Herbert, S. Balibar, and F. Caupin, "Cavitation Pressure in Water" *Phys. Rev. E*, vol. 74, pp. 041603, Oct. 2006.

CHAPTER 3

Modeling and Simulation of Cavitation Bubble Behavior

3.1 Motivations

The objectives of the work presented in this chapter are to gain a better understanding of the behavior of cavitation bubbles driven by ultrasound fields, and to model and simulate the physical characteristics and behavior of cavitation bubbles generated by enhanced histotripsy and lithotripsy treatment with acoustic bubble coalescence and dispersion (ABCD) in order to improve ABCD processes. The formation of cavitation bubbles on the surface of tissue or urinary stones causes the desirable erosion during histotripsy and lithotripsy treatments; however, the same acoustic bursts produce pre-focal cavitation bubbles that may shield or attenuate the next therapy pulses [1-2]. Instead of waiting for the bubbles to passively dissolve away before applying the next histotripsy pulse or shockwave, properly tuned low amplitude acoustic pulses can be applied to actively force the residual nuclei from the surrounding fluid to coalesce and disperse away from the propagation path. One of the main goals of this simulation model is to optimize the acoustic parameters of ABCD pulses [3-8].

3.2 Theory and Methods

3.2.1 Single Bubble Model

Numerical simulation of bubble radius under different pulse sequences was performed in order to understand the behavior of cavitation bubbles, their growth and collapse, and characteristics of their oscillation during enhanced histotripsy or lithotripsy treatment with acoustic bubble coalescence and dispersion. We have developed both Rayleigh-Plesset (Eq. 3.1) and Gilmore's model (Eq. 3.2) for single bubble radius that can be solved for any arbitrary input pressure function [9].

Rayleigh-Plesset Equation:

$$R\ddot{R} + \frac{3}{2}\dot{R}^2 + \rho^{-1}\left[\frac{2\sigma}{R} - \left(P_0 + \frac{2\sigma}{R_0}\right)\left(\frac{R_0}{R}\right)^{3\eta} + P_0 + P_A\cos(\omega t)\right] = 0 \qquad \text{Eq. 3.1}$$

Gilmore's Equation:

$$\frac{dR_0}{dt} = \frac{DR_gT}{R_0}\left(P_0 + \frac{4\sigma}{3R_0}\right)^{-1} * \left[A + R_0\left(\frac{B}{\pi Dt}\right)^{\frac{1}{2}} C_{sn}\left(\frac{C_i}{C_{sn}} - \frac{A}{B}\right)\right. \qquad \text{Eq. 3.2}$$

$$A = \frac{1}{T_b}\int_0^{T_b}\frac{R}{R_0}dt,\ B = \frac{1}{T_b}\int_0^{T_b}\left(\frac{R}{R_0}\right)^4 dt,\ C_{sn} = C_0\left[1 + \left(\frac{2\sigma}{R_0P_0}\right)\right]$$

R_0 : equilibrium radius, R : time varying radius

P_0: absolute pressure, σ : surface tension of the host fluid

ρ : density of the liquid, D : diffusion constant

C_0 : equilibrium saturation concentration of the gas in moles/unitvolume

C_i : concentration of dissolved gas in the liquid far from bubble

Oscillation of acoustic field pressure gradient causes the bubble volume to oscillate as well. This oscillation is in-phase with the sound field for bubbles smaller than resonant size and out-of-phase for bubbles larger than resonant size. The plot in figure 3.1 shows the phase difference

between the acoustic field and bubble oscillation for different bubble sizes under three different driving frequencies. The vertical lines show the resonant size of each frequency, and bubbles on each side of the line will be oscillating almost in phase with one another. For the range of parameters generally used in ABCD pulses, the oscillation of bubbles is stable and almost linear; with acoustic field of $p(t) = p_0 + P_A \cos(\omega t - kx)$, bubble radius is close to equation 3.3.

$$R(t) = R_0 + R_\varepsilon \cos(\omega t - \theta) \qquad \text{Eq. 3.3}$$

with $R_\varepsilon = -\frac{P_A}{R_0 \rho} \frac{1}{\sqrt{(\omega_0^2 - \omega^2)^2 + (2\beta_{tot}\omega)^2}}$, and $\tan\theta = \frac{2\beta_{tot}\omega}{\omega_0^2 - \omega^2}$

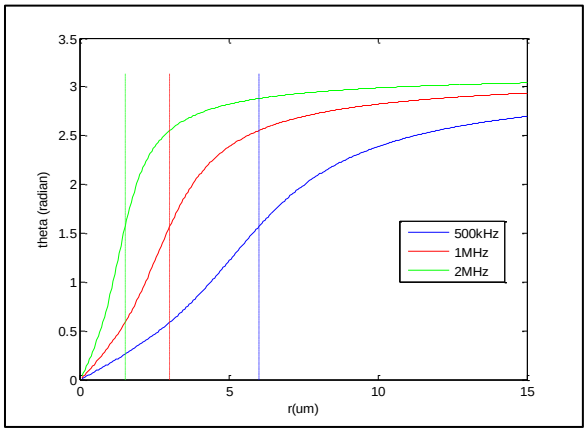

Figure 3.1. The phase difference between the field and bubble oscillation for different bubble sizes under three different driving frequencies: .5, 1, and 2 MHz.

3.2.2 Behavior of Cavitation Bubbles Driven by Ultrasound Fields

Acoustic field inducing size oscillations in the bubbles give rise to two major forces; primary and secondary Bjerknes forces. The primary Bjerknes force (Eq. 3.4,3.5) describes the tendency of bubbles smaller (or larger) than resonant size to move up (or down) a pressure gradient, and congregate at pressure antinodes (or nodes). Primary Bjerknes force component in x direction is given by Eq. 3.4, and its time average over one cycle in Eq. 3.5. Solving the pressure

gradient for each of the traveling and standing acoustic field, time average of radiation force can be simplified as Eq. 3.6 and Eq. 3.7 [10-16].

$$F_x = -\frac{\partial p}{\partial x}\Big|_{x0} \Delta x \Delta y \Delta z \quad \text{Eq.3.4}$$

$$< \vec{F} >= -< V\vec{\nabla}P > \quad \text{Eq.3.5}$$

$$\bar{F}_{B,trav} = \frac{4\pi}{\rho_0 c} R_0 P_A^2 \omega \, sin(ky) \quad \text{Eq. 3.6}$$

$$\bar{F}_{B,stand} = \frac{3}{2R_o} k P_A V_o R_\epsilon \, sin(2ky) \quad \text{Eq. 3.7}$$

The secondary Bjerknes force (Eq. 3.8) describes an attractive force between bubbles which are oscillating in phase with one another depending on their size and the acoustic field frequency. The secondary Bjerknes force is hypothesized to be the dominant mechanism for bringing the remnant bubbles from SWL cavitation together to coalesce and clear the propagation path.

$$\bar{F}_{rad2} = -\left(\frac{3}{1+2f}\right)\left(\frac{f}{1+2f}\right)\left(\frac{V_{\varepsilon 01}\omega^2}{4\pi r_b^2}\right)(V_{\varepsilon 02}\rho_{2\varepsilon}\cos\theta_b) \quad \text{, with } f = \frac{\rho_{1e}}{\rho} \quad \text{Eq.3.8}$$

A 2D model of bubble dynamics simulation was programmed in MATLAB. An initial population of cavitation bubbles can be generated with any arbitrary size and number of bubbles, or with a distribution of an averaged size, or by image processing of a given image/video. The medium, e.g. water, was assumed to be homogeneous and under a given acoustic field, which can be set to a standing wave, traveling wave, or a given map of a pressure field. The model then applies radiation forces –oscillation, primary and secondary Bjerknes forces –and then real time coalescence of bubbles is simulated. Bubble coalescence is a complex and not fully understood process; however, in this simulation we simplified this process by assuming that when shells of

two or more bubbles come into contact, they immediately become a single bubble with total mass as sum of the coalescing bubbles' masses.

3.2.3 Experimental Setup

A series of experiments with histotripsy combined with ABCD pulses were performed to evaluate the simulation results. The experiment setup is shown in figure 3.2. All experiments were conducted in deionized degassed water. The growth and collapse of the histotripsy bubble cloud and the behavior of residual bubbles during ABCD pulses were monitored using high speed photography using Photron Fastcam SA1.1 high speed camera (Photron USA Inc., San Diego, CA). The high speed camera was utilized with a 10X super-long working distance microscope objective (T Plan SLWD 10X/0.20, Nikon Instruments Inc., Tokyo, Japan) coupled to a 70 mm macro lens (Sigma 70 mm 1:2:8 DG Macro, Sigma Corporation of America, Ronkonkoma, NY) in order to provide required optical power to monitor micron sized residual cavitation bubbles. Initial cavitation bubble cloud was generated by an in-house built transducer array consisted of eight individual 2 MHz histotripsy transducer modules confocally aligned and arranged in a spherical pattern. ABCD pulses were applied following each histotripsy pulse by a 1 MHz transducer module aligned to the focus of histotripsy modules. More details of the construction of this histotripsy array transducer is described in Duryea, et al. [3]. The following general pulse scheme was examined in this series of experiments: (a) cavitation initiation pulses: cavitation bubbles were initiated by the 2 MHz histotripsy transducer array using a single very short intense pulse (P- > 30 MPa), and (b) ABCD pulses: residual bubble nuclei following the collapse of histotripsy bubble cloud were sonicated by the ABCD pulses for a duration of 5 ms and different pressure amplitudes over the range of 80 kPa to 900kPa.

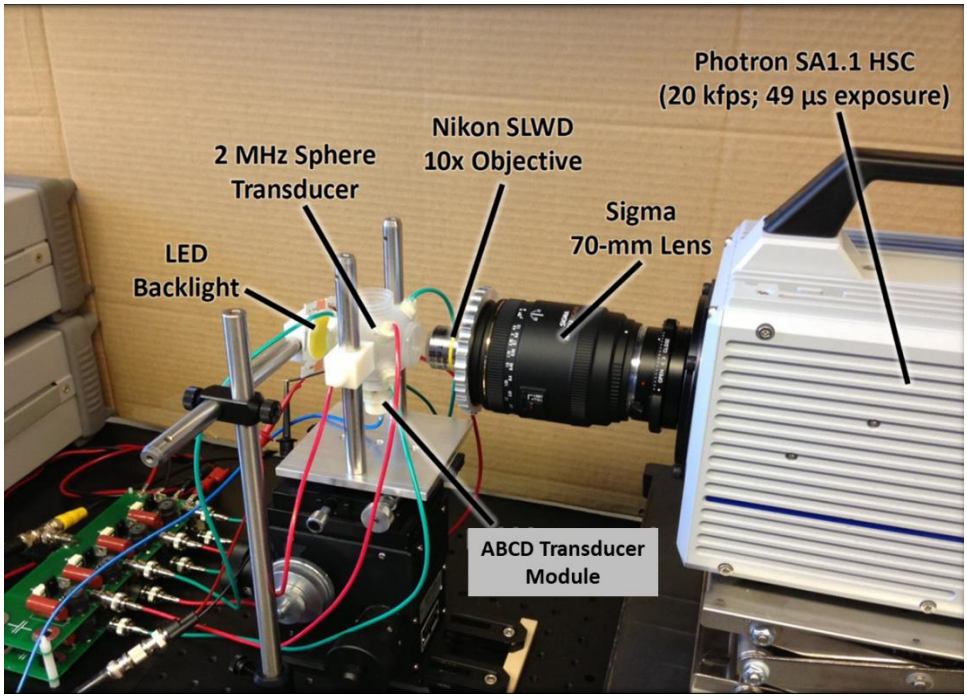

Figure 3.2. Experimental setup. A spherical in-house made histotripsy transducer with used and backlit cavitation bubbles were captured with a high speed camera.

3.3 Results

Simulation results were compared and evaluated with experimental results. The simulation results were found to be in agreement with the experimental results for cases in which primary or secondary Bjerknes forces were the dominant factors and oscillation of bubbles were stable. At lower pressures, under standing wave field, the primary Bjerknes force was dominant, and cavitation bubbles congregated around pressure nodes, an example of which is shown in figure 3.3. The ABCD pulses with frequency of 1 MHz and amplitude of 350 kPa were applied for the experimental and simulation results shown in figure 3.3. As expected, the distance between nodes for both the simulation and experimental results is 370 µm. At higher pressures the secondary

Bjerknes forces were the dominant factors, and cavitation bubbles were forced more effectively to come together and coalesce.

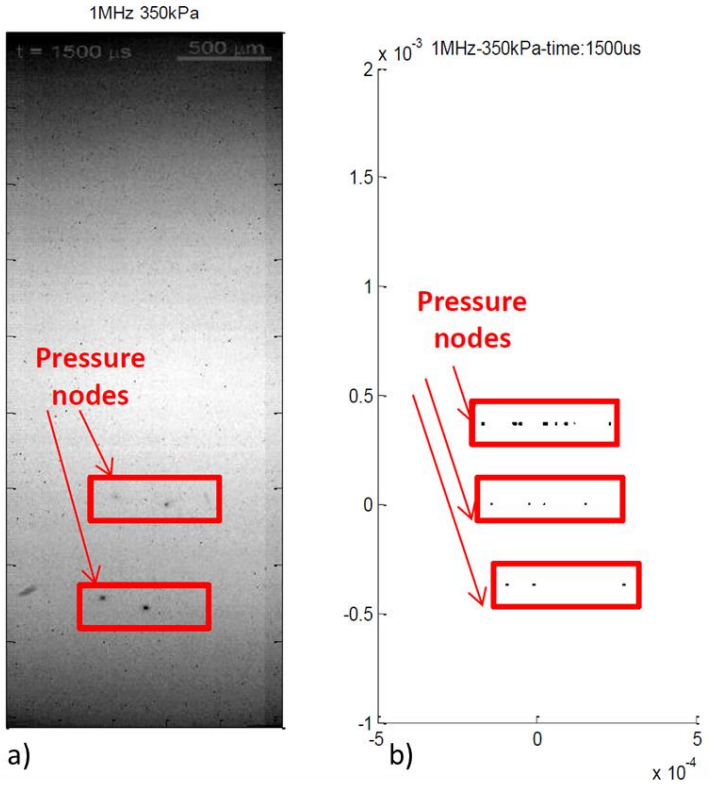

Figure 3.3. Comparison of a) Experimental and b) simulated results. The pattern of congregation of bubbles at pressure nodes. ABCD pulses were applied at 1 MHz and 350 kPa.

Figure 3.4 shows the normalized total area of cavitation bubbles as a function of time following the histotripsy pulse and during the time that ABCD pulses are applied for both simulation predictions, figure 3.4(a), and experimental results, figure 3.4(b). It can be observed from the experimental results that at higher pressure (600kPa), cavitation bubbles start to coalesce faster than at lower pressure (350kPa) case, and there is a large drop in backlit area within the first 100µs. After about 2500µs of ABCD pulses, the backlit area reaches its minimum. The same trend is also predicted by simulation.

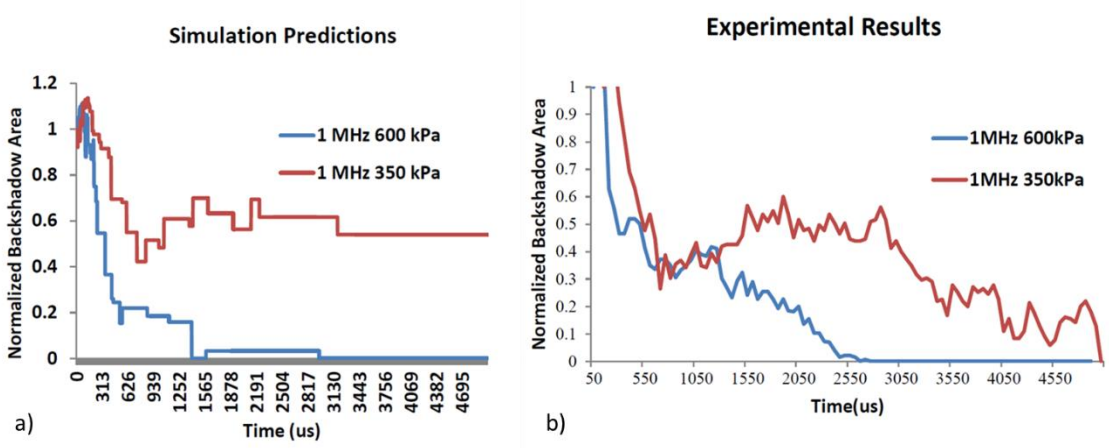

Figure 3.4. Quantitative comparison of experimental and simulated results.The backlit area of bubble cloud shadow as a function of time as a quantitative measure to compare (a)simulation prediction to (b)experimental results.

3.4 Discussion

Despite the simplified assumptions that were made in the simulation model, the results demonstrated that the model correlated well with experiments when primary or secondary Bjerknes forces were the dominant factors and the bubble oscillation was stable (Mechanical index <2). The acoustic parameters of ABCD pulses are within this range, and as a result the simulation developed in this study can be used for optimization of ABCD parameters. This simulation can be performed for different frequencies and pressures within the working parameter range, and results of most effective ABCD pulses can be selected for experimental implementation. However, the simulation model was unable to predict the bubble dynamics at higher pressures under which cavitation bubbles go under violent growth and collapse. A simulation of cavitation behavior for a population of 100 bubbles, with normal distribution size with average radius of 3 μm, under ABCD pulses with frequency of 1 MHz and duration of 3 ms with different pressure levels was performed. The results for the normalized total area of cavitation bubbles as a function of time is illustrated in

figure 3.5. Simulation predictions suggests that lower pressures of ABCD pulses of 80 kPa and 210 kPa were not effective in coalescence and dispersion of cavitation bubbles. After 3 ms of ABCD pulses over half of residual bubbles remained in the propagation path. With higher pressure ABCD pulses, the total area of cavitation bubbles reduced to 10% of the initial bubble cloud size after only 600 µs of ABCD pulses with 660 kPa, and 900 kPa. These predictions can be used to minimize the amount of ABCD pulses that is needed to be delivered for effective bubble coalescence and dispersion.

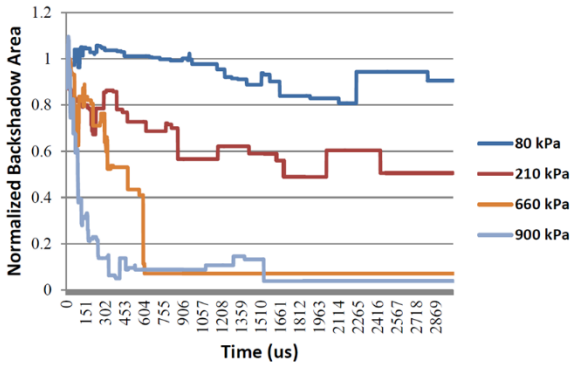

Figure 3.5. Experimental and simulated results for the total area of bubble cloud as a function of time for different ABCD pressure levels.

Figure 3.6 shows the duration of ABCD pulses needed for effective bubble coalescence and dispersion for different pressure levels between 280 kPa and 900 kPa. Again, experimental evaluation of simulation predictions confirmed that primary and secondary Bjerknes forces that were modeled in this simulation were the dominant factors.

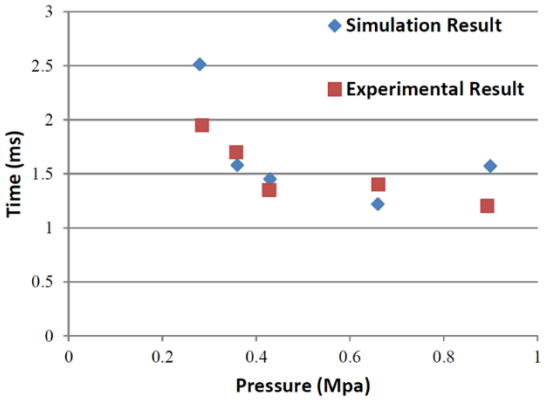

Figure 3.6 The averaged amount of time of ABCD pulses needed for effective bubble coalescence and dispersion for different pressure levels between 280 kPa and 900 kPa with frequency of 1 MHz.

3.5 References

[1] M. Delius, F. Ueberle, W. Eisenmenger, “Extracorporeal shock waves act by shock wave-gas bubble interaction,” *Ultrasound in medicine & biology*, vol. 24, no. 7, pp. 1055-9. Sep. 1998.

[2] A. Philipp, M. Delius, C. Scheffczyk, A. Vogel, W. Lauterborn, “Interaction of lithotripter-generated shock waves with air bubbles,” *The Journal of the Acoustical Society of America*, vol. 93, no. 5, pp. 2496-509, May. 1993.

[3] A. P. Duryea, C. A. Cain, H. A. Tamaddoni, W. W. Roberts and T. L. Hall, "Removal of residual nuclei following a cavitation event using low-amplitude ultrasound," *IEEE Transactions on Ultrasonics, Ferroelectrics, and Frequency Control*, vol. 61, no. 10, pp. 1619-1626, Oct. 2014.

[4] A. P. Duryea, W. W. Roberts, C. A. Cain and T. L. Hall, "Removal of residual cavitation nuclei to enhance histotripsy erosion of model urinary stones," *IEEE Transactions on Ultrasonics, Ferroelectrics, and Frequency Control*, vol. 62, no. 5, pp. 896-904, May 2015.

[5] A. P. Duryea, H. A. Tamaddoni, C. A. Cain, W. W. Roberts and T. L. Hall, "Removal of residual nuclei following a cavitation event: a parametric study," *IEEE Transactions on Ultrasonics, Ferroelectrics, and Frequency Control*, vol. 62, no. 9, pp. 1605-1614, Sep. 2015.

[6] A. P. Duryea, C. A. Cain, W. W. Roberts and T. L. Hall,, "Removal of residual cavitation nuclei to enhance histotripsy fractionation of soft tissue," *IEEE Transactions on Ultrasonics, Ferroelectrics, and Frequency Control*, vol. 62, no. 12, pp. 2068-2078, Dec. 2015.

[7] A. P. Duryea, W. W. Roberts, C. A. Cain, H. A. Tamaddoni and T. L. Hall, "Acoustic bubble removal to enhance SWL efficacy at high shock rate: an in vitro study," *Journal of Endourology*, vol. 28, no. 1, pp. 90-95, Jan. 2014.

[8] H. Alavi Tamaddoni, W. W. Roberts, A. P. Duryea, C. A. Cain, and T. L. Hall, "Enhanced High-Rate Shockwave Lithotripsy Stone Comminution in an *in vivo* Porcine Model Using Acoustic Bubble Coalescence," *Journal of Endourology*, vol. 30, no. 12, pp. 1321-1325, Dec. 2016.

[9] C. C. Church, "Prediction of rectified diffusion during nonlinear bubble pulsations at biomedical frequencies." *The Journal of the Acoustical Society of America*, vol. 83, no. 6, pp. 2210-2217, Jun. 1988.

[10] V. Bjerknes, *Fields of Force*, 1906.

[11] M. Kornfeld and L. Suvorov, "On the destructive action of cavitation," *Journal of Applied Physics*, vol. 15, no.6, pp. 495-506, 1944.

[12] F. G. Blake, "Bjerknes Forces in Stationary Sound Fields," *The Journal of the Acoustical Society of America*, vol. 21, no. 5, pp. 551-551, Jun. 1949.

[13] E. A. Neppiras, "Subharmonic and Other Low-Frequency Emission from Bubbles in Sound-Irradiated Liquids," *The Journal of the Acoustical Society of America*, vol. 46, no. 3B, pp. 587-601, Sep. 1969.

[14] L. A. Crum and A. I. Eller, "Motion of Bubbles in a Stationary Sound Field," *The Journal of the Acoustical Society of America*, vol. 48, no. 1B, pp. 181-189, Jul. 1970.

[15] L. A. Crum, "Bjerknes forces on bubbles in a stationary sound field," *The Journal of the Acoustical Society of America*, vol. 57, no 6, pp. 1363-1370, Jun. 1975.

[16] T. G. Leighton, *The Acoustic Bubble*. San Diego, CA: Academic Press Inc, 1997.

CHAPTER 4

Enhanced High Rate Shockwave Lithotripsy Stone Comminution in an *in vivo* Porcine Model Using Acoustic Bubble Coalescence

A majority component of this chapter has been published in the the *Journal of Endourology*. © 2018 J Endourol, with permission, from [1].

4.1 Introduction

A strong rate dependence in the efficacy of stone comminution for shockwave lithotripsy (SWL) has been shown by many *in vitro* [2-5], *in vivo* [6], and human studies [7-9]. It is hypothesized that a major component of this effect is due to the presence of cavitation bubbles persisting from shockwave to shockwave which shield or attenuate the amplitude of subsequent lithotripter shockwaves [10-12]. At low firing rates, there is sufficient time for a majority of the bubbles to passively dissolve, while at high firing rates the per shockwave efficacy is significantly reduced due to persisting bubbles.

The fragmentation of renal calculi by SWL is understood to be produced through mechanical stresses caused by a combination of incident shockwaves and the collapse of cavitation bubbles on the surface of the urinary stones [13-14]. Although mechanical stress generated by the incident shockwave causes the initial disintegration of the stone, cavitation is a necessary component for efficient fragmentation, and particularly for producing fine passable fragments

(<2mm) [14]. The effect of cavitation on the fragmentation process is thought to be primarily through erosion on the stone surface, but it may also help in the formation of crack lines through which damage is spread from the surface into the bulk of the stone. This damage on the surface of the stone makes the structure weaker and as a result more susceptible to subsequent shockwaves [14-16].

The growth and collapse lifespan of a cavitation bubble cloud produced by a lithotripter shockwave has been shown to be on the order of 1ms – much shorter than the interval between shockwaves at typical lithotripter firing rates of 0.5–2Hz. However, the residual micron sized bubbles following a cavitation cloud collapse have a longer lifespan on the order of 1 second and thus a large fraction would be expected to persist between subsequent shockwaves particularly at higher firing rates [3, 17-19]. On subsequent pulses, these nuclei absorb energy from the negative pressure phase of the lithotripter waveform reducing cavitation on the surface of the stone, which in turn reduces the efficacy of stone comminution [3].

In our previous studies, low amplitude acoustic bursts were used with *in vitro* models to actively remove residual cavitation bubbles through forced coalescence [2, 20-21]. Significant improvement was demonstrated in the comminution efficacy of SWL at higher rates (120 and 60 SW/min). In this study, the feasibility of SWL stone comminution at 120 SW/min with acoustic bubble coalescence (ABC) was evaluated on a porcine model and compared to standard SWL at the same rate.

4.2 Methods

After IACUC approval, a total of twelve 45-50kg female pigs were used in this study. Throughout the procedure, the pigs were anesthetized with 2-2.5% inhaled isoflurane, while their vital signs including body temperature, heart rate, oxygen saturation, and respiration were monitored by a Vet/Ox Plus 4800 Vital Signs Monitor (Heska, Loveland, CO). Each pig was placed prone on a surgical table. Flexible cystoscopy (Olympus CYF-3) was performed to visualize and cannulate the right ureter with an access wire. An 8 Fr silicone urinary catheter was passed partially up the ureter and the balloon inflated with 5-10cc saline to produce ureteral occlusion. One hour later, the animal was repositioned semi-prone (left flank up) and transcutaneous ultrasound (Ultrasonics, Richmond, Canada) confirmed hydronephrosis. With ultrasound guidance, percutaneous access was obtained above the 12^{th} rib to enter the collecting system through an upper-pole renal calyx. An angled glide wire was advanced into the collecting system and manipulated down the ureter, then replaced with an Amplatz stiff wire, over which sequentially dilation was performed up to 26 Fr and a sheath placed. Through this sheath, endoscopy of the collecting system was performed using the flexible ureteroscope. Once the designated lower pole calyx (occasionally a mid-renal calyx was used) was identified, the cystoscope was removed and reloaded with a zero-tip 1.9 Fr wire basket grasping a 6 mm diameter cylindrical stone. The cystoscope and basket were passed through the sheath into the collecting system and navigated into the previously identified lower pole calyx where the stone was released. Any air introduced during implantation was aspirated with the flexible cystoscope while flushing degassed water through the ureteral access catheter.

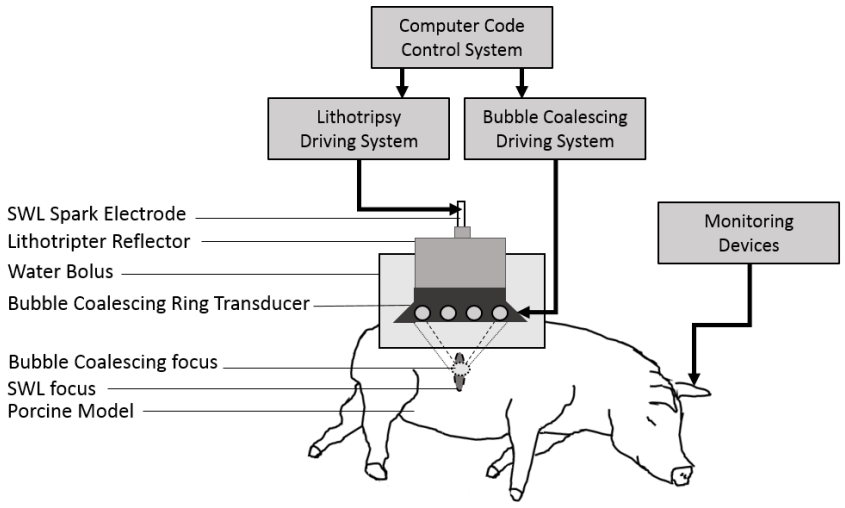

Figure 4.1. Experiment setup: the model stone implanted in right kidney of the porcine model is targeted and treated by a laboratory electro-hydraulic lithotripter patterned after Dornier HM3 along with a separate annular transducer array generating the acoustic bubble coalescence pulses. The water bolus is filled with degassed water with gas concentration below 10% saturation and contains a 15 cm cut out for direct coupling of sound from the water to the skin. The animal's vital signs including oxygen saturation, heart rate, respiration and core body temperature were monitored throughout the experiment.

The model stones were cylindrical in shape 6 mm diameter, about 7mm height, with an average hydrated mass of 281.7mg (std=33.8mg). The stones were made by a mixture of BegoStone plaster (BEGO, Smithfield, RI), albumin (Carolina Biological Supply Co., Burlington, NC), and water using the method described by Simmons, et al. [22] formed in an acetal mold. The mass ratio of mixture was 73% BegoStone, 2.5% albumin, and 24.5% water. Model stones were formulated to imitate the structural strength of cysteine composition stones. The stones were stored in degassed water under vacuum for at least 24 hours before use to minimize any gas incorporated during formation.

After the stone was implanted into the subject and air evacuated from the collecting system, the access sheath and wire were removed, and the incision was sealed with superglue. The occlusion catheter in the ureter was deflated to allow urinary drainage and the animal was left to rest for about 30 minutes before the treatment. The incision was not part of the subsequent acoustic window for the lithotripsy treatment. The skin over the targeted area was shaved and treated with depilatory cream in order to improve ultrasound coupling. The location of the target was marked on the skin and a water bolus consisting of a large plastic bag was placed on the pig over the targeted area. To ensure optimal sound coupling, the bolus was glued directly to the skin around a 15cm cut out hole so that there was no membrane between fluid and skin (equivalent to an immersion bath). The bolus was filled with degassed water at room temperature of about 21°C and the dissolved gas concentration maintained below 10% saturation by continuous recirculation and degassing. A stereotactic positioning setup was used where a curvilinear imaging array probe (C4 on P6 scanner, GE Medical Systems, Waukesha, WI) was positioned with a 3-axis motorized system to target the implanted stone. The imaging probe assembly was then removed and replaced with the lithotripter head assembly where the focus was aligned to the ultrasound image.

A laboratory electro-hydraulic lithotripter (EHL) was used for all the treatments modeled on the design of Coleman, et al. [23] to simulate the acoustic field generated by a Dornier HM3 (Dornier Medical Systems, Kennesaw, GA). One modification was that the system used a straight downward firing configuration to facilitate rapid electrode changes [23-24]. Additionally, water was drawn continuously through the head via small ports at the highest point on the reflector and recirculated into the water bolus to remove any cavitation bubbles formed by the electrode. The lithotripter was operated at a firing rate of 120 SW/min and charging voltage of 20kV generating shockwaves with a peak positive pressure (P+) of 34MPa, and a peak negative (P-) of 8MPa. All

EHL electrodes (HealthTronics, Austin, TX) used in the experiments were preconditioned with 500 break-in shocks at 20kV and 120 SW/min the day before usage for maximum acoustic output. In each treatment two electrodes were used to generate a total of 2500 shocks; 1250 uninterrupted shocks on each of the electrodes.

Acoustic bubble coalescence sequences were applied during five of the ten experiments interleaved between each shockwave. The ABC transducer was constructed in-house, consisting of an annular array of eight 500kHz transducers each 50mm diameter surrounding the lithotripter reflector. ABC sequences consisted of alternating tone bursts of 2 cycles from each transducer at a PRF of 100kHz and amplitude of 1MPa for a total duration of 16ms. The bubble coalescence pulses were applied after 10ms delay in order to let the initial bubble cloud to grow and collapse first. (Figure 4.2) This pulse sequence was designed to provide a relatively uniform unfocused sound field from a ring transducer geometry similar to the one in our previous *in vitro* study [2].

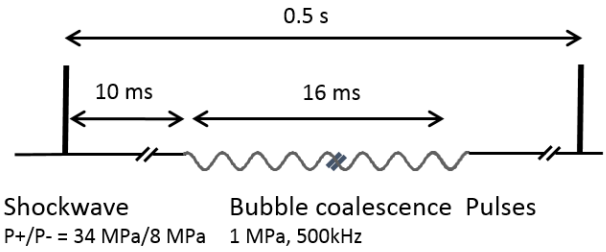

Figure 4.2. Acoustic pulse sequence for shockwave lithotripsy and bubble coalescing. The SWL rate was 120 SW/min interleaved with bubble coalescing pulses applied for duration of 16 ms.

Post-treatment position of the targeted kidney stone was confirmed by removing the lithotripter head and reattaching the GE imaging probe assembly. The subject was then euthanized and the kidney harvested including a portion of distal ureter. The kidney was carefully dissected and all stone fragments remaining in the collecting system were recovered by flushing with water

and further dissection. Collected fragments were filtered through 4, 2, 1, and ½ mm hole size perforated brass plates. The fragments of each bin size were dried for 48 hours and then weighed. Three control stones not implanted were allowed to dry as well to serve as a correction factor for the amount of water lost during dehydration. The mass of the fragments smaller than 0.5mm was calculated by subtracting the sum of all the collected fragments from the initial mass of the stone.

4.3 Results

During one of the experiments, the water bolus leaked requiring the SWL treatment to be stopped. In a second case, the percutaneous implantation was unsuccessful. After excluding these two subjects a total of ten remained for the final data set reported here, five using normal SWL and five using SWL with ABC. It should be noted that the position of the stones during the treatment was not monitored, and some movement due to respiratory excursion is expected, however post treatment position of the targeted stone in the kidney was confirmed by ultrasound imaging to have not moved significantly for nine treated subjects. In a tenth case which used SWL with ABC, a majority of fragments were observed to have dropped into the renal pelvis. On dissection, this stone was found to be nearly completely fragmented. The small variation in the initial mass of the implanted stones was found to have no statistically significant effect on the efficacy of stone comminution (T-Test, p-value=0.8).

Figure 4.3 shows typical results for normal SWL treatments (a, c) and when combined with ABC (b, d). Qualitatively, the fragmentation was more complete for nearly every treatment using ABC.

Figure 4.3. Typical results from normal SWL treatment (a, c) and SWL with ABC (b, d). Recovered fragments from treatments with normal SWL (c) were visibly larger than treatments with SWL and ABC (d).

Resulting fragment distributions from all ten experiments are summarized in Figure 4.4. The most striking finding was the change in distribution of stone fragments larger than 4mm when using ABC. Whereas all normal SWL treatments had at least one remaining fragment larger than 4mm averaging 65% of the initial stone mass, only one of five treatments using SWL with ABC had any remnant fragment larger than 4mm. Looking at a smaller size threshold, the normal SWL treatment left behind on average 75% of the stone mass in fragments larger than 2mm, while the SWL treatment combined with ABC left on average only 25% of the mass larger than 2mm (T-Test, p-value=0.003).

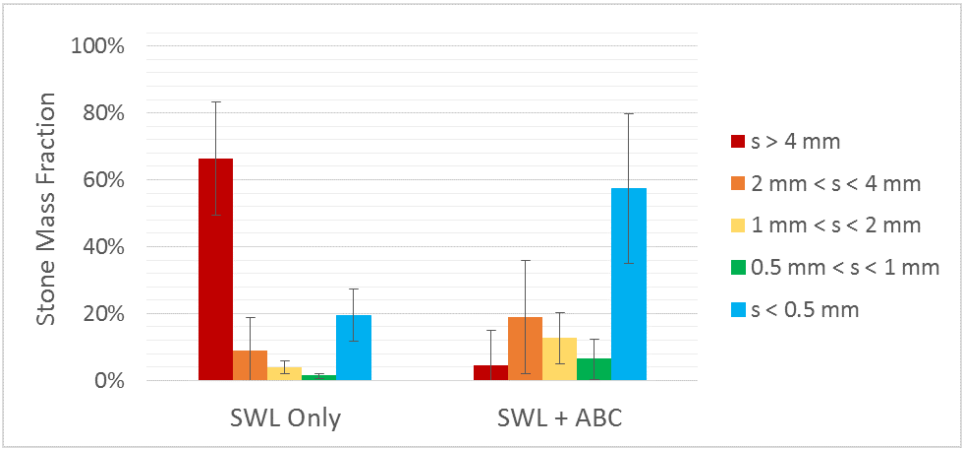

Figure 4.4. Post-treatment stone fragment distribution normalized to initial stone mass for normal SWL and SWL combined with ABC. The distribution is significantly shifted toward smaller fragments for SWL with ABC.

4.4 Discussion

In this study, low pressure acoustic pulses were utilized to stimulate residual cavitation bubbles to coalesce and clear the path for the subsequent shockwaves. This occurs through the acoustic field inducing size oscillations in the bubbles and gives rise to two major forces. The primary Bjerknes force describes the tendency of bubbles smaller (or larger) than resonant size to move up (or down) a pressure gradient and congregate at pressure antinodes (or nodes). The secondary Bjerknes force describes an attractive force between bubbles oscillating in phase depending on their size and the acoustic field frequency. This secondary Bjerknes force is hypothesized to be the dominant mechanism bringing the remnant bubbles from SWL cavitation together to coalesce and clear the propagation path [2,21]. In general, the degree of coalescence required for effective clearance of the propagation path to mitigate effects of bubble shielding is not known. This suggests the potential for further optimization of acoustic parameters for ABC for further improvement in fragmentation efficiency.

The shockwave rate used for this study was 120 SW/min which is a common rate used in clinical SWL. This high rate was chosen to reduce experiment time and possibly enhance the difference between study groups. In vitro work [2] has shown that a significant though somewhat reduced difference also occurs at 60 SW/min. The goal here was to understand the barriers to higher rate SWL and consider methods to alleviate them. Although, this study does not show that pre-focal cavitation and the shielding effect is the only barrier to higher rate SWL, reducing the

population of pre-focal cavitation by means of forced coalescence appears to improve the efficiency of higher rate SWL significantly.

One of the major differences between distribution of stone fragments in subjects with and without ABC was the presence of at least one larger than 4mm stone fragments in subjects without ABC. In previous studies, we have shown that shielding effect reduces the cavitation on the surface of the stone [3], which is a significant factor in producing fine fragments by means of surface erosion and weakening the structure of stone that makes the further fragmentation to smaller pieces more probable during subsequent shockwaves [14-16]. As a result, by removing pre-focal cavitation from the propagation path and reducing the shielding effect, it was expected to see lower amount of large fragments when ABC was applied.

An additional problem with higher rate SWL is increased risk for collateral tissue damage. Cavitation within the kidney parenchyma is thought to be the source of this damage. It is possible that ABC with SWL could help reduce this damage by preventing a proliferation of cavitation bubbles expanding into the kidney tissue. However, it is also possible that cavitation damage could be exacerbated by additional forced oscillation of bubbles outside the collecting system. A separate study of tissue damage in SWL with and without ABC will be required to assess the extent of tissue damage without the trauma associated with stone implantation.

Related work has shown improvement in stone comminution by interleaving SWL with auxiliary shockwaves produced by a piezoelectric annular array shockwave generator [25, 26]. The auxiliary shockwaves in the mentioned study are extremely short duration and on the order of 8MPa pressure timed to arrive right after the initial collapse of bubble cloud produced by each lithotripter shockwave, generating a secondary intensified collapse near the surface of the stone. It

is important to note the significant differences in the amplitude and duration of the acoustic fields used compared to the present study. Interestingly, the acoustic sound sources have a remarkably similar geometry.

Optimal bubble coalescence requires a non-focused acoustic field that exposes as much of the propagation path as possible where cavitation may occur. Ultrasound guided lithotripters with central access port for imaging are ideally suited for ABC because the coalescence generator could be a simple small unfocused transducer. Systems lacking this port (generally x-ray guided) require a slightly more complex annular array transducer to generate the coalescence field such as the device demonstrated here, but still possible without modification of the shockwave source.

4.5 Conclusions

This study demonstrates the feasibility of utilizing acoustic bubble coalescence in enhancing higher rate shockwave lithotripsy. The results suggest significant improvement in the stone fragmentation process when using bubble coalescence with shockwaves which implies that ABC can mitigate the shielding effect of residual cavitation bubbles resulting in a more efficient SWL treatment.

4.6 References

[1] H. Alavi Tamaddoni, A. P. Duryea, E. Vlaisavljevich, Z. Xu, T. L. Hall, "Acoustic Methods for Increasing the Cavitation Initiation Pressure Threshold," *IEEE transactions on ultrasonics, ferroelectrics, and frequency control*, vol. 65, no. 11, pp. 2012-2019. Nov. 2018.

[2] A. P. Duryea, W. W. Roberts, C. A. Cain, H. A. Tamaddoni and T. L. Hall, “Acoustic bubble removal to enhance SWL efficacy at high shock rate: an in vitro study,” *Journal of Endourology*, vol. 28, no. 1, pp. 90-95, Jan. 2014.

[3] Y. A. Pishchalnikov, J. A. McAteer, Jr. J. C. Williams, I. V. Pishchalnikova and R. J. Vonderhaar, “Why stones break better at slow shockwave rates than at fast rates: in vitro study with a research electrohydraulic lithotripter,” *Journal of Endourology*, vol. 20, no. 8, pp. 537-41, Aug. 2006

[4] M. J. Weir, N. Tariq, and R. J. Honey, "Shockwave frequency affects fragmentation in a kidney stone model," *J Endourol*, vol. 14, pp. 547-50, Sep 2000.

[5] A. Greenstein and H. Matzkin, "Does the rate of extracorporeal shock wave delivery affect stone fragmentation?," *Urology*, vol. 54, pp. 430-432, 1999.

[6] R. F. Paterson, D. A. Lifshitz, J. E. Lingeman, A. P. Evan, B. A. Connors, N. S. Fineberg, *et al.*, "Stone fragmentation during shock wave lithotripsy is improved by slowing the shock wave rate: studies with a new animal model," *J Urol*, vol. 168, pp. 2211-5, Nov 2002.

[7] K. T. Pace, D. Ghiculete, and M. Harju, "Shock wave lithotripsy at 60 or 120 shocks per minute: A randomized, double-blind trial," *The Journal of Urology*, vol. 174, pp. 595-599, 2005.

[8] E. Yilmaz, E. Batislam, M. Basar, D. Tuglu, C. Mert, and H. Basar, "Optimal frequency in extracorporeal shock wave lithotripsy: prospective randomized study," *Urology*, vol. 66, pp. 1160-4, Dec 2005.

[9] K. Madbouly, A. M. El-Tiraifi, M. Seida, S. R. El-Faqih, R. Atassi, and R. F. Talic, "Slow versus fast shock wave lithotripsy rate for urolithiasis: a prospective randomized study," *J Urol*, vol. 173, pp. 127-30, Jan 2005.

[10] M. Delius, F. Ueberle, W. Eisenmenger, “Extracorporeal shock waves act by shock wave-gas bubble interaction,” *Ultrasound in medicine & biology*, vol. 24, no. 7, pp. 1055-9. Sep. 1998.

[11] A. Philipp, M. Delius, C. Scheffczyk, A. Vogel, W. Lauterborn, “Interaction of lithotripter-generated shock waves with air bubbles,” *The Journal of the Acoustical Society of America*, vol. 93, no. 5, pp. 2496-509, May. 1993.

[12] Y. A. Pishchalnikov, J. A. McAteer, M. R. Bailey, I. V. Pishchalnikova, J. C. Williams, and A. P. Evan, "Acoustic shielding by cavitation bubbles in shock wave lithotripsy (SWL)," in *17th International Symposium on Nonlinear Acoustics* 2005, pp. 319-322.

[13] M. Lokhandwalla, B. Sturtevant, “Fracture mechanics model of stone comminution in ESWL and implications for tissue damage,” *Physics in medicine and biology*, vol. 45, no. 7, pp. 1923, Jul. 2000.

[14] S. Zhu, F. H. Cocks, G. M. Preminger, P. Zhong, “The role of stress waves and cavitation in stone comminution in shock wave lithotripsy,” *Ultrasound in medicine & biology*, vol. 28, no. 5, pp. 661-71, May. 2002.

[15] P. Zhong, C. J. Chuong, G. M. Preminger, “Characterization of fracture toughness of renal calculi using a microindentation technique,” *Journal of materials science letters,* vol. 12, no. 1, pp. 1460-2, Jan. 1993.

[16] A. P. Duryea, W. W. Roberts, C. A. Cain, and T. L. Hall, "Controlled cavitation to augment SWL stone comminution: mechanistic insights in vitro," *IEEE Trans Ultrason Ferroelectr Freq Control*, vol. 60, pp. 301-9, Feb 2013.

[17] H. G. Flynn, “Generation of transient cavities in liquids by microsecond pulses of ultrasound,” *Journal of the Acoustical Society of America*, vol. 72, no. 6, pp. 1926-32, Dec. 1982.

[18] J. B. Fowlkes and L. A. Crum, “Cavitation threshold measurements for microsecond length pulses of ultrasound,” *Journal of the Acoustical Society of America,* vol. 83, no. 6, pp. 2190–2201, Jun. 1988.

[19] Y. A. Pishchalnikov, J. A. McAteer, I. V. Pishchalnikova, J. C. Williams, M. R. Bailey, and O. A. Sapozhnikov, "Bubble proliferation in shock wave lithotripsy occurs during inertial collapse," in *18th International Symposium on Nonlinear Acoustics*, 2008, pp. 460-463.

[20] Duryea A, Cain C, Roberts W, Tamaddoni H, Hall T. Active removal of residual bubble nuclei following a cavitation event. InUltrasonics Symposium (IUS), 2013 IEEE International 2013 Jul 21 (pp. 1813-1816). IEEE.

[21] A. P. Duryea, C. A. Cain, H. A. Tamaddoni, W. W. Roberts and T. L. Hall, "Removal of residual nuclei following a cavitation event using low-amplitude ultrasound," *IEEE Transactions on Ultrasonics, Ferroelectrics, and Frequency Control*, vol. 61, no. 10, pp. 1619-1626, Oct. 2014.

[22] W. N. Simmons, F. H. Cocks, P. Zhong, and G. Preminger, "A composite kidney stone phantom with mechanical properties controllable over the range of human kidney stones," *J Mech Behav Biomed Mater,* vol. 3, pp. 130-3, Jan 2010.

[23] A. J. Coleman, J. E. Saunders, and M. J. Choi, "An experimental shock wave generator for lithotripsy studies," *Phys Med Biol,* vol. 34, pp. 1733-42, Nov 1989.

[24] A. P. Duryea, W. W. Roberts, C. A. Cain, and T. L. Hall, "Optically triggered solid state driver for shock wave therapy," in *Int. Society for Therapeutic Ultrasound Symp.*, 2011, pp. 76-80.

[25] X. Xi and P. Zhong, "Improvement of stone fragmentation during shock-wave lithotripsy using a combined EH/PEAA shock-wave generator—in vitro experiments," *Ultrasound in Medicine & Biology*, vol. 26, pp. 457-467, 2000

[26] Y. Zhou, F. H. Cocks, G. M. Preminger, P. Zhong. “Innovations in shock wave lithotripsy technology: updates in experimental studies,” *The Journal of Urology*, vol. 172, no. 5, pp.1892-8, Nov. 2004.

CHAPTER 5

Enhanced Shockwave Lithotripsy with Acoustic Bubble Coalescence and Dispersion

5.1 Introduction

Shockwave lithotripsy (SWL) is a non-invasive method for the treatment of urinary stones. SWL is utilized to replace surgical removal of urinary stones. In SWL, stones are fragmented by applying acoustic energy from outside of the body. One of the main issues with the current clinical use of SWL is the incomplete fragmentation of stones. These incomplete fragments can cause extreme pain when they are discarded. They can also act as nidus for additional stone formation [1-3]. In SWL treatments, mechanical stresses of incident shockwave and the collapse of cavitation bubble cloud on the surface of the stone are the main causes of stone fragmentation [4-5]. Generally, the mechanical stress produced by the incident shockwave is believed to be the primary factor in stone fragmentation, and particularly for the initial disintegration of the stones. However, cavitation is also a necessary component for efficient fragmentation and particularly for producing fine passable debris (fragments smaller than 2 mm) [5-7]. Cavitation bubbles are formed by the tensile portion of the lithotripsy waveform following the peak positive, and typically have a lifespan of about 1 ms, which is much shorter than the time interval between consequent shockwaves in lithotripsy with typical firing rates rage of 0.5-2 Hz. However, the residual micron sized bubbles following a cavitation cloud collapse have a longer lifespan on the order of 1 second, and thus are expected to persist between subsequent shockwaves particularly at higher firing rates

[8-11]. At low firing rates, there is sufficient time for a majority of the bubbles to passively dissolve, while at high firing rates, efficacy is significantly reduced due to persisting bubbles. On subsequent shocks, these nuclei along the propagation path may attenuate subsequent shockwave, and particularly absorb energy from the negative pressure phase of the lithotripter waveform, reducing cavitation on the surface of the stone, which in turn reduces the efficacy of treatment in producing fine fragments [8].

The efficacy of stone comminution for shockwave lithotripsy (SWL) is strongly rate dependent [8,12-18]. Presence of cavitation bubbles persisting from shockwave to shockwave, which may shield or attenuate the amplitude of subsequent lithotripsy shockwaves, is hypothesized to be the cause of reduced per shock efficacy of SWL at higher rates [19-20]. At low firing rates, there is sufficient time for a majority of the residual nuclei bubbles to passively dissolve away; however, at higher firing rates, efficacy is significantly reduced due to persisting cavitation bubbles. In clinical use generally 120 SW/min is used even with lower per shock efficacy, as the treatment still would be more time/cost efficient.

The solution that we propose in this study to overcome the adverse effects of persisting bubbles is Acoustic Bubble Coalescence and Dispersion (ABCD) by forcing cavitation bubbles to coalesce or disperse away from the propagation path before the arrival of next therapy pulse. In our previous *in vivo* and *in vitro* studies, low amplitude acoustic bursts were used to actively remove residual cavitation bubbles through forced coalescence [12,21-25]. The secondary radiation force that bubble coalescence relies upon is significantly stronger when bubbles are close together – i.e. a high cloud density. This occurs immediately after the cavitation cloud collapse- about a millisecond after the shockwave- after which bubbles tend to spread apart. Thus, previous

experiments have applied the ABCD field after a relatively short time of a few milliseconds post shockwave. An alternate strategy to investigate is to wait until immediately before the next shockwave in order to force the bubbles to coalesce and disperse any persisting bubbles that have not fully dissolved. In previous studies, we have shown that applying properly tuned low pressure pulse sequences, Acoustic Bubble Coalescing (ABC) pulses, can improve the efficacy of histotripsy and lithotripsy treatments by actively stimulating bubble coalescence and removing residual bubble nuclei from the propagation path [12,21-25]. This process may also reduce collateral tissue damage. The specific objectives of this study were to optimize the parameters of bubble coalescing pulses, particularly for the shockwave lithotripsy in comminution of kidney stones, and to conduct a feasibility investigation of acoustic bubble dispersion by forcing the residual bubble nuclei to disperse from the propagation path away or to the targeted area before arrival of the next therapy pulse. The goal of ABCD is to compliment the current SWL treatment to avoid incomplete fragmentation, and improve the efficacy of treatment in producing fine passable debris.

5.2 Methods

5.2.1 Acoustic Pulse Sequence

A clinical lithotripter (Dornier Compact Delta) was used for all the treatments. The lithotripter was operated at a firing rate of 30 SW/min and 120 SW/min at power setting 3, which produced a peak positive pressure of 20.5 MPa, and a peak negative of 5.2 MPa, calibrated by an in-house built fiber-optic probe hydrophone [26]. The waveform for lithotripter is shown in figure 5.1.

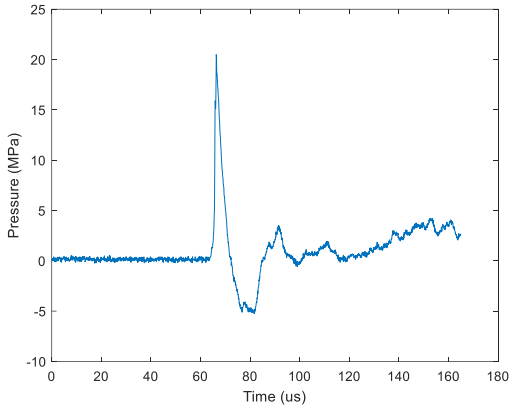

Figure 5.1. Dornier Lithotripter waveform

Complete treatments were defined as 2500 shocks delivered to each sample. In order to have a better understanding of the process of fragmentation under different pulse sequences, a second set of experiments were performed stopping after only 500 shocks.

Acoustic bubble coalescence and dispersion sequences were applied following each shockwave. The ABCD transducer was constructed in-house, consisting of an annular array of eight confocal 500 kHz transducers, each 50 mm diameter surrounding the lithotripter reflector. ABCD sequences consisted of alternating tone bursts of 2 cycles from each transducer in sequence at a PRF of 100 kHz and amplitude of 1 MPa or 0.5 MPa for a total duration of 8 ms.

The experiments were performed with six different pulse schemes, as shown in figure 5.2. Scheme 1, the control case, consisted of SWL at a rate of 120 shocks/min without any ABCD pulse sequence. The next four schemes all employed ABCD where the SWL pulses at a rate of 120 shocks/min were interleaved with low amplitude acoustic pulses at different time delays and different pressure levels. For ABCD 1 (post), SWL at 120 shocks/min was interleaved with low amplitude acoustic pulses applied beginning 3 ms after each shock in order to allow only enough time for the initial bubble cloud that was generated by the lithotripter shockwave to grow and

collapse. For ABCD 2 (post + pre), shockwaves were interleaved with two sets of low amplitude acoustic pulses applied between each shock; one set was applied 3 ms following the shock, and the second set was applied right before the next shock beginning 450 ms after the first shock. For ABCD 3 (pre), low amplitude acoustic pulses were applied beginning 450 ms after each shockwave ending right before the next shockwave arrived. For ABCD 4 (pre, extra low amp), similar to ABCD 3, the high rate shocks were interleaved with low amplitude acoustic pulses just before the next shockwave arrived to maximize dispersion, but for this case the pressure amplitude of ABCD pulses were reduced to 0.5 MPa. The result of these five cases were compared to a final scheme consisting of low shock rate pulses only applied at 30 shocks/min (no ABCD). Each experiment was repeated for 10 trials for each of these six schemes.

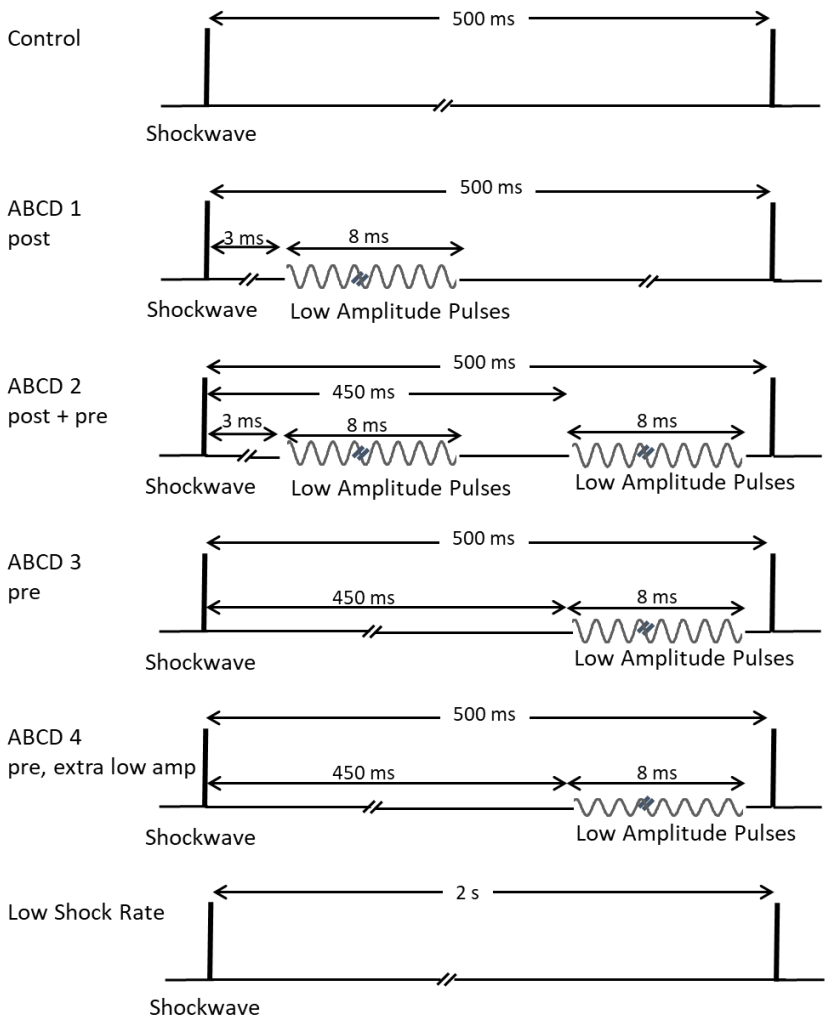

Figure 5.2. Acoustic pulse sequences for shockwave lithotripsy and bubble coalescence and dispersion pulses.

5.2.2 Experiment Setup

Model stones were placed inside a finger cot filled with deionized water degassed to an oxygen level of about 80% saturation, which is close to that of the urine. The finger cot assembly, enclosed with a sealing clip at the top, was positioned inside a water tank at the focus of a clinical Dornier lithotripter and ABCD ring transducer. An acoustic window was embedded in the bottom of the tank for the lithotripter head. The water tank was filled with deionized water at room

temperature of about 21°C and dissolved gas concentration in the water was maintained below 30% saturation by continuous recirculation and degassing. Figure 5.3 shows a schematic of experiment setup.

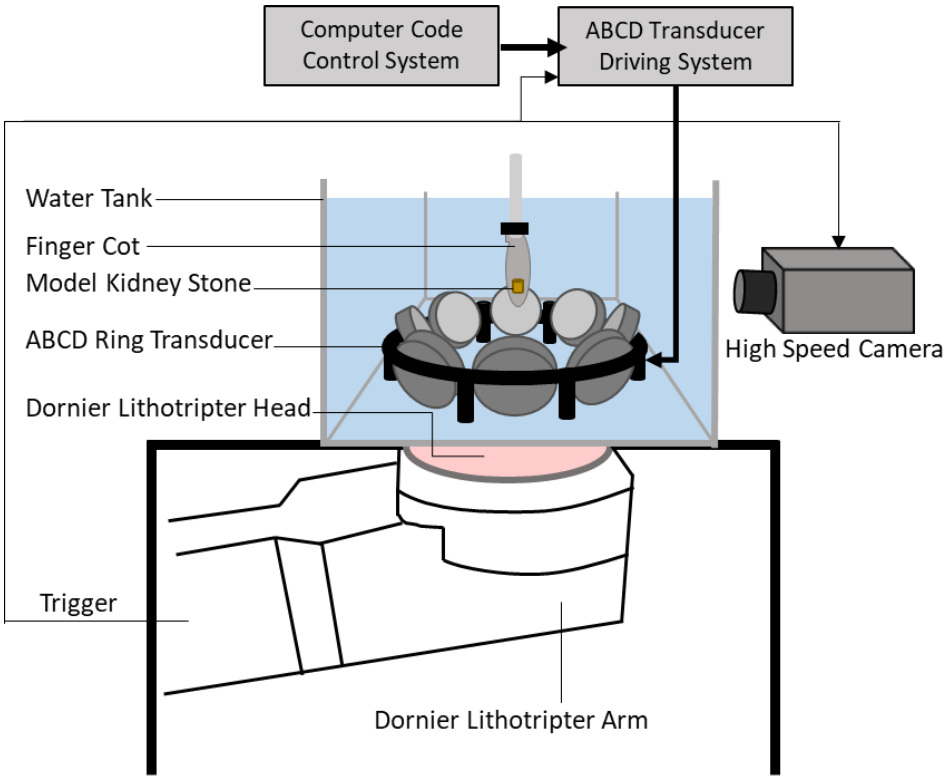

Figure 5.3. Experiment setup: the model stones were placed inside a finger cot filled with deionized degassed water and was positioned inside the water tank at the focus of a clinical Dornier lithotripter and ABCD transducer.

Model kidney stones were made from a mixture of BegoStone plaster (BEGO, Smithfield, RI), and water formed in an acetal mold. They were cylindrical in shape with 10 mm diameter and 10 mm height with an average hydrated mass of 1557 mg and with a standard deviation of 28.9 mg. The mass ratio of mixture was 75% BegoStone, 25% water. Stones were hydrated for 24 hours before the experiments. These model stones were formulated to imitate the structural strength of cysteine composition stones [27]. Model stones were used because they have very consistent

mechanical properties reducing variability in results and ultimately the number of experimental repetitions required when compared to real stones.

Optical images from a high speed camera (Photron, FASTCAM SA1.1, Lens: Nikon ED, AF Micro NIKKOR 200mm 1:4 D) were recorded and processed to analyze cavitation behavior following the collapse of initial bubble cloud and forced bubble coalesce and dispersion.

5.2.3 Stone Measurements

Upon completion of each experiment, stone fragments in the finger cot were recovered and filtered through 4, 2, and 1 mm hole size perforated brass plates. The fragments of each bin size were dried for 48 hours and then weighed. Seven untreated control stones were allowed to dry as well to serve as a correction factor for the amount of water lost during dehydration. The mass of the fragments smaller than 1 mm was then calculated by subtracting the sum of all the collected fragments from the initial mass of the stone estimated with the hydration correction factor.

5.3 Results

The resulting average stone fragment distributions for all six schemes is summarized in figure 5.4. The high shock rate control case had the lowest efficacy in stone comminution, while the low shock rate case had the highest. All ABCD pulse schemes were found to improve stone comminution efficacy at a shock rate of 120 shock/min achieving results closer to the 30 shocks/min low rate case. ABCD 4 (applying pulses immediately before each shock) was found to be the most effective, particularly for producing fine passable fragments (< 2 mm). The average percentage of untreated stone fragments larger than 2 mm was 15.81% for the control case and

only 0.19% for ABCD 4 (p-value = 8.53e-5) – very close to the low shock rate results of 0.16% fragments larger than 2mm (p-value = 0.87).

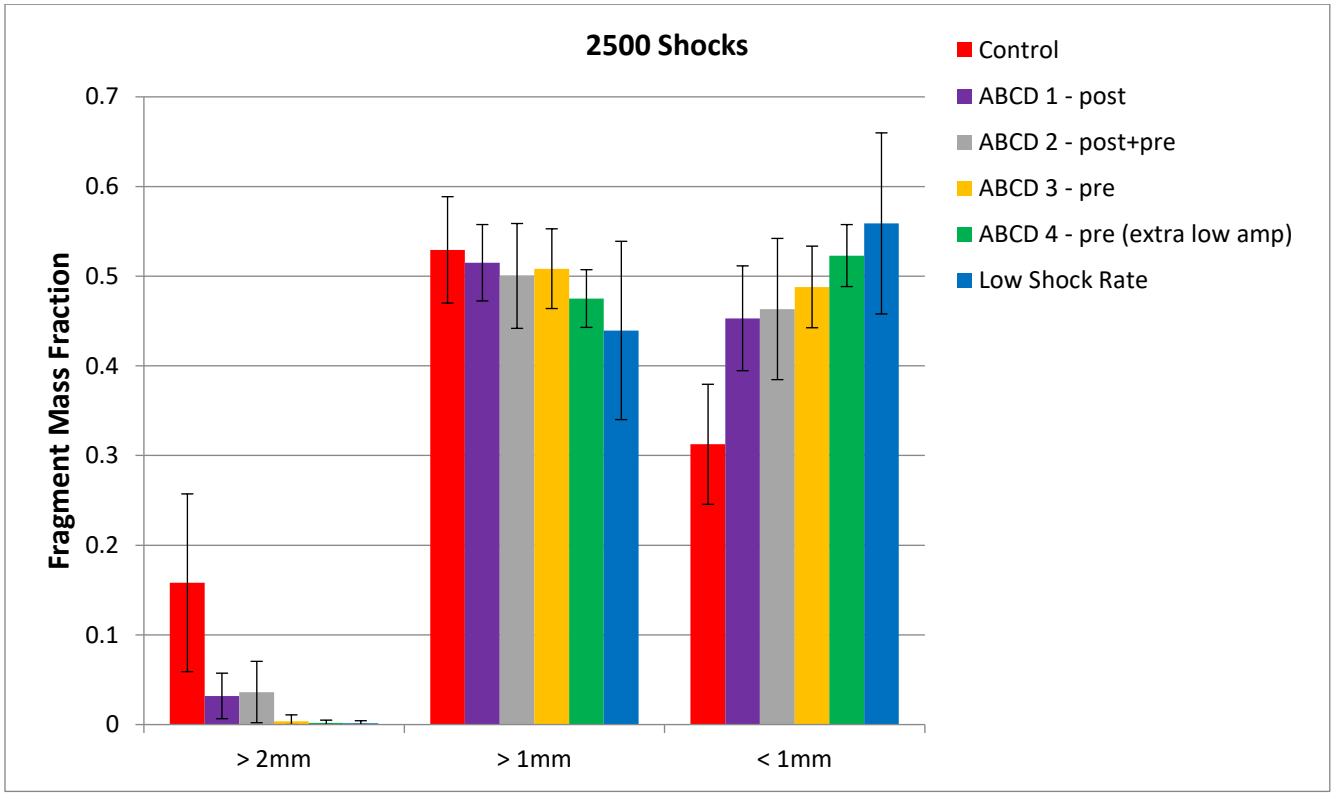

Figure 5.4. Post-treatment stone fragment distribution normalized to initial stone mass and averaged over 10 trials for normal SWL and SWL combined with different ABCD pulse sequences for complete treatments of 2500 shocks.

The second series of experiments was performed with only 500 shocks instead of 2500 shocks, in order to observe the process of stone fragmentation in the early stages of treatment for the different pulse sequences. Figure 5.5 shows the average fragments mass fraction of four pulse schemes. In complete treatments, applying low amplitude acoustic pulses right before the arrival of the next shocks to disperse residual bubbles were shown to result in more efficacious stone comminution than applying these pulses right after each shock to force the residual bubbles to coalesce. However, the early breakage of stone after 500 shocks demonstrate no significant

different between ABCD 1 (post) and ABCD 4 (pre, extra low amp) cases. Both ABCD 1 and ABCD 4 cases achieved similar reductions in stone fragments larger than 4 mm.

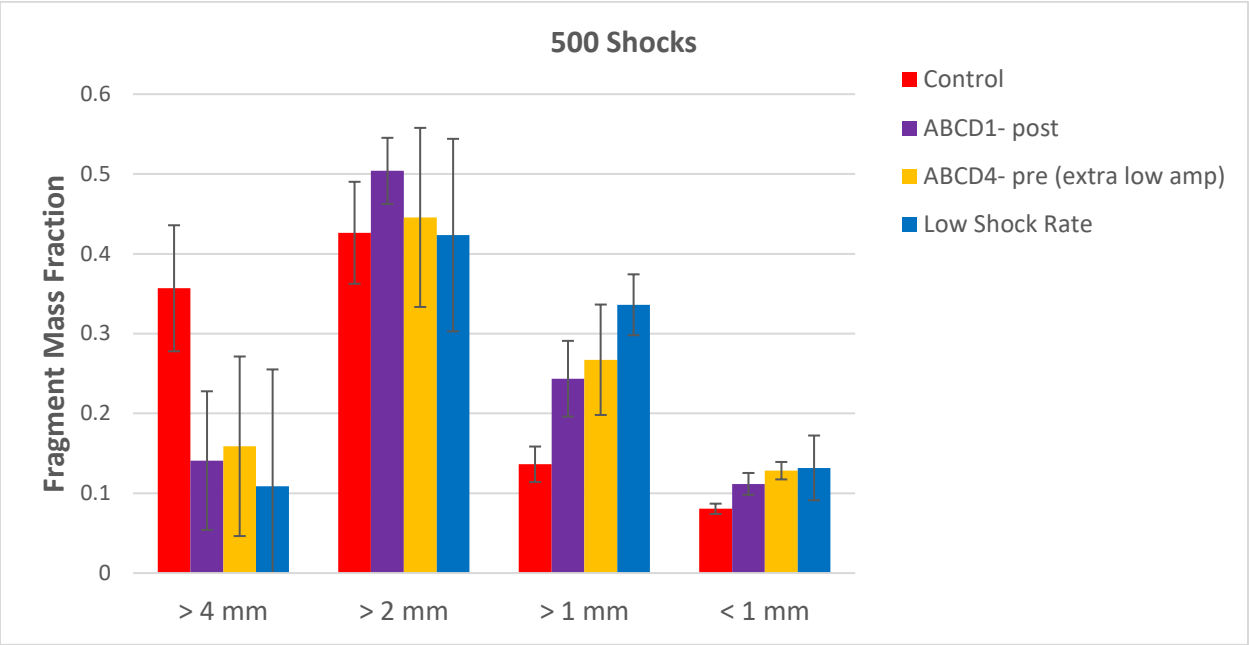

Figure 5.5. Post-treatment stone fragment distribution normalized to initial stone mass and averaged over 7 trials for normal SWL and SWL combined with different ABCD pulse sequences for 500 shocks.

Figure 5.6 shows typical results of remnant debris for SWL treatments only (6a) and when combined with ABCD 1 (6b), and ABCD 4(6c), and low shock rate SWL(6d). Qualitatively, the fragmentation was more complete for every treatment in any of the ABCD cases; however, ABCD 4 seems to be more successful in producing fine debris.

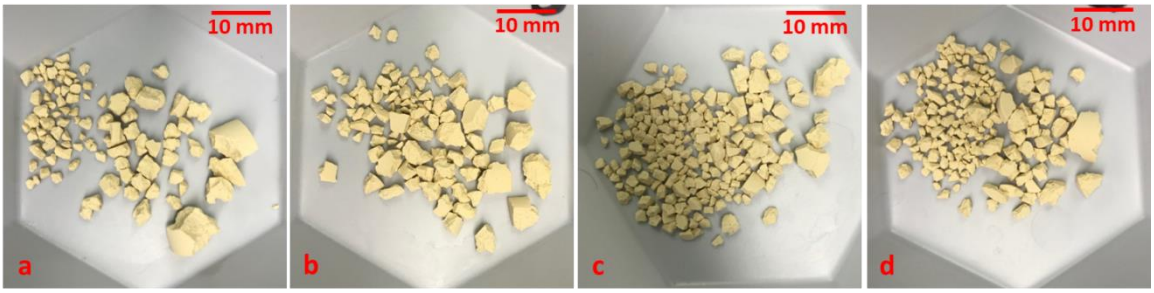

Figure 5.6. Typical results for stone fragments for normal SWL and SWL combined with different ABCD pulse sequences after 500 shocks; a)high rate SWL only, b)high rate SWL+ABCD 1, c)high rate SWL+ABCD 4, d)low rate SWL.

5.4 Discussion

This study demonstrated the feasibility of utilizing acoustic bubble coalescence and dispersion in enhancing high rate shockwave lithotripsy on a clinical device. The efficacy of stone comminution for high rate SWL was significantly improved for any of the four ABCD sequences tested, and the results for the best sequence were very close to low rate SWL of 30 shocks/min. The shockwave rate used in this study (120 SW/min) is still in common clinical practice at many locations despite its reduced efficacy because of the need for shorter procedure times. This work shows that it is possible to restore good efficacy for these faster procedures through the use of ABCD. Enhancing SWL with ABCD pulses can help complete comminution through increasing the safety of the treatment as well. The increased risk for collateral tissue damage in high rates SWL is hypothesized to be due to cavitation within the kidney parenchyma, SWL enhanced with ABCD would reduce this damage by preventing a proliferation of cavitation bubbles expanding into the kidney tissue. Currently the FDA limit for number of shocks that can safely be applied in one session is 2500 shocks. However, with reduced collateral tissue damage, a higher number of pulses could be applied to ensure complete stone comminution.

The low pressure acoustic pulses making up the various ABCD sequences explored in this study achieve their effects by stimulating residual cavitation bubbles to either coalesce or disperse from the propagation path and the lithotripter focus. Forced coalescence was the strategy previously employed to avoid negative effects of persisting residual cavitation bubbles [12,21-25]. The mechanism of bubble coalescence occurs through the acoustic field inducing size oscillations in the bubbles, which gives rise to two major forces. The primary Bjerknes force describes the tendency of bubbles smaller (or larger) than resonant size to move up (down) a pressure gradient and congregate at pressure antinodes (or nodes). The secondary Bjerknes force describes an attractive (or repulsive) force between bubbles, which are oscillating in phase (or out of phase) with one another depending on their size and the acoustic field frequency [28-34]. This secondary Bjerknes force is hypothesized to be the dominant factor bringing the remnant bubbles together to coalesce. During stable bubble oscillations, this force increases with higher amplitude and higher frequency of the driving sound field. The amplitude and frequency of acoustic bubble coalescence pulses in this study are set to mechanical index of one, which would result in stable oscillation. An example of bubble coalescence in ABCD 1 (post) can be seen in figure 5.7. Our attempt in this study was to use both coalescence and dispersion to overcome the negative effects of persisting residual cavitation bubbles. An example of bubble coalescence and dispersion in ABCD 3 (pre) can be seen in figure 5.8. The primary Bjerknes force is hypothesized to be the dominant factor in dispersing residual cavitation bubbles away from the focus, and becomes more dominant than the secondary Bjerknes force at mechanical indexes lower than 1; therefore, it was expected that lower pressures for ABCD pulses would result in more effective dispersion, while higher pressure maximize coalescence. In this set of experiments the results demonstrated that ABCD 4 (pre, extra

low amp) pulses with pressure amplitude of 500 kPa, was more efficacious than ABCD 3 (pre) pulses with pressure amplitude of 1 MPa.

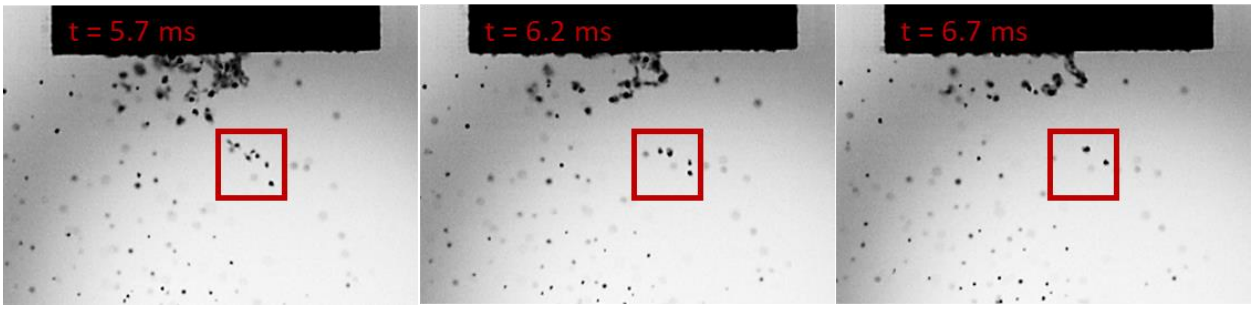

Figure 5.7. An example of bubble coalescence is shown in the red square; few bubbles coalesce to two remaining bubbles in 1 milisecond. ABCD 1 (post), after 10 shocks, ABCD pulses are applied from t = 3 ms to t = 11 ms. The 3 frames above are taken at 10 kfps and show only 1ms of during of ABCD pulses.

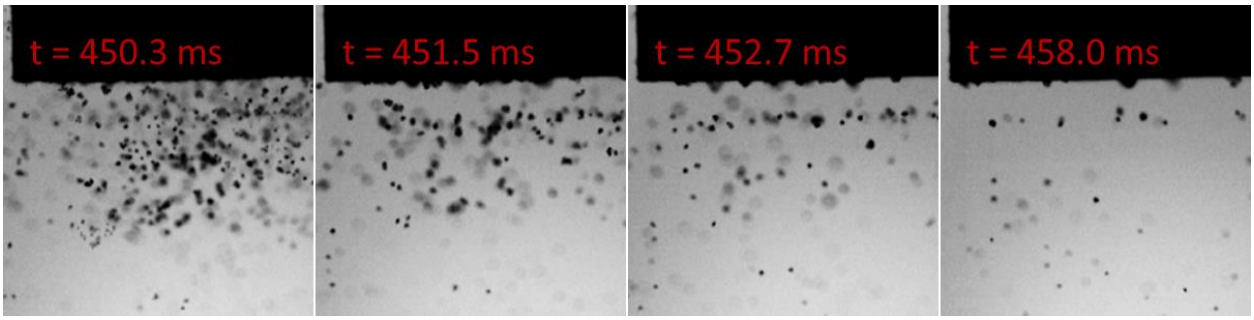

Figure 5.8. Process of coalescence and dispersion for a typical ABCD 3 (pre). ABCD pulses begin at 450 ms following the shock, and it can be seen that during the 8 ms of these pulses large amount of scattered cavitation in the first frame is mainly cleared in the last frame.

An example of the cavitation bubble cloud generated following the shockwave for SWL only and SWL when combined with ABCD 1 (post) and ABCD 4 (pre, extra low amp) is shown in figure 5.9. Comparing the large scattered cavitation in SWL only case in figure 5.9(a) with minimal cavitation along the propagation path in figure 5.9(b, c), we can see that ABCD pulses can mitigate the shielding effect of residual bubble nuclei, by removing them from the propagation

path. For ABCD 1 (post) case, figure 5.9(b), it appears that by applying low amplitude pulses right after the shockwave, the majority of residual bubbles are coalesced to a few larger bubbles. However, for ABCD 4 (pre, extra low amp) case, figure 5.9(c), by applying low amplitude pulses right before the shockwave, bubble coalescence occurs when residual bubbles are further apart, and are either dispersed from the propagation path, or coalesced to a larger number of smaller bubbles in comparison with ABCD 1 (post) case. Higher efficacy of ABCD 4 (pre, extra low amp) case in producing fine debris could be due to increased cavitation on the surface of the stone, as well as reduced shielding effect.

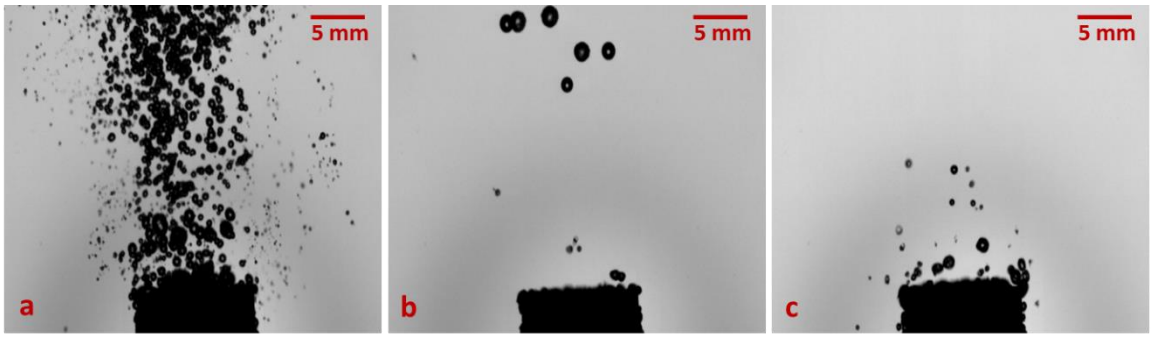

Figure 5.9 – Cavitation bubble cloud after 10 shocks: a)high rate SWL only, b)high rate SWL+ABCD 1 (post), c)high rate SWL+ABCD 4 (pre,low amp).

These results suggest that manipulation of residual bubbles after each shockwave can be further optimized by acoustic bubble coalescence and dispersion, which can reduce the shielding effect of residual bubble nuclei more efficiently than relying only on the immediate coalescence of residual bubbles, resulting in a more efficient SWL treatment.

Cavitation bubble dynamics and forced dispersion are expected to have a high dependency on the medium and surrounding space. This set of experiments was performed in free degassed deionized water, and the stone was placed in an enclosed finger cot filled with slightly degassed

deionized water to mimic the medium and the space inside of a kidney. However, further studies and *in vitro* and *in vivo* experiments in kidneys are needed to show if similar results can be obtained in real life treatments.

5.5 References

[1] Lingeman JE, Smith LH, Wood JR. Bioeffects and long term effects of ESWL. In: Urinary Calculi: ESWL, Endourology and Medical Therapy. Philadelphia: Lea & Febiger. 1989; 285.

[2] Politis G, Griffith DP. ESWL: Stone free efficacy based upon the stone size and location. World J Urol. 1987; 5: 255–258.

[3] Cass AS. Comparison of first generation (Dornier HM3) and second generation (Medstone STS) lithotriptors: treatment results with 13,864 renal and ureteral calculi. J Urol. 1995 Mar; 153 (3 Pt 1): 588-92. PMID: 7861488.

[4] M. Lokhandwalla, B. Sturtevant, “Fracture mechanics model of stone comminution in ESWL and implications for tissue damage,” *Physics in medicine and biology*, vol. 45, no. 7, pp. 1923, Jul. 2000.

[5] S. Zhu, F. H. Cocks, G. M. Preminger, P. Zhong, “The role of stress waves and cavitation in stone comminution in shock wave lithotripsy,” *Ultrasound in medicine & biology*, vol. 28, no. 5, pp. 661-71, May. 2002.

[6] P. Zhong, C. J. Chuong, G. M. Preminger, “Characterization of fracture toughness of renal calculi using a microindentation technique,” *Journal of materials science letters*, vol. 12, no. 1, pp. 1460-2, Jan. 1993.

[7] A. P. Duryea, W. W. Roberts, C. A. Cain, and T. L. Hall, "Controlled cavitation to augment SWL stone comminution: mechanistic insights in vitro," *IEEE Trans Ultrason Ferroelectr Freq Control*, vol. 60, pp. 301-9, Feb 2013.

[8] Y. A. Pishchalnikov, J. A. McAteer, Jr. J. C. Williams, I. V. Pishchalnikova and R. J. Vonderhaar, “Why stones break better at slow shockwave rates than at fast rates: in vitro study with a research electrohydraulic lithotripter,” *Journal of Endourology*, vol. 20, no. 8, pp. 537-41, Aug. 2006

[9] H. G. Flynn, “Generation of transient cavities in liquids by microsecond pulses of ultrasound,” *Journal of the Acoustical Society of America*, vol. 72, no. 6, pp. 1926-32, Dec. 1982.

[10] J. B. Fowlkes and L. A. Crum, “Cavitation threshold measurements for microsecond length pulses of ultrasound,” *Journal of the Acoustical Society of America*, vol. 83, no. 6, pp. 2190–2201, Jun. 1988.

[11] Y. A. Pishchalnikov, J. A. McAteer, I. V. Pishchalnikova, J. C. Williams, M. R. Bailey, and O. A. Sapozhnikov, "Bubble proliferation in shock wave lithotripsy occurs during inertial collapse," in *18th International Symposium on Nonlinear Acoustics*, 2008, pp. 460-463.

[12] A. P. Duryea, W. W. Roberts, C. A. Cain, H. A. Tamaddoni and T. L. Hall, “Acoustic bubble removal to enhance SWL efficacy at high shock rate: an in vitro study,” *Journal of Endourology*, vol. 28, no. 1, pp. 90-95, Jan. 2014.

[13] M. J. Weir, N. Tariq, and R. J. Honey, "Shockwave frequency affects fragmentation in a kidney stone model," *J Endourol*, vol. 14, pp. 547-50, Sep 2000.

[14] A. Greenstein and H. Matzkin, "Does the rate of extracorporeal shock wave delivery affect stone fragmentation?," *Urology*, vol. 54, pp. 430-432, 1999.

[15] R. F. Paterson, D. A. Lifshitz, J. E. Lingeman, A. P. Evan, B. A. Connors, N. S. Fineberg, *et al.*, "Stone fragmentation during shock wave lithotripsy is improved by slowing the shock wave rate: studies with a new animal model," *J Urol*, vol. 168, pp. 2211-5, Nov 2002.

[16] K. T. Pace, D. Ghiculete, and M. Harju, "Shock wave lithotripsy at 60 or 120 shocks per minute: A randomized, double-blind trial," *The Journal of Urology*, vol. 174, pp. 595-599, 2005.

[17] E. Yilmaz, E. Batislam, M. Basar, D. Tuglu, C. Mert, and H. Basar, "Optimal frequency in extracorporeal shock wave lithotripsy: prospective randomized study," *Urology*, vol. 66, pp. 1160-4, Dec 2005.

[18] K. Madbouly, A. M. El-Tiraifi, M. Seida, S. R. El-Faqih, R. Atassi, and R. F. Talic, "Slow versus fast shock wave lithotripsy rate for urolithiasis: a prospective randomized study," *J Urol*, vol. 173, pp. 127-30, Jan 2005.

[19] M. Delius, F. Ueberle, W. Eisenmenger, “Extracorporeal shock waves act by shock wave-gas bubble interaction,” *Ultrasound in medicine & biology*, vol. 24, no. 7, pp. 1055-9. Sep. 1998.

[20] A. Philipp, M. Delius, C. Scheffczyk, A. Vogel, W. Lauterborn, “Interaction of lithotripter-generated shock waves with air bubbles,” *The Journal of the Acoustical Society of America*, vol. 93, no. 5, pp. 2496-509, May. 1993.

[21] A. P. Duryea, C. A. Cain, H. A. Tamaddoni, W. W. Roberts and T. L. Hall, "Removal of residual nuclei following a cavitation event using low-amplitude ultrasound," *IEEE Transactions on Ultrasonics, Ferroelectrics, and Frequency Control*, vol. 61, no. 10, pp. 1619-1626, Oct. 2014.

[22] A. P. Duryea, W. W. Roberts, C. A. Cain and T. L. Hall, "Removal of residual cavitation nuclei to enhance histotripsy erosion of model urinary stones," *IEEE Transactions on Ultrasonics, Ferroelectrics, and Frequency Control*, vol. 62, no. 5, pp. 896-904, May 2015.

[23] A. P. Duryea, H. A. Tamaddoni, C. A. Cain, W. W. Roberts and T. L. Hall, "Removal of residual nuclei following a cavitation event: a parametric study," *IEEE Transactions on Ultrasonics, Ferroelectrics, and Frequency Control*, vol. 62, no. 9, pp. 1605-1614, Sep. 2015.

[24] A. P. Duryea, C. A. Cain, W. W. Roberts and T. L. Hall,, "Removal of residual cavitation nuclei to enhance histotripsy fractionation of soft tissue," *IEEE Transactions on Ultrasonics, Ferroelectrics, and Frequency Control*, vol. 62, no. 12, pp. 2068-2078, Dec. 2015.

[25] H. Alavi Tamaddoni, W. W. Roberts, A. P. Duryea, C. A. Cain, and T. L. Hall, “Enhanced High-Rate Shockwave Lithotripsy Stone Comminution in an *in vivo* Porcine Model Using Acoustic Bubble Coalescence,” *Journal of Endourology*, vol. 30, no. 12, pp. 1321-1325, Dec. 2016.

[26] J. E. Parsons, C. A. Cain, and J. B. Fowlkes, “Cost-effective assembly of a basic fiber-optic hydrophone for measurement of high amplitude therapeutic ultrasound fields,” *Journal of the Acoustical Society of America*, vol. 119, no. 3, pp. 1432–1440, Mar. 2006.

[27] W. N. Simmons, F. H. Cocks, P. Zhong, and G. Preminger, "A composite kidney stone phantom with mechanical properties controllable over the range of human kidney stones," *J Mech Behav Biomed Mater*, vol. 3, pp. 130-3, Jan 2010.

[28] V. Bjerknes, *Fields of Force*, 1906.

[29] M. Kornfeld and L. Suvorov, "On the destructive action of cavitation," *Journal of Applied Physics*, vol. 15, no.6, pp. 495-506, 1944.

[30] F. G. Blake, "Bjerknes Forces in Stationary Sound Fields," *The Journal of the Acoustical Society of America*, vol. 21, no. 5, pp. 551-551, Jun. 1949.

[31] E. A. Neppiras, "Subharmonic and Other Low-Frequency Emission from Bubbles in Sound-Irradiated Liquids," *The Journal of the Acoustical Society of America,* vol. 46, no. 3B, pp. 587-601, Sep. 1969.

[32] L. A. Crum and A. I. Eller, "Motion of Bubbles in a Stationary Sound Field," *The Journal of the Acoustical Society of America,* vol. 48, no. 1B, pp. 181-189, Jul. 1970.

[33] L. A. Crum, "Bjerknes forces on bubbles in a stationary sound field," *The Journal of the Acoustical Society of America,* vol. 57, no 6, pp. 1363-1370, Jun. 1975.

[34] T. G. Leighton, *The Acoustic Bubble*. San Diego, CA: Academic Press Inc, 1997.

CHAPTER 6

Non-Focal Acoustic Lens Design for Cavitation Bubble Consolidation

6.1 Introduction

During high rate shockwave lithotripsy and histotripsy treatments, persisting pre-focal cavitation bubbles following the lithotripsy shockwave or histotripsy pulse may shield or block the subsequent pulse, and potentially induce collateral tissue damage [1-11]. The study presented in this chapter, similar to those in chapters 3-5, attempts to mitigate the adverse effect of persisting residual bubbles. Studies in previous chapters demonstrate that properly tuned low amplitude acoustic pulses can be utilized to actively stimulate acoustic bubble coalescence and dispersion (ABCD) and help alleviate the effects of persisting bubbles [12-17]. This chapter explores the effects of different sound field patterns in the efficacy of ABCD and further optimization of the ABCD process by designing transducer lenses that generate more efficient ABCD pulses.

Bubble coalescence and dispersion is a strong function of spatial distribution of the sound field. A suitable sound field for effective coalescing of bubbles should have a broad region of uniform amplitude that could be readily generated by a small unfocused transducer aligned coaxially with the lithotripter or histotripsy transducer. Optimal bubble coalescence requires a non-focused acoustic field that exposes as much of the propagation path as possible where cavitation may occur. Some of the histotripsy transducers and lithotripters such as ultrasound guided lithotripters, have a central access port for imaging, which are ideally suited for the ABCD

transducer, since the coalescence generator could be a simple small unfocused transducer. Nevertheless, there is still room for more enhancement and optimization in the spatial distribution of the sound field to achieve more efficient coalescence and dispersion. A traditional elliptical transducer lens design produces the maximum focal gain possible for a given aperture. However, this design results in a sound field that might not be optimal for bubble consolidation, since its effective field volume is limited and the primary and secondary radiation forces may act against each other.

In the work presented in this chapter, we designed and fabricated non-focal transducer lenses with more complex surface geometries than traditional designs using rapid prototyping stereolithography to produce more effective acoustic fields for optimal bubble consolidation during lithotripsy or histotripsy therapy. We developed a design methodology using inverse problem techniques to map a desired acoustic field back to the surface of the transducer lens in order to determine the correct phase shift at every point on the lens surface. This method could be also applied to other acoustics problems where non-focused acoustic fields are desired.

6.2 Methods

We explored two approaches for designing non-spherically focused surfaces for ABCD transducer lenses: one was to examine different geometry functions for the surface of the lens that would result in desirable sound fields. The other was a more general approach that starts with a target sound field and traces it back to a lens surface design that would produce such a sound field.

6.2.1 Sound Field Simulation

We looked into different surface geometries, which translates to setting different time delays and phase shifts for each point on the transducer. The ABCD transducer that is placed in the central access port of the histotripsy transducer, as shown in figure 6.1, has a radius of 25.4 mm. The sound field simulation was done by populating the surface of the lens with a large number of small rectangular transducers using FOCUS [18-21], a Matlab toolbox developed at Michigan State University to generate the pressure map. The surface of the transducer lens model with a diameter of 50.8 mm was populated by 2500 rectangular transducers. The first example was a typical spherically focused lens, with surface modeled as in Eq. 6.1. Figure 6.1 shows the 2-dimensional radial cross section, 3-dimensional view of the surface of transducer lens, and the simulation result for a field pressure at a transverse plane at a distance of 150mm from the surface of the transducer, which is at the focus of the histotripsy transducer as well as that of the ABCD transducer.

Surface model of a spherically focused lens:

$$z = f(x, y) = x^2 + y^2 \qquad \text{Eq. 6.1}$$

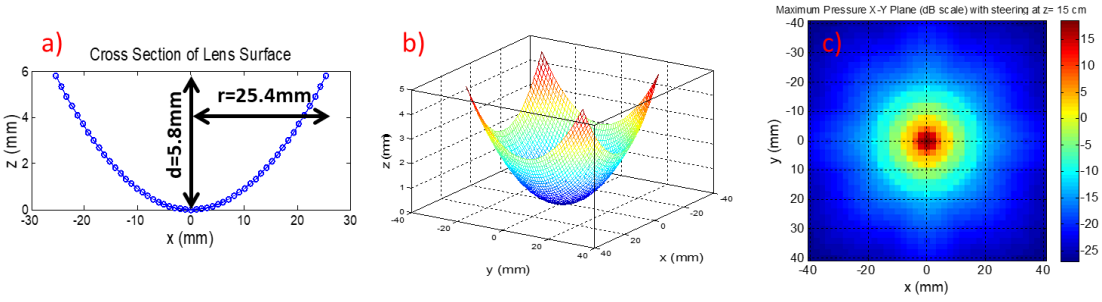

Figure 6.1. a) 2-dimensional cross section, and b) 3-dimensional view of the surface of transducer lens, c) the simulation result for field pressure (dB) at transverse plane at a distance of 150mm from the surface of the transducer with spherically focused lens.

The spherically focused lens resulted in a small and high amplitude focus. We hypothesized that a large uniform high pressure field would maximize secondary Bjerknes forces and should result in more pronounced bubble coalescence. The Gaussian lens model, as can be seen in figure 6.2(c), resulted in a large uniform focal zone that has a diameter of about 20mm, which would cover the extent of bubble cloud and its collapse generated by the histotripsy transducer that is used in this study.

Surface model of a Gaussian lens:

$$z = f(x, y) = 1 - e^{-c(x^2+y^2)} \qquad \text{Eq. 6.2}$$

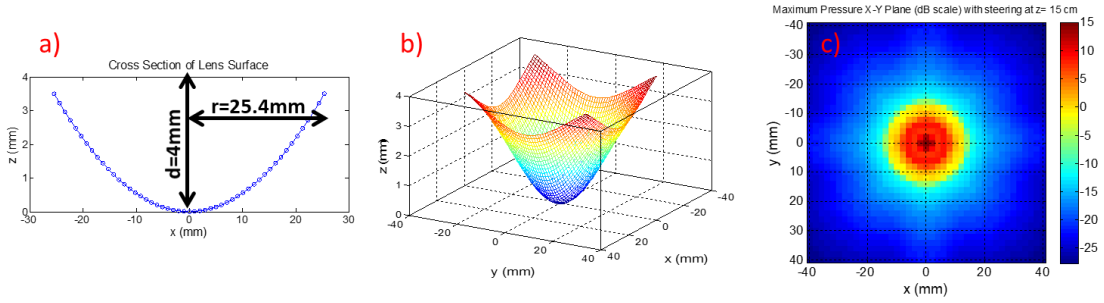

Figure 6.2. a) 2-dimensional cross section, and b) 3-dimensional view of the surface of transducer lens, c) the simulation result for field pressure (dB) at transverse plane at a distance of 150mm from the surface of the transducer with Gaussian function surface model (constant c=1, normalized to maximum d=4mm).

Another geometrical model that we examined was sinc function, Eq. 6.3, which would result in a Bessel shaped surface. We were interested to see if we could generate a sound field with

a high pressure gradient that increased primary Bjerknes forces. Figure 6.3 shows the surface of a sinc shaped lens, and the corresponding simulated acoustic field. In this field, the primary radiation force pushes bubbles with sizes smaller than the resonant size away from the peripheral zones toward the center, where they coalesce and form larger bubbles. The resulting larger bubbles are then pushed away from the propagation path.

Surface model of a sinc lens:

$$z = f(x,y) = \frac{\sin\left(c\sqrt{x^2+y^2}\right)}{\left(c\sqrt{x^2+y^2}\right)} \qquad \text{Eq. 6.3}$$

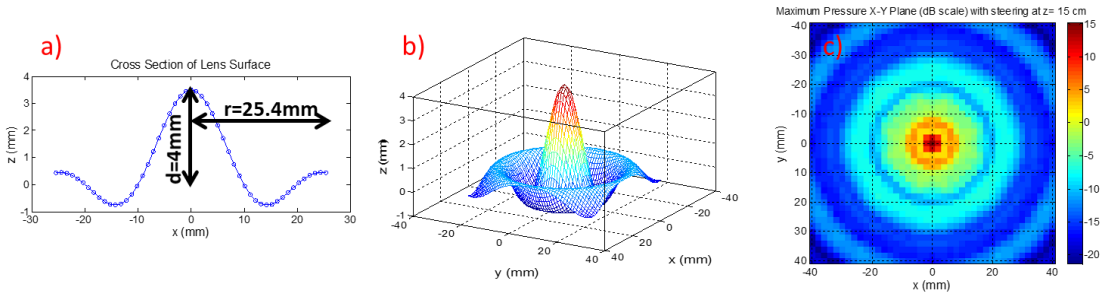

Figure 6.3. a) 2-dimensional cross section, and b) 3-dimensional view of the surface of transducer lens, c) the simulation result for field pressure (dB) at transverse plane at a distance of 150mm from the surface of the transducer with sinc function surface model (constant c=8, normalized to maximum d=4mm).

6.2.2 Lens Surface Design Optimization for an Arbitrary Sound Field

The goal of this approach is to trace back a desired sound field to a particular design for a non-spherically focused surface containing ABCD transducer lenses. The first step was to define the desired field pattern, and translate it to the utility function to be optimized as shown in Eq. 6.4.

Hence, the goal of the optimization is to maximize optimization factors (Φ) subject to constraint factors (Π):

$$\mathcal{U} = \sum_i \beta_i \, \Phi_i - \sum_j \nu_j \Pi_j \qquad \text{Eq. 6.4}$$

$\mathcal{U}$: Utility function, β_i, ν_j: Weight constants, Φ_i: Optimizing factors, Π_j: Constraint factors

For more effective bubble coalescence, our goal is to maximize the pressure in the focal zone at the center within a large enough area to cover the extent of the collapse of the bubble cloud (which for our experiment setup is about 20 mm wide), while keeping the pressure amplitude in the focal zone uniform. For amplitude uniformity we set the bound of no more than 3dB difference across the field. There are also some physical design constraints, including lens thickness and surface gradient, to insure continuity of the surface for build feasibility. The optimizing and constraint factors that we defined for the desired field for the ideal ABCD lens were summarized as:

- Optimizing factor: to maximize pressure at the focus

$\Phi_1 = p_{max}$, Max Pressure at focus Eq. 6.5

- Constraint factor #1: Pressure uniformity

$$\Pi_1 = (p_{max} - p_{min}) > 3dB \qquad \text{Eq. 6.6}$$

- Constraint factor #2: Lens thickness

$$\Pi_2 = |z| > 5mm \qquad \text{Eq. 6.7}$$

- Constraint factor #3: Lens surface gradient

$$\Pi_3 = |\Delta z| < 1mm \qquad \text{Eq. 6.8}$$

The surface of the lens is assumed to be circular and formed by M square transducers. Hence, the pressure at any point of the field is contributed by each element and can be calculated as the sum of all M transducers. The coordinate system of each element is defined by the Cartesian system (x, y, z) where height z is a function of (x, y). For the sake of simplicity, it is assumed that the lens surface has circular symmetry, and hence, as shown in figure 6.4, the surface can be defined by a radial profile by n equally-spaced data points in the form of $[z_1,\ z_2,\ \ldots, z_n]$.

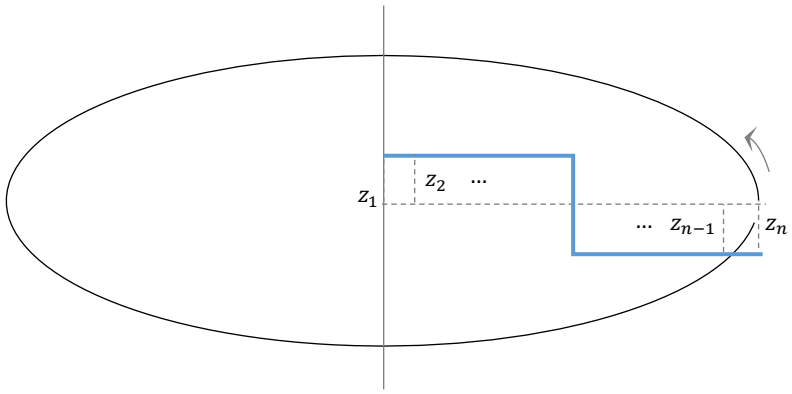

Figure 6.4. Radial profile of lens surface defined by equally spaced data points $z_1, z_2, \ldots, z_n$.

With this assumption, the optimization problem will be reduced to solving for *n* transducer height z_i along the radius:

$$Z_{Optimization} = [z_1,\ z_2,\ \ldots, z_n], \text{ where: n} \ll M \qquad \text{Eq. 6.9}$$

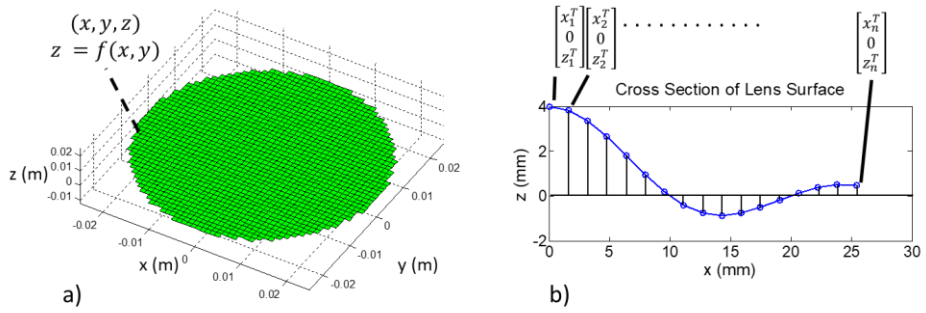

Figure 6.5. Simulation of surface of the lens and coordination of each transducer on the surface a) simulated array transducer with m square transducers populating a circular surface with a diameter of 50.8 mm, b) cross section of lens surface.

To achieve a global optimum, Genetic Algorithm (GA) was adopted in this study. Starting with a reasonable initial population, for instance a flat disk or a traditional elliptical surface profile, a mixed random number of solutions were generated with a predefined population size. Then using the defined constraints and utility function, as defined in Eq. 6.4-6.8, the population was ranked, and only an elite percentage of the population were kept to mutate and produce the next generation. This process was then iterated for a number of generations to find the optimal solution. This optimization process was done in MATLAB using Genetic Algorithm Toolbox with the following setting:

- Total number of transducers (M): 256
- Number of data points on radial profile (n): 8
- Population size:10
- Elite fraction: 50% and 80%
- Total number of generations: 100

6.2.3 Experimental Setup for Sound Field Measurement

To evaluate the design approaches described earlier, different non-spherically focused surfaces for ABCD transducer lenses were generated and assessed; some with arbitrary shape functions to examine different geometry functions for the surface of the lens, and some with optimized shapes to achieve a target sound field. A number of designed lenses with different parameters were fabricated using 3D printer. The resulting sound fields generated by ABCD transducer using these lenses were then experimentally measured and compared with the simulation results. The measurements were performed using a fiber-optic probe hydrophone that was built in-house [22]. The ABCD transducer was maintained stationary during the measurements, while the fiber-optic hydrophone was translated via a motorized positioning system (Anaheim Automation Inc., Anaheim, CA) scanning the sound field pressure of 50mm by 50mm plane at 150 mm distance from the surface of the ABCD transducer.

6.2.4 Experimental Evaluation

The proposed optimal lens design methodology for enhanced coalescence and dispersion were adopted for histotripsy treatments. In our current setup, histotripsy pulses were generated by an in-house made hemisphere transducer array of 112 individual transducers with a frequency of 500 kHz. Individual transducer module housings were fabricated from Accura 60 plastic (3D Systems Inc., Rock Hill, SC) using rapid prototyping stereolithography, each consisting of two 1 MHz Pz36 disc elements (Ferroperm Piezoceramics A/S, Kvistgaard, Denmark) stacked on top of each other and driven to produce 500 kHz, and a flat Accura-60 disc as the matching layer between element and water. This histotripsy array transducer generates a focal zone of -6-dB beamwidth measuring 2.0 mm in the lateral dimension and 6.3 mm in the axial [23]. The histotripsy transducer

was driven to produce 5 bursts of histotripsy pulses exceeding 30 MPa, which is the pressure threshold to initiate cavitation. The histotripsy pulses were followed with ABCD pulses with 500 µs delay, which is enough time for the bubble cloud generated by histotripsy pulses to grow and collapse. The ABCD pulses were generated by an in-house made individual 1 MHz transducer module placed in the central port of histotripsy array transducer scaffold. The ABCD transducer module consisted of a single 1 MHz PZT-4 disc element (Steiner & Martins Inc., Miami, FL) with a diameter of 50 mm, and an acoustic interchangeable lens as matching layer with a focal length of 150 mm, which coincide with the histotripsy focus. This ABCD transducer module design with interchangeable lens allowed for convenient change of the lenses during the experiments. The pressure amplitude of ABCD pulses were 0.6 MPa. The pulse sequence used for all experiments for this study is shown in figure 6.6.

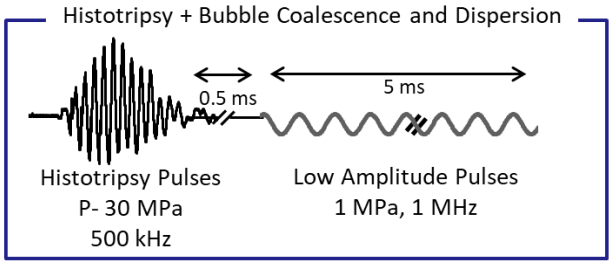

Figure 6.6. Histotripsy and bubble coalescence and dispersion pulses, in which each histotripsy pulse is followed by low amplitude acoustic pulses for 5 ms.

A schematic of the experimental setup is depicted in figure 6.7. All experiments and measurements were conducted in a water tank, filled with deionized water that was degassed to about 80% of saturation. The histotripsy and ABCD transducers were placed in the water tank with a positioning system. Cavitation events were monitored by a Photron Fastcam SA1.1 high speed camera (Photron USA Inc., San Diego, CA).

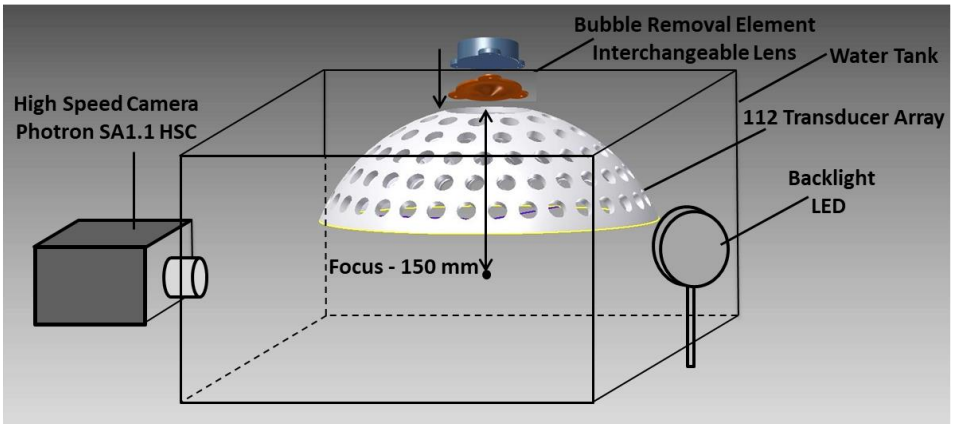

Figure 6.7. Schematic of experiment setup for simulation evaluation.

6.3 Results

Figure 6.8 shows examples of simulation and measure sound fields of ABCD transducer using designed lenses. The acoustic sound fields of ABCD transducer using two different lenses, explained in section 6.2.1, is shown in figure 5.8: from simulation on the top (a,b) and from measured sound field scans for the corresponding lenses on at the bottom (c,d). Figure 6.8 a) and c) show the simulated and measured sound field for a Gaussian lens (with constant c=1), and figure 6.8 b) and d) show the simulated and measured sound field for a sinc funcion lens (with constant c=8). As it can be seen in this figure, the resulting sound field shape from the experimental measurements correlate well with the simulation results.

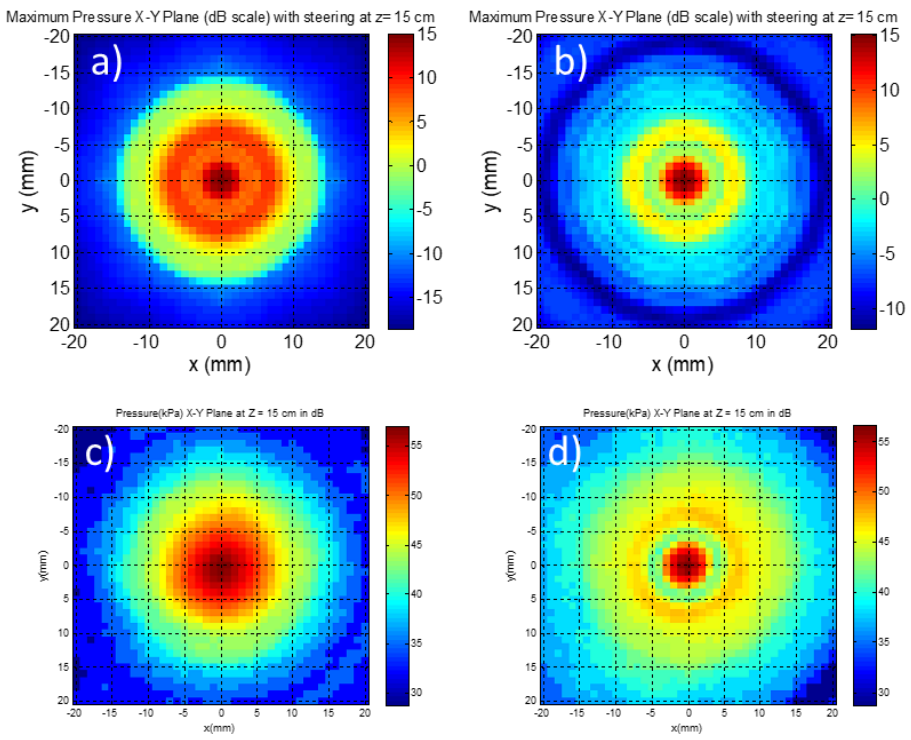

Figure 6.8. Comparison of sound field simulation (a and b) with corresponding measured sound field (c and d). a) and c) show the simulation and measured sound field for Gaussian lens with constant c=1, b) and d) show the simulation and measured sound field for a sinc funcion lens with constant c=8.

The genetic algorithm optimization process successfully achieved surface profile designs that would result in defined desired fields. Desired fields with sharp edges were generally harder to achieve. The results for a few different GA optimizations are shown below in the next three figures.

Figure 6.9 shows the results for GA optimization for a desired field with high pressure square-shaped focal zone of width of 20 mm, using GA population size of 10, elite fraction of 80%, and 100 number of generations with a mesh of 256 transducer elements. The simulated sound

field shown in figure 6.9(b) is calculated at a plane with 150mm distance from the ABCD transducer surface.

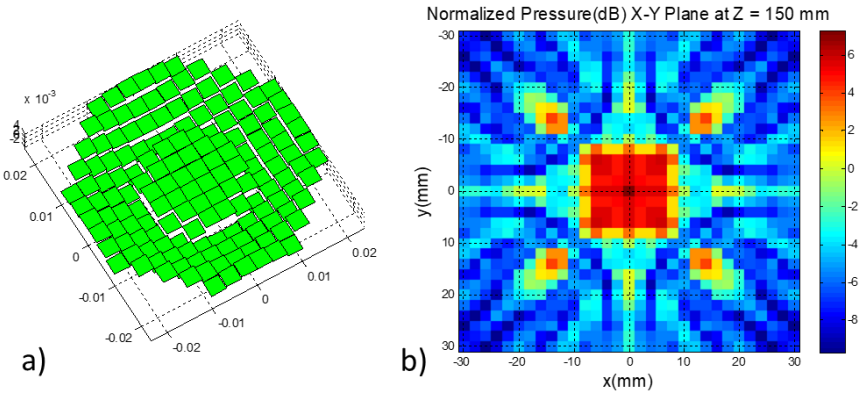

Figure 6.9. Results for GA optimization for high pressure square at the focus with 256 transducers a) three-dimensional view of the optimal lens surface, b) normalized pressure field at z=150mm.

Figure 6.10 shows the results for GA optimization for a desired field with high pressure at the focus with width of 20 mm, using GA population size of 10, elite fraction of 50%, and 100 number of generations with 2500 transducer populating the surface of the lens. The simulated sound field shown in figure 6.10(b) is calculated at a plane with 150mm distance from the ABCD transducer surface.

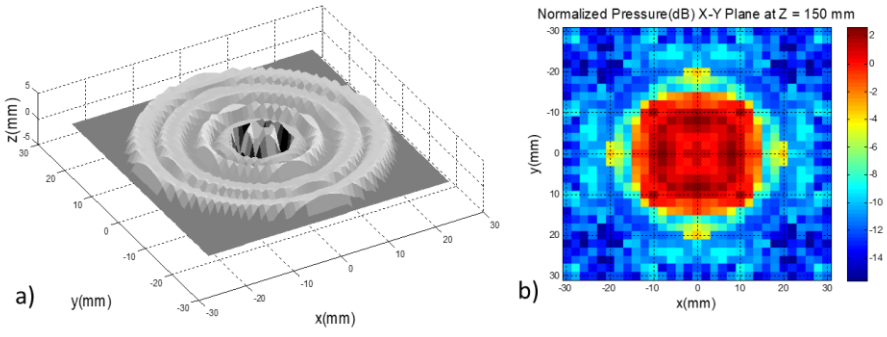

Figure 6.10. Results for GA optimization for high pressure area at the focus with 2500 transducers a) three-dimensional view of the optimal lens surface, b) normalized pressure field at z=150mm.

Figure 6.11 shows the results for GA optimization for a desired field with high pressure at the focus surrounded by a low pressure ring that would maximize the pressure gradient and primary Bjerknes forces. Similar to the sinc shaped lens described earlier, in sound fields with high pressure gradient, the primary Bjerknes forces are increased, hence, will push the bubble smaller than the resonant size from the low pressure ring in the periphery of the focus to the high pressure center to coalesce. This GA optimization was performed with population size of 10, elite fraction of 50%, and 100 generations with 2500 transducer populating the surface of the lens.

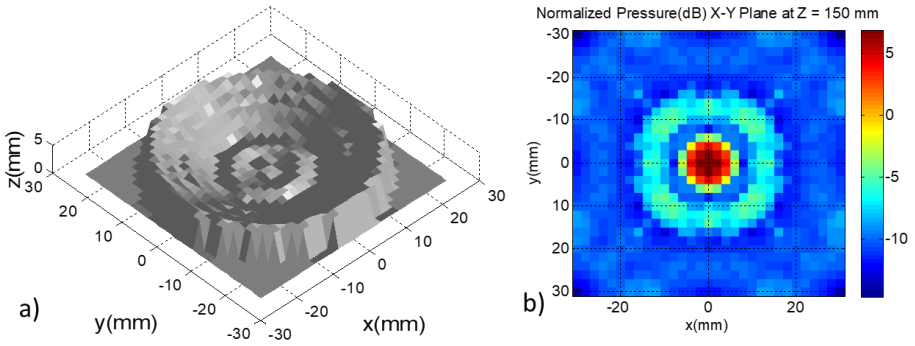

Figure 6.11. Results for GA optimization for high pressure at focus with low pressure ring shaped around it with 2500 transducers a) three-dimensional view of the optimal lens surface, b) normalized pressure field at z=150mm.

We further investigated the effects of these lenses on bubble consolidation in histotripsy treatments. A more effective ABCD process would result in a denser bubble cloud at the focus of the histotripsy transducer, and minimal scattered cavitation in the periphery of the focus. Figure 6.12 shows the bubble cloud size after the 5th pulse for the control case, in which the histotripsy

pulse was applied without ABCD pulses, and for three other cases in which histotripsy pulses were interleaved with ABCD pulses with elliptical, gaussian, and sinc shaped lenses. Scattered cavitation was significantly reduced when ABCD pulses were applied and while Gaussian and sinc shaped lenses were more effective than the elliptical lens.

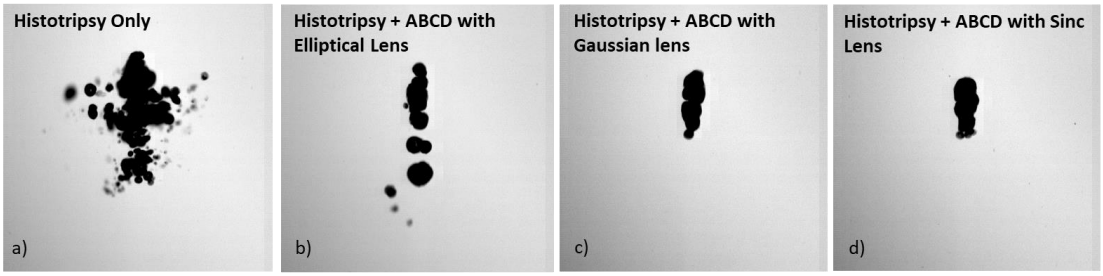

Figure 6.12. Bubble cloud size after five histotripsy pulses: a) histotripsy only, b) histotripsy and bubble coalescence and dispersion pulses by an elliptical lens, c) histotripsy and bubble coalescence and dispersion pulses by a sinc (with constant c=8) shaped designed lens, and d) histotripsy and bubble coalescence and dispersion pulses by a Gaussian shaped lens.

Figure 6.13 shows a quantitative measure for the shape and density of the bubble cloud. Since an effective ABCD should result in a dense bubble cloud at the focus with minimal scattered cavitation similar to that of the first pulse, we defined two areas: a focal area and a periphery area. The averaged area of the backlit bubble cloud at the first pulse over 60 trials is calculated as the target focal area in which a dense bubble cloud is produced, and any cavitation outside of this area is labeled as scattered cavitation. Measurements were done after five pulses for the control case and ABCD cases with a few different elliptical, gaussian, and sinc shaped lenses. The measurements for the total area of scattered cavitation in figure 6.13 is normalized to the averaged target focal area. For the control case, the average scattered area was 3.23 times of the target focal area; this value was reduced to 0.47 for ABCD with typical elliptical transducer lens, and further

improved to zero scattered cavitation with two of the new lens designs with sinc and Gaussian shapes.

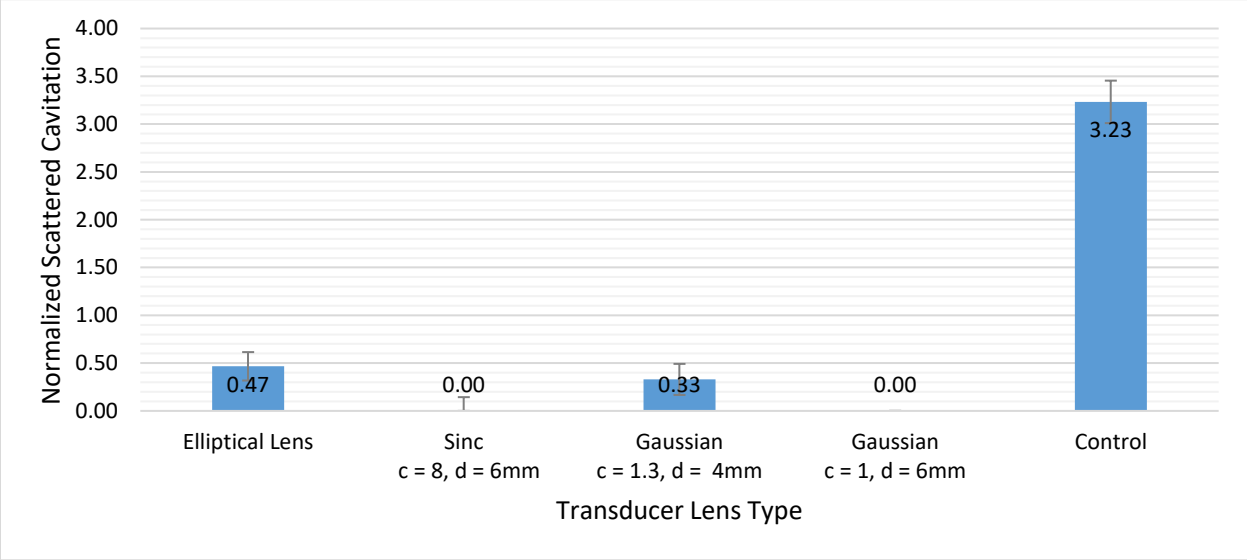

Figure 6.13. Scattered Cavitation in the periphery zone after 5th pulse for ABCD cases with different elliptical, gaussian, and sinc shaped lenses averaged over 3 samples normalized to the target area as the average area of bubble cloud at first pulse.

6.4 Discussion

This study demonstrated the feasibility of utilizing non-focal transducer lenses designed with complex surface geometries in order to produce more effective acoustic fields for bubble consolidation during lithotripsy or histotripsy.

An optimization design methodology was developed using a genetic algorithm to map any desired acoustic field to the transducer lens surface. This method can be applied to other acoustics problems where non-focused acoustic fields are desired.

The overall goal is to avoid or minimize the shielding effect and memory effect of persisting cavitation bubbles along the propagation path. The solution that we examined in this work is to actively consolidate cavitation by forced coalescence and dispersion. Previous chapters explored different pulse sequences for acoustic bubble coalescence and dispersion, employing primary and secondary Bjerknes forces to force the remaining persisting cavitation bubbles to consolidate and coalesce in order to clear the propagation path before the arrival of the next therapy pulse. In this chapter however, we explored further improvement of the ABCD process by optimizing the sound field of the ABCD transducer for more efficient primary and secondary Bjerknes forces.

The Secondary Bjerknes force, which describes an attractive force between bubbles that oscillate in phase with one another, and a repulsive force between bubbles that oscillate out of phase with one another, is hypothesized to be the dominant factor in bringing the remnant bubbles together to coalesce [24-26]. The secondary Bjerknes force is maximized with higher pressure within parameters that generate stable oscillation. The ideal for maximum bubble coalescence was to generate a high pressure focal zone with large beamwidth. One of the issues with typical focused lenses is that the focal zone has a small beamwidth. The size of the bubble cloud in lithotripsy is generally large to begin with, but even in histotripsy applications where a small and dense bubble cloud is generated, still the extent of the area in which cavitation bubbles may be found following the collapse of bubble cloud is much larger than the focal zone of a single element ABCD transducer with a typical focused elliptical lens. The goal of ABCD is to clear the entire propagation path. The typical Elliptical lens that we used in our experiments had a -6 dB beamwidth of 6 mm. However, we were able to attain a -6 dB beamwidth of 18 mm with one of the Gaussian lens designs. The results confirmed our hypothesis that transducer lens geometries

with larger focal areas result in more effective bubble consolidation. The Gaussian transducer lens with a focal zone of 18 mm width had the highest reduction of scattered cavitation.

Another approach was to maximize the primary Bjerknes force and attempt to attain a sound field in which primary and secondary Bjerknes forces would not act against each other. The goal was to maximize the primary Bjerknes force by maximizing pressure gradient [24, 29-30]. We hypothesized that a sound field with high pressure amplitude at the center focal area surrounded by a low pressure ring would increase the primary Bjerknes force, which would push the bubbles smaller than resonant size to the high amplitude focal zone, where the secondary Bjerknes force is strong and would force the bubbles to coalesce. The results confirmed our hypothesis and a sinc function transducer lens with a Bessel shaped surface resulted in more effective bubble consolidation than a typical elliptical lens transducer.

6.5 References

[1] Y. A. Pishchalnikov, J. A. McAteer, Jr. J. C. Williams, I. V. Pishchalnikova and R. J. Vonderhaar, “Why stones break better at slow shockwave rates than at fast rates: in vitro study with a research electrohydraulic lithotripter,” *Journal of Endourology*, vol. 20, no. 8, pp. 537-41, Aug. 2006

[2] H. G. Flynn, “Generation of transient cavities in liquids by microsecond pulses of ultrasound,” *Journal of the Acoustical Society of America*, vol. 72, no. 6, pp. 1926-32, Dec. 1982.

[3] J. B. Fowlkes and L. A. Crum, “Cavitation threshold measurements for microsecond length pulses of ultrasound,” *Journal of the Acoustical Society of America,* vol. 83, no. 6, pp. 2190–2201, Jun. 1988.

[4] M. J. Weir, N. Tariq, and R. J. Honey, "Shockwave frequency affects fragmentation in a kidney stone model," *J Endourol,* vol. 14, pp. 547-50, Sep 2000.

[5] A. Greenstein and H. Matzkin, "Does the rate of extracorporeal shock wave delivery affect stone fragmentation?," *Urology,* vol. 54, pp. 430-432, 1999.

[6] R. F. Paterson, D. A. Lifshitz, J. E. Lingeman, A. P. Evan, B. A. Connors, N. S. Fineberg, *et al.*, "Stone fragmentation during shock wave lithotripsy is improved by slowing the shock wave rate: studies with a new animal model," *J Urol*, vol. 168, pp. 2211-5, Nov 2002.

[7] K. T. Pace, D. Ghiculete, and M. Harju, "Shock wave lithotripsy at 60 or 120 shocks per minute: A randomized, double-blind trial," *The Journal of Urology*, vol. 174, pp. 595-599, 2005.

[8] E. Yilmaz, E. Batislam, M. Basar, D. Tuglu, C. Mert, and H. Basar, "Optimal frequency in extracorporeal shock wave lithotripsy: prospective randomized study," *Urology*, vol. 66, pp. 1160-4, Dec 2005.

[9] K. Madbouly, A. M. El-Tiraifi, M. Seida, S. R. El-Faqih, R. Atassi, and R. F. Talic, "Slow versus fast shock wave lithotripsy rate for urolithiasis: a prospective randomized study," *J Urol*, vol. 173, pp. 127-30, Jan 2005.

[10] M. Delius, F. Ueberle, W. Eisenmenger, “Extracorporeal shock waves act by shock wave-gas bubble interaction,” *Ultrasound in medicine & biology*, vol. 24, no. 7, pp. 1055-9. Sep. 1998.

[11] A. Philipp, M. Delius, C. Scheffczyk, A. Vogel, W. Lauterborn, “Interaction of lithotripter-generated shock waves with air bubbles,” *The Journal of the Acoustical Society of America*, vol. 93, no. 5, pp. 2496-509, May. 1993.

[12] A. P. Duryea, W. W. Roberts, C. A. Cain, H. A. Tamaddoni and T. L. Hall, “Acoustic bubble removal to enhance SWL efficacy at high shock rate: an in vitro study,” *Journal of Endourology*, vol. 28, no. 1, pp. 90-95, Jan. 2014.

[13] A. P. Duryea, C. A. Cain, H. A. Tamaddoni, W. W. Roberts and T. L. Hall, "Removal of residual nuclei following a cavitation event using low-amplitude ultrasound," *IEEE Transactions on Ultrasonics, Ferroelectrics, and Frequency Control*, vol. 61, no. 10, pp. 1619-1626, Oct. 2014.

[14] A. P. Duryea, W. W. Roberts, C. A. Cain and T. L. Hall, "Removal of residual cavitation nuclei to enhance histotripsy erosion of model urinary stones," *IEEE Transactions on Ultrasonics, Ferroelectrics, and Frequency Control*, vol. 62, no. 5, pp. 896-904, May 2015.

[15] A. P. Duryea, H. A. Tamaddoni, C. A. Cain, W. W. Roberts and T. L. Hall, "Removal of residual nuclei following a cavitation event: a parametric study," *IEEE Transactions on Ultrasonics, Ferroelectrics, and Frequency Control*, vol. 62, no. 9, pp. 1605-1614, Sep. 2015.

[16] A. P. Duryea, C. A. Cain, W. W. Roberts and T. L. Hall,, "Removal of residual cavitation nuclei to enhance histotripsy fractionation of soft tissue," *IEEE Transactions on Ultrasonics, Ferroelectrics, and Frequency Control,* vol. 62, no. 12, pp. 2068-2078, Dec. 2015.

[17] H. Alavi Tamaddoni, W. W. Roberts, A. P. Duryea, C. A. Cain, and T. L. Hall, "Enhanced High-Rate Shockwave Lithotripsy Stone Comminution in an *in vivo* Porcine Model Using Acoustic Bubble Coalescence," *Journal of Endourology*, vol. 30, no. 12, pp. 1321-1325, Dec. 2016.

[18] R. J. McGough, T. V. Samulski, and J. F. Kelly, "An efficient grid sectoring method for calculations of the near-field pressure generated by a circular piston," *J Acoust Soc Am,* vol. 115, pp. 1942-54, May 2004.

[19] R. J. McGough, "Rapid calculations of time-harmonic nearfield pressures produced by rectangular pistons," *J Acoust Soc Am,* vol. 115, pp. 1934-41, May 2004.

[20] J. F. Kelly and R. J. McGough, "A time-space decomposition method for calculating the nearfield pressure generated by a pulsed circular piston," *IEEE Trans Ultrason Ferroelectr Freq Control,* vol. 53, pp. 1150-9, Jun 2006.

[21] D. Chen and R. J. McGough, "A 2D fast near-field method for calculating near-field pressures generated by apodized rectangular pistons," *J Acoust Soc Am,* vol. 124, pp. 1526-37, Sep 2008

[22] J. E. Parsons, C. A. Cain, and J. B. Fowlkes, "Cost-effective assembly of a basic fiber-optic hydrophone for measurement of high amplitude therapeutic ultrasound fields," *Journal of the Acoustical Society of America,* vol. 119, no. 3, pp. 1432–1440, Mar. 2006.

[23] A. P. Duryea, W. W. Roberts, C. A. Cain and T. L. Hall, "Removal of residual cavitation nuclei to enhance histotripsy erosion of model urinary stones," *IEEE Transactions on Ultrasonics, Ferroelectrics, and Frequency Control*, vol. 62, no. 5, pp. 896-904, May 2015.

[24] V. Bjerknes, *Fields of Force,* 1906.

[25] M. Kornfeld and L. Suvorov, "On the destructive action of cavitation," *Journal of Applied Physics,* vol. 15, no.6, pp. 495-506, 1944.

[26] F. G. Blake, "Bjerknes Forces in Stationary Sound Fields," *The Journal of the Acoustical Society of America,* vol. 21, no. 5, pp. 551-551, Jun. 1949.

[27] E. A. Neppiras, "Subharmonic and Other Low-Frequency Emission from Bubbles in Sound-Irradiated Liquids," *The Journal of the Acoustical Society of America,* vol. 46, no. 3B, pp. 587-601, Sep. 1969.

[28] L. A. Crum and A. I. Eller, "Motion of Bubbles in a Stationary Sound Field," *The Journal of the Acoustical Society of America*, vol. 48, no. 1B, pp. 181-189, Jul. 1970.

[29] L. A. Crum, "Bjerknes forces on bubbles in a stationary sound field," *The Journal of the Acoustical Society of America,* vol. 57, no 6, pp. 1363-1370, Jun. 1975.

[30] T. G. Leighton, *The Acoustic Bubble*. San Diego, CA: Academic Press Inc, 1997.

CHAPTER 7

Summary and Future Work

7.1 Summary

This dissertation explored acoustical methods for cavitation control during histotripsy and shockwave lithotripsy (SWL) treatments in order to improve efficacy and safety of these treatments, particularly at higher rates by minimizing shielding and memory effects of remnant residual bubbles, active tissue protection, and focal sharpening. More specifically, this research 1) demonstrated that the pressure threshold at which histotripsy cavitation bubble cloud is generated can be actively modified, 2) developed numerical simulation models for cavitation bubble behavior under different histotripsy, lithotripsy and acoustic bubble coalescence pulses, 3) performed *in vivo* studies to demonstrate the feasibility of applying acoustic bubble coalescence (ABC) pulses immediately after each shockwave to increase efficacy of stone comminution in high rate SWL, 4) investigated the effects of utilizing acoustic bubble coalescence and dispersion (ABCD) pulses in enhancing high rate SWL, and showed that the per shock efficacy of stone comminution for high rate SWL (120 shocks/min) was significantly improved to that of the low rate SWL (30 shocks/min), and furthermore, 5) demonstrated the feasibility of design and optimization of non-focal transducer lenses with complex surface geometries to produce more effective acoustic fields for bubble consolidation during lithotripsy or histotripsy.

7.1.1 Active Modulation of Cavitation Initiation Threshold

The motivation for this study was to achieve active tissue protection during histotripsy treatments by modulating cavitation initiation threshold. We hypothesized that by applying a properly tuned low amplitude acoustic pulse sequences before or during histotripsy pulses, the initiation pressure threshold and the growth of the cavitation bubble cloud could be modified. This hypothesis was examined in three different mediums of degassed water, tissue phantom gel, and bovine liver tissue and results confirmed that applying bubble suppressing pulses before or during shock scattering histotripsy treatment increases the cavitation initiation pressure threshold by 20% in the targeted area [1]. This study demonstrated that by applying bubble suppressing pulses during treatment, the residual nuclei are forced to coalesce. As a result, the probability of presence of nuclei at the focus of histotripsy transducer and shock scattering is decreased, which consequently increases the initiation pressure threshold. Furthermore, the results demonstrated that by applying bubble suppressing and pre-conditioning pulses, the shape and density of the resulting cavitation bubble cloud can be modified to obtain a dense bubble cloud at the focus with minimum scattered cavitation in the periphery of the focus, which in turn would increase the efficacy of the treatment and decrease collateral tissue damage. (Chapter 2)

7.1.2 Acoustic Bubble Coalescence and Dispersion

The main motivation for different studies presented in this dissertation on bubble consolidation and ABCD is to minimize the adverse effects of persisting residual bubbles during high rate SWL and histotripsy, and possibly reduce collateral tissue damage.

The feasibility of utilizing acoustic bubble coalescence in enhancing higher rate SWL in an *in vivo* porcine model was examined (Chapter 4). The results from this *in vivo* study demonstrated significant improvement in the efficacy of high rate SWL in stone comminution when ABC pulses were applied. Complete comminution (<2mm) of implanted kidney stones increased from average of 25% of the initial stone mass for SWL only case to 75% of the initial stone mass for SWL+ABC case (p-value=0.003) [2]. This study suggested that ABC pulses can mitigate the shielding effect of residual bubble nuclei. The higher efficacy of enhanced SWL, particularly in producing fine passable debris, could be due to increased cavitation on the surface of stones. This improvement in efficacy of high rate SWL treatments can in turn be translated to reduced treatment time, and potentially reduced collateral tissue damage. SWL enhanced with ABC requires smaller dose of shockwaves to obtain the same result, this could be translated to lower amount of tissue damage. Moreover, increased risk of collateral tissue damage in higher rate SWL is hypothesized to be due to cavitation within the kidney parenchyma which again is reduced by ABC pulses.

We attempted to further optimize the parameters of bubble coalescence, and investigated the feasibility of acoustic bubble coalescence and dispersion pulses in an *in vitro* study. This study examined the effects of applying low amplitude acoustic pulse sequences at different amplitudes and different time delays following each shockwave, which resulted in different interactions among residual microbubbles during stone comminution (Chapter 5). We hypothesized that by utilizing ABCD, we can mitigate the shielding effects of residual cavitation bubbles more efficiently, and further improve the therapy efficacy, particularly at higher rates. The results demonstrated that the average percentage of untreated stone fragments (>2mm) was significantly reduced from 15.81% of the initial mass for the control case to 0.19% of the initial mass for the

best ABDC enhanced case. These results suggested that manipulation of residual bubbles can be further improved by applying acoustic bubble coalescence and dispersion immediately before each shockwave, which can reduce the shielding effects of residual bubble nuclei more efficiently than relaying only on immediate coalescence of residual bubbles, resulting in a more efficient SWL treatment.

Furthermore, we explored the effects of different non-spherically focused transducer lenses for the ABCD transducer. The goal of this study was to design transducer lenses that produce acoustic sound fields that maximize the primary and secondary Bjerknes forces in order to more effectively force the residual cavitation bubbles to coalesce and disperse them away from the propagation path (Chapter 6). Genetic algorithm was adopted for design of these optimal transducer lens surfaces. This study demonstrated that our new transducer lens designs were more effective than typical elliptical transducer lenses in producing a dense bubble cloud at the focus with minimum scattered cavitation during histotripsy treatment. The averaged normalized scattered cavitation was reduced from 3.23 times of the target focal area for the control case to 0.47 for ABCD with a typical elliptical transducer lens, and further improved to zero scattered cavitation with two of the new lens designs with sinc and Gaussian shapes.

The research presented in this dissertation demonstrated the feasibility of acoustical methods for control of initiation of the cavitation bubble cloud and control of pre-focal cavitation in different therapy modes, and provided insight into physical processes underlying cavitation bubble behavior during enhanced SWL and histotripsy. Future work, as explained in the remainder of this chapter, will aim to build upon the work detailed in this dissertation in order to advance our understanding of the physical characteristics and behavior of cavitation bubbles in enhanced SWL

and histotripsy treatments, and to take further steps required to improve and translate findings of this research to clinical applications.

7.2 Future Work

7.2.1 Cavitation Initiation Threshold Modulation

While the cavitation initiation threshold modulation study (Chapter 2) demonstrated the feasibility of actively modifying the threshold for cavitation initiation, there is still work to be done to optimize the parameters of the bubble suppressing pulses, and moreover, to translate the findings of this study to active tissue protection in clinical treatments.

7.2.1.1 Parameter Optimization

Based on the results obtained from this study (Chapter 2), the acoustic parameters of bubble suppressing and pre-conditioning pulses, including frequency, amplitude, and pulse duration are to be optimized. The frequency of pre-conditioning and bubble suppressing pulses applied before and during the histotripsy pulses was the same in this research, each of which is subject to further optimization. The efficacy of forced bubble coalescence for a given bubble population is highly dependent on the driving frequency, particularly if its corresponding resonant size is close to the existing bubble nuclei size range. Furthermore, the pre-conditioning process is expected to rely on the primary Bjerknes forces as well as the secondary Bjerknes forces, and as a result, separate optimization for each mechanism is required since there are different phenomena in play in each mechanism.

In order to gain a better understanding of the cavitation nuclei population in tissue and their role in the histotripsy process, and as first steps in optimizing the acoustic parameters for pre-

conditioning before the treatment as well as bubble suppressing during the treatment, future work should be conducted in order to determine the potential nuclei characteristics, including investigation of size distribution of the existing cavitation nuclei population. Generally, for analysis of the cavitation bubble size following a cavitation event, such as collapse of a bubble cloud, we can use high resolution optical images to explore the size of residual cavitation bubbles, or by an ultrasound B-mode imaging transducer. This method can be used for larger size bubble populations; however, for exploring any free weak nuclei before the treatment, we need to excite the bubbles in order to grow them to a sufficiently detectable size by camera or any ultrasound imaging devices. Post-processing of images will include utilizing the bubble model that we had already developed for the study presented in chapter 3 to project the bubble size pre-excitation. We expect to observe the bubble radius to be in range of 1-5 microns for the bubble population following the histotripsy pulse (for the experiment setting detailed in chapter 2) based on previous observations, as well as the theoretical value for the resonant size of the 1 MHz histotripsy transducer, which is close to 3 microns. However, the size of cavitation nuclei prior to treatment pulses is expected to be much lower, and in the sub-micron range. Next steps will include modifying and advancing the developed cavitation bubble model (explained in Chapter 3) to simulate the effects of preconditioning and bubble suppressing pulses in the nucleation process for cavitation bubbles with a range of radii that are obtained by the size analysis study explained earlier. The simulation and parameter optimization can be done for a range of initial bubble sizes, since it is expected to observe some variation in the size of the weak nuclei. The model will be used to optimize the acoustic parameter of pre-conditioning and bubble suppressing pulses, including frequency, amplitude and duration of acoustic pulses. We expect to observe more effective change in cavitation initiation threshold modulation by employing the optimized

parameters, particularly since the mechanical index of pressures and frequencies applied in this study (Chapter 2) are in the range in which secondary Bjerknes force, and consequently bubble coalescence, is the dominant factor. However, optimized parameters for pre-conditioning which utilizes dispersion as well as coalescence may introduce more significant change.

7.2.1.2 Modulating the Cavitation Initiation Pressure Threshold in an *in vivo* Model

The cavitation initiation threshold modulation study detailed in chapter 2 included series of experiments in different mediums: degassed water, tissue phantom gel, and bovine liver tissue. The results of this work showed that similar trends of change in the cavitation initiation threshold was carried out in different mediums. However, an *in-vivo* validation of the results obtained in this study is an important next step in the development of active tissue protection. It is expected that similar results to that of the *ex-vivo* tissue would be attained in an *in-vivo* model.

7.2.2 Cavitation Control and ABCD

A significant portion of this dissertation was dedicated to developing acoustical methods for minimizing the adverse effects of pre-focal cavitation bubbles during histotripsy and lithotripsy treatments. Future work includes exploring the feasibility of active bubble dissolution, further optimization and *in vivo* validation of ABCD process, and investigation of the safety of ABCD in SWL and exploring possible reduction in collateral tissue damage.

7.2.2.1 Active Bubble Dissolution

In previous studies, we have shown that applying properly tuned low amplitude pulse sequences can improve the efficacy of histotripsy or lithotripsy treatments by actively stimulating bubble coalescence and dispersing them away from the propagation path. Another approach to

explore to minimize the adverse effects of pre-focal cavitation is active bubble dissolution. The goal of this study is to investigate the feasibility of actively forcing the residual bubbles to dissolve away. In the absence of a sound field, bubbles will dissolve away slowly to due to an excess of internal gas pressure in comparison with a surface tension pressure of $2\sigma/R_0$. Bubbles with radius of 10 μm dissolve away completely in about 1.17 s in air-free water, and in 6.63 s in saturated water. In the presence of a sound field, when liquid is saturated, passive dissolution is negligible. If input pressure is smaller than a threshold, bubble will dissolve away through active dissolution; otherwise, they will grow by rectified diffusion. Cavitation bubble models developed in this work (Chapter 3) can be unitized in designing acoustic pulse sequences that could be applied between histotripsy pulses for active bubble dissolution.

7.2.2.2 Simulation and Optimization of ABCD

Future work will aim to develop more complete cavitation bubble models and simulation of forced bubble coalescence and dispersion, which could be then utilized for further optimization of acoustic parameters of ABCD. The behavior and interactions of residual microbubbles following the collapse of lithotripsy or histotripsy bubble cloud is extremely complicated. The simplified modeling and simulation of bubble behavior developed in this research (Chapter 3) was useful for applications of ABCD that were performed in this dissertation. The simulation results were found to be in agreement with experimental results for the range of parameters for which primary or secondary Bjerknes forces were the dominant factors and the bubble oscillations were stable (MI<1). However, further optimization of the ABCD process calls for more complete models for cavitation nucleation, bubble coalescence, active dissolution, and behavior and movement of bubbles in inhomogeneous mediums.

And finally, the optimized ABCD design is to be evaluated in an *in vivo* porcine model similar to the model detailed in chapter 4.

7.2.2.3 Study of Proliferation of Cavitation Bubbles and Safety of SWL enhanced with ABCD

Utilizing acoustic bubble coalescence in shockwave lithotripsy can potentially reduce collateral tissue damage in two different ways. Increased risk for collateral tissue damage in high rates SWL is hypothesized to be due to cavitation within the kidney parenchyma. ABCD with SWL could help reduce this damage by preventing a proliferation of cavitation bubbles expanding into the kidney tissue. Additionally, since SWL enhanced with ABCD requires smaller doses of shockwaves for achieving the same result, lower amounts of tissue damage are expected to occur. On the other hand, forced coalescence and dispersion might introduce some collateral tissue damage through forced movements of cavitation bubbles. One of the goals of future studies would be to examine the safety of ABCD in SWL, and to explore possible reductions in collateral tissue damage in an *in vitro* model. Porcine kidneys will be obtained from a local slaughterhouse and used on the day of harvest. Kidneys will be kept in saline under vacuum for four hours prior to use to minimize dissolved gas. A model stone will be inserted through an incision in the proximal ureter into the lower pole. The stone will then be targeted with shockwaves at various rates while imaging with ultrasound. The locations of enhancement on harmonic imaging within the parenchyma will be tracked during treatment. SWL at various rates with and without ABCD will be tested. The experiment will also be performed on a set of kidneys without a stone to determine if the presence of the stone affects the proliferation of cavitation. The tissues will be sent for histology for further analysis.

7.3 References

[1] H. Alavi Tamaddoni, A. P. Duryea, E. Vlaisavljevich, Z. Xu, T. L. Hall, "Acoustic Methods for Increasing the Cavitation Initiation Pressure Threshold," *IEEE transactions on ultrasonics, ferroelectrics, and frequency control*, vol. 65, no. 11, pp. 2012-2019. Nov. 2018.

[2] H. Alavi Tamaddoni, W. W. Roberts, A. P. Duryea, C. A. Cain, and T. L. Hall, "Enhanced High-Rate Shockwave Lithotripsy Stone Comminution in an *in vivo* Porcine Model Using Acoustic Bubble Coalescence," *Journal of Endourology*, vol. 30, no. 12, pp. 1321-1325, Dec. 2016.